Dissertation submitted to the

Combined Faculty of Natural Sciences and Mathematics

of the Ruperto Carola University Heidelberg, Germany

for the degree of

Doctor of Natural Sciences

Presented by

Philipp Alexander Voss, M.Sc.

born in Weißenburg in Bayern.

Oral examination July 22nd, 2020

Cellular processes underlying symbiosis establishment in *Aiptasia*, a model for cnidarian-dinoflagellate endosymbiosis

Referees:

Prof. Dr. Annika Guse

Prof. Dr. Thomas Holstein

Contents

Previous publications of work presented in this thesis

The work presented in this thesis has partially been published. The results presented in chapter 2 of this thesis have been published in the following publication under a CC-BY 4.0 International license:

> Wolfowicz, I., Baumgarten, S., Voss, P.A., Hambleton, E.A., Voolstra, C.R., Hatta, M., and Guse, A. (2016). *Aiptasia sp.* larvae as a model to reveal mechanisms of symbiont selection in cnidarians. Sci Rep *6*.

Results presented in chapter 3 have partially been published in the following publication under a CC-BY-NC-ND 4.0 International license:

> Voss, P.A., Gornik, S.G., Jacobovitz, M.R., Rupp, S., Dörr, M.S., Maegele, I., and Guse, A. (2019). Nutrient-dependent mTORC1 signaling in coral-algal symbiosis. BioRxiv.

Contributions

Parts of the results in chapter 3 were obtained by the following contributors: Cell proliferation assays were conducted by Melanie Dörr and Sebastian Rupp, KEGG enrichment analysis, as well as MITF-family phylogeny and CLOVER analysis of E-box motifs by Sebastian Gornik, and LAMP1 antibody verification and immunofluorescence staining by Marie Jacobovitz.

Publications in pre-print servers and journals

Wolfowicz, I., Baumgarten, S., Voss, P.A., Hambleton, E.A., Voolstra, C.R., Hatta, M., and Guse, A. (2016). *Aiptasia sp.* larvae as a model to reveal mechanisms of symbiont selection in cnidarians. Sci Rep *6*.

Voss, P.A., Gornik, S.G., Jacobovitz, M.R., Rupp, S., Dörr, M.S., Maegele, I., and Guse, A. (2019). Nutrient-dependent mTORC1 signaling in coral-algal symbiosis. BioRxiv.

Jacobovitz, M.R., Rupp, S., Voss, P.A., Gornik, S.G., and Guse, A. (2019). Dinoflagellate symbionts escape vomocytosis by host cell immune suppression. BioRxiv.

List of Figures

List of Tables

List of Supplemental Files

Abstract

Coral reefs are the most biodiverse ecosystems on Earth. Their productivity is powered by the symbiotic association between corals and unicellular photosynthetic dinoflagellates of the family Symbiodiniaceae. These symbionts reside inside the corals' cells in specialized organelles, the symbiosomes, from where they transfer energy-rich compounds to the corals to support their nutrition. Interestingly, symbiosis is re-established every generation, as most corals produce symbiont-free offspring, which acquire symbionts from the surrounding sea water by phagocytosis. Despite the importance of symbiosis establishment for the coral life cycle, it is unclear how corals identify compatible symbionts and which mechanisms allow the symbionts to persist in their intracellular niche. For example, it is unknown how symbionts escape the host immune response and how symbiont-derived nutrients are integrated into the host cell metabolism. Using the sea anemone *Aiptasia* as a model, I characterized the underlying processes of symbiosis establishment. *Aiptasia* engages in symbiosis with similar species of Symbiodiniaceae as corals, and can be induced to produce larvae under laboratory conditions, providing access to symbiont-free larvae to study symbiosis establishment year-round. In a first step, I compared the uptake of compatible symbionts to that of free-living Symbiodiniaceae and inert beads in *Aiptasia* larvae. I uncovered that selection of symbionts occurs already prior to their phagocytosis and that while phagocytosis was size-selective, all tested particles were phagocytosed. This implies that additional mechanisms for the selection of compatible symbionts occur once potential symbionts have been phagocytosed. To assess the molecular mechanisms underlying symbiosis establishment in more detail, I developed a cell-specific method to compare gene expression in symbiotic and non-symbiotic cells. This revealed a major down regulation of various catabolic processes, including autophagy, as a response to symbiont uptake. Specifically, I found evidence that the shutdown of autophagy is regulated by a conserved gene-regulatory network under the control of the master regulator of cell growth and proliferation, mTOR (mechanistic target of rapamycin). mTOR is activated by symbiont-derived nutrients and symbiosis resulted in increased lipid storage and cell proliferation. Thus, I propose a model where symbiont-derived nutrients activate mTOR signaling, which acts as a mechanism of symbiont selection. Beneficial symbionts activate mTOR, resulting in their maintenance and allowing them to proliferate in the host tissue, while failure to activate mTOR would result in their autophagy. Currently, coral reefs are declining world-wide at unprecedented rates, mostly caused by global warming disrupting the symbiotic interaction leading to loss of symbionts from the host, a process known as 'coral bleaching'. This thesis lays the foundation for future work studying the molecular mechanisms underlying symbiont selection and symbiosis establishment in cnidarian-dinoflagellate symbiosis. Understanding how corals select and stably integrate symbionts may help to predict how corals adapt to changing environments, a prerequisite to combat the loss of these important ecosystems.

Zusammenfassung

Korallenriffe sind die artenreichsten Ökosysteme der Erde. Ihre Produktivität basiert auf der Symbiose zwischen Korallen und einzelligen photosynthetischen Dinoflagellaten der Familie Symbiodiniaceae. Diese Symbionten leben in speziellen Organellen, den Symbiosomen, innerhalb der Korallenzellen. Sie teilen energiereiche Verbindungen mit den Korallen und sichern somit deren Ernährung ab. Die Symbiose wird in jeder Genereration neu etabliert, da die meisten Korallen Nachkommen zeugen, die keine Symbionten besitzen. Symbionten werden deshalb aus dem umgebenden Meerwasser durch Phagozytose aufgenommen. Obwohl die Etablierung der Symbiose so zentral für den Lebenszyklus der Korallen ist, ist immer noch unklar, wie Korallen kompatible Symbionten erkennen und welche Mechanismen es den Symbionten erlauben in ihrer intrazellulären Nische zu überleben. Zum Beispiel ist noch unklar wie Symbionten dem Immunsystem der Koralle entgehen und wie die vom Symbionten transferierten Nährstoffe in den Metabolismus der Wirtszelle integriert werden. Im Modellorganismus *Aiptasia*, einer Seeanemone, charakterisiere ich die zugrundeliegenden Prozesse der Etablierung der Symbiose. *Aiptasia* formt eine Symbiose mit ähnlichen Symbiodiniaceae-Spezies wie Korallen. Außerdem kann in *Aiptasia* die Produktion von Larven im Labor stimuliert werden, was den Zugang zu Larven ohne Symbionten erlaubt, mit denen das ganze Jahr über die Etablierung der Symbiose untersucht werden kann. Zunächst verglich ich die Aufnahme kompatibler Symbionten zur Aufnahme von frei lebenden Symbiodiniaceae und inerten Plastikkügelchen. Dabei stellte sich heraus, dass die Selektion von Symbionten bereits vor deren Phagozytose einsetzt. Die Phagozytose selbst war größenselektiv, aber alle Partikel wurden phagozytiert, was darauf hinweist, dass nach der Phagozytose zusätzliche Mechanismen zur Selektion von Symbionten existieren. Um die molekularen Vorgänge der Etablierung der Symbiose genauer zu untersuchen, entwickelte ich eine Methode um die Genexpression in symbiotischen und nichtsymbiotischen Zellen miteinander zu vergleichen. Dabei stellte sich heraus, dass mehrere katabolische Prozesse, darunter Autophagie, als Reaktion auf die Aufnahme von Symbionten massiv herunterreguliert waren. Ich fand Hinweise darauf, dass das Abschalten der Autophagie durch ein konserviertes Genregulationsnetzwerk gesteuert wird, welches wiederum durch mTOR (mechanistic target of rapamycin) kontrolliert wird. mTOR selbst wird durch symbiontische Nährstoffe aktiviert und die Symbiose bewirkte eine erhöhte Einlagerung von Lipiden sowie Zellteilung. Darauf basierend stelle ich ein Modell vor, in dem die Aktivierung des mTOR Signalweges durch symbiontische Nährstoffe als Mechanismus für die Selektion von Symbionten dient. Nutzbringende Symbionten aktivieren mTOR durch das Teilen von Nährstoffen, was ihnen erlaubt in der Wirtszelle zu überleben und sich dort zu teilen. Symbionten die keine Nährstoffe teilen, hingegen, schaffen es nicht mTOR zu aktivieren, was zu ihrem Verdau durch Autophagie führt. Korallenriffe werden derzeit weltweit in noch nie dagewesenem Ausmaß durch die Folgen des Klimawandels geschädigt. Dabei wird die

Symbiose zwischen Korallen und Symbiodiniaceae gestört, was zum Verlust der Symbionten und letztendlich zum Verhungern der Korallen führt. Diese Arbeit stellt eine erste Untersuchung der molekularen Mechanismen der Symbioseetablierung und Selektion von Symbionten dar. Das Verständnis, wie Korallen Symbionten auswählen und stabil integrieren, kann dazu beitragen, vorherzusagen, wie sich Korallen an sich verändernde Umgebungen anpassen, eine wichtige Voraussetzung, um den Verlust dieser fragilen Ökosysteme zu verhindern.

1 General Introduction

1.1 Coral reef ecosystems

Coral reefs are biodiverse ecosystems found in shallow tropical waters. Despite covering less than 0.1% of the ocean surface, they provide habitat for about one quarter of marine species (Spalding and Grenfell, 1997). Due to their high biodiversity, coral reefs have been called the rainforests of the sea. Similar to the tropical rainforests on land, which exist on poor soils, coral reefs occur in regions of oligotrophic (nutrient-poor) tropical waters. In fact, the areas where reefs currently exist were sparsely populated before the evolution of reef-building stony corals (Scleractinia) in the Triassic (Muscatine et al., 2005), which form the basis of coral reef ecosystems.

1.1.1 Coral reef ecology

Reef-building corals form the basis of coral reefs, as the foundation of reefs is formed on top of limestone deposits originating from the skeletons of stony corals (Scleractinia) and the remains of other limestone-depositing organisms collectively referred to as 'reef-builders'. Corals contribute the most limestone, followed by calcareous algae (e.g. coralline algae), which deposit limestone in their cell walls (Sorokin, 2013). Further reef-builders include sponges, mollusks (e.g. the giant clams), and foraminifers (unicellular eukaryotes with a limestone shell). The reef-builders form the limestone by precipitation of calcium and carbonate ions from the sea water. Limestone pieces of all sizes accumulate on the floor of the reef between the coral skeletons where they are compacted into sheets of limestone, which can become several hundred meters thick over time (Sorokin, 2013). This physical foundation acts as a structure into which many species bore caves or on which new limestone structures are built to provide habitat for many other species. This allowed reef ecosystems to become the most biodiverse ecosystems on earth harboring 32 out of the 34 recognized animal phyla, more than in any other ecosystem (tropical rainforests house 17 phyla) (Porter and Tougas, 2001). This immense biodiversity is additionally supported by efficient recycling of scarce nutrients within a complex food web.

The primary producers in coral reefs are phototrophic algae, cyanobacteria, as well as the corals, which house photosynthetic algae (Sheppard et al., 2018). These primary producers act as food for primary consumers, mostly zooplankton and filter feeders such as sea squirts (tunicates), snails, sponges, and herbivorous fish. At a higher trophic level are carnivorous species, including fish and many crustaceans, that eat the primary consumers and other carnivorous species. The dense living conditions on the reef enable the efficient recycling of nutrients up and down the food chain. Interestingly, the coral meta-organism (comprised of corals and their photosynthetic symbionts) can be considered to simultaneously be primary producer, primary consumer, and carnivorous, as the symbionts fix carbon and the corals feed on both phyto- and zooplankton (Ferrier-Pagès et al., 2011).

Besides their importance for biodiversity, coral reefs provide important ecosystem services for approximately 500 million people around the globe (Wilkinson, 2004). By forming a living physical barrier to waves, reefs protect coastlines from erosion during storms or tsunamis. They are a prerequisite to many people's income by supporting fishery and tourism and are the source of medical compounds isolated from coral reef organisms. Altogether, the ecosystem services of coral reefs are estimated to surmount up to 9.9 trillion USD annually (Costanza et al., 2014). Coral reefs can only provide these services when they are healthy, but they are increasingly threatened by human interventions (see section 1.1.3).

1.1.2 Coral reefs depend on scleractinian corals

The coral reef ecosystem strictly depends on Scleractinia (stony corals), for maintaining both structural and trophic stability (Dubinsky, 1990; Harrison and Booth, 2007; Sheppard et al., 2018). Stony corals are corals that build skeletons under their living tissue. The skeletons consist of limestone (calcium carbonate) in the form of aragonite and grow continually over the lifetime of a coral (Sheppard et al., 2018), facilitating the growth of the coral towards the light. Limestone from coral skeletons and other reef-builders forms the foundation of the coral reef.

Besides creating the physical foundation of coral reefs, Scleractinia also support the reef's trophic cascade (Dubinsky, 1990). They live in symbiosis with unicellular algae of the family Symbiodiniaceae (Boschma, 1925; Brandt, 1881; Krueger, 2017), which are among the main primary producers in the ecosystem (Sheppard et al., 2018). By living inside of the coral host, these algae can efficiently recycle waste products of coral metabolism, such as nitrate and phosphate, allowing them to support not only their own growth, but also that of their host (Tremblay et al., 2012). In fact, the corals are so dependent on this symbiosis, that when the symbiosis breaks down under stress conditions, a process known as bleaching, failure to re-establish the symbiosis is lethal and can lead to reef decline (Hoegh-Guldberg et al., 2007).

1.1.3 Threats to coral reefs

Extensive coral death can lead to destruction of entire reef ecosystems. Unfortunately, this is occurring at a higher rate than ever before, due to a number of anthropogenic factors (Eakin et al., 2019; Porter and Tougas, 2001). One major cause, particularly in close proximity to land-based agriculture and urban centers, is eutrophication, i.e. increasing nutrient levels (Porter and Tougas, 2001). In the naturally oligotrophic waters, coral symbionts benefit from their association with corals by recycling nitrogen and phosphorus – waste products of coral respiration. Increased nutrient levels in the water due to human activity take away this competitive advantage and favor the growth of macroalgae, which can shade out the corals (Lapointe, 1999).

The effects of human activity have increased so drastically that even remote coral reefs are threatened. Elevated atmospheric carbon dioxide levels due to industrial carbon emission lead to ocean acidification

which results in to reduced calcification in corals (Kleypas and Langdon, 2006). Additionally, global warming leads to sea surface temperatures above the temperature tolerance of corals, which can lead to coral bleaching (loss of symbionts) and death (Hoegh-Guldberg et al., 2007). The most damaging coral bleaching event ever recorded occurred from 2014 to 2017, when sea surface temperatures were at record highs (Eakin et al., 2019).

1.2 Symbiodiniaceae

1.2.1 Symbiodiniaceae phylogeny and systematics

Coral reefs rely on the symbiosis between corals and unicellular eukaryotes of the family Symbiodiniaceae. Symbiodiniaceae belong to the phylum Dinoflagellata (Greek *dinos* "whirling" and Latin *flagellum* "whip, scourge"). Dinoflagellates are flagellated unicellular eukaryotes belonging to the superphylum Alveolata within the SAR supergroup comprising Stramenopiles (incl. diatoms); Alveolata (ciliates, apicomplexans, and dinoflagellates), and Rhizaria, (incl. radiolarians and foraminiferans) (Figure 1.1) (Brown et al., 2018).

Dinoflagellates are one of the most diverse groups of eukaryotes in marine surface waters (de Vargas et al., 2015). There are almost 2,400 extant described species living both in the oceans and freshwater, with diverse lifestyles and with different trophic and morphological adaptations (Taylor, 1987). The dinoflagellates include photoautotrophic, heterotrophic, and mixotrophic species. About half of the dinoflagellate species are photoautotrophs and the other half are heterotrophs (Gómez, 2012). Around 1% of dinoflagellates are symbiotic mutualists and around 7% are parasitic (Gómez, 2012).

The plastids of most photosynthetic dinoflagellates originated from a secondary endosymbiosis, i.e. the uptake and incorporation of a photosynthetic eukaryote that arose from a primary endosymbiosis of a cyanobacterium (as in the ancestor of land plants) by another eukaryote (Bhattacharya et al., 2004).

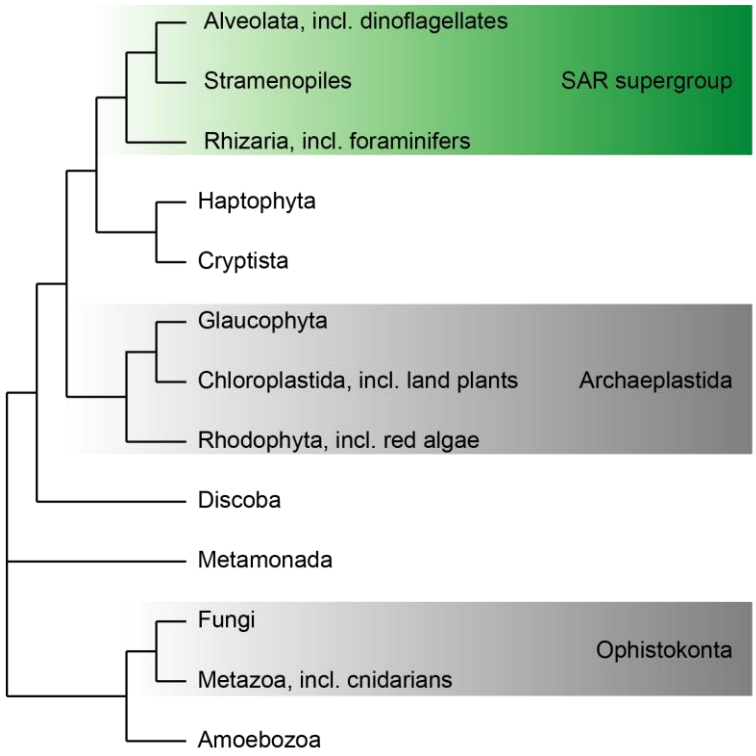

Figure 1.1. Phylogenetic position of the SAR supergroup within the eukaryotes. Based on data from (Brown et al., 2018). Branch lengths arbitrary.

As the ability to photosynthesize was lost in the dinoflagellates several times, heterotrophic species arose, which in some cases regained photosynthesis through tertiary, and potentially quaternary, endosymbioses of eukaryotes with primary and secondary symbionts, respectively (Waller and Kořený, 2017).

Of the few symbiotic dinoflagellates, perhaps the most well-known belong to the family Symbiodiniaceae, members of which form endosymbioses with corals and some other hosts. All members of Symbiodiniaceae (formerly genus *Symbiodinium*) were originally regarded as a single widely distributed species, *Symbiodinium microadriaticum* (Freudenthal, 1962), but genetic evidence revealed tremendous diversity within the taxon (Rowan and Powers, 1991, 1992). Once the diversity was discovered, nine clades A-I were described based on 18S rRNA sequences (Rowan and Knowlton, 1995). Two of these clades (H and I) are exclusively associated with foraminifers; other unicellular eukaryotes belonging to the SAR supergroup (Pochon and Gates, 2010). Species from clades A, B, C, D, and F establish symbiosis with cnidarians, including corals (LaJeunesse et al., 2018; Rodriguez-Lanetty et al., 2003). The division into clades was recently augmented when several new genera in the family Symbiodiniaceae were defined based on genetic, morphological, physiological, ecological, and biogeographic evidence for several taxa (LaJeunesse et al., 2018; Nitschke et al., 2020) (Figure 1.2). Within the Symbiodiniaceae, species belonging to the genera *Symbiodinium* (clade A), *Breviolum* (clade

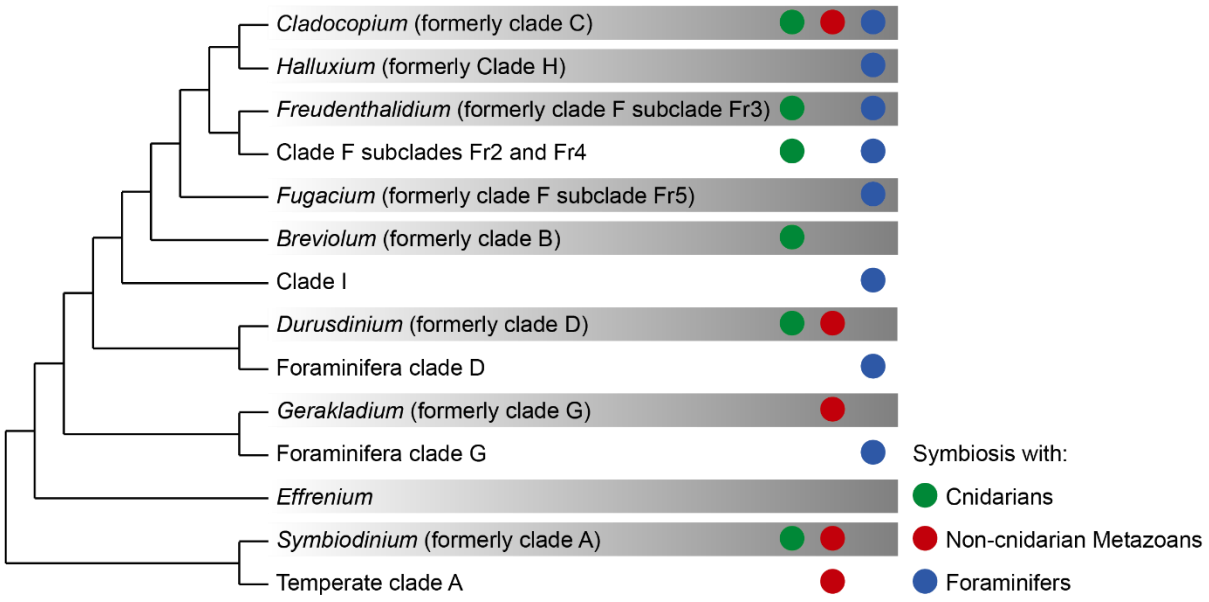

Figure 1.2. Phylogeny of Symbiodiniaceae based on nuclear small subunit of rRNA. Only genera and clades likely to represent genera are shown. Previous clade names of new genera indicated in brackets. Branch lengths arbitrary. Based on data from LaJeunesse et al., 2018.

B), *Cladocopium* (clade C), *Durusdinium* (clade D), as well as species belonging to clade F establish symbiosis with cnidarians (LaJeunesse et al., 2018; Rodriguez-Lanetty et al., 2003).

1.2.2 Symbiotic relationships of Symbiodiniaceae

Symbiotic interactions of Symbiodiniaceae are not restricted to corals. Within Cnidaria, Symbiodiniaceae form symbioses with members of all orders of Hexacorallia (including Scleractinia), various other Anthozoa, Scyphozoa (jellyfish), and the Milleporidae (fire corals) belonging to the Hydrozoa (see also Figure 1.4). Symbiodiniaceae also form symbioses with other animals including Porifera (sponges) (Carlos et al., 1999; Hill et al., 2011), Acoelomorpha (acoel flatworms) (Barneah et al., 2007), and Mollusca (e.g. the giant clam *Tridacna sp.* and various nudibranchs) (Kempf, 1984; Norton et al., 1992). Symbiodiniaceae also establish symbiosis with various species of unicellular eukaryotes, e.g. Foraminifera (reviewed in (Pochon and Pawlowski, 2006)) and Ciliophora (ciliates) (Lobban et al., 2005).

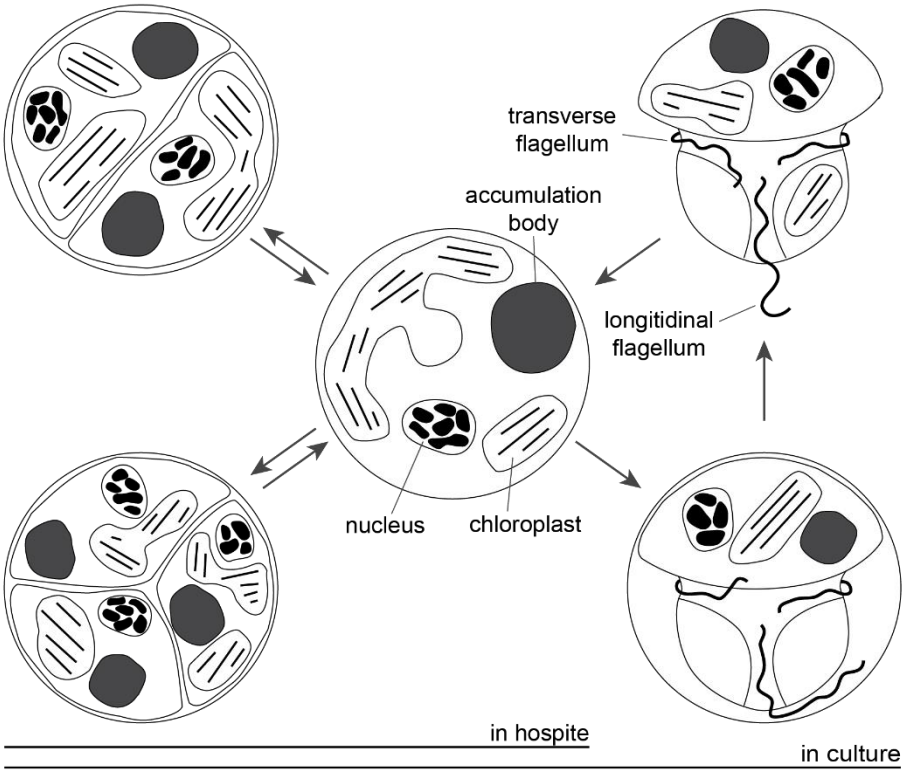

Figure 1.3. Life stages of Symbiodiniaceae. Center and left show the vegetative cyst. The motile zoospore is shown on the right. Note that the cell wall is usually significantly thicker in cultured Symbiodiniaceae than in hospite. Adapted from Freudenthal, 1962.

1.2.3 Basic biology of Symbiodiniaceae

Symbiodiniaceae are unicellular photosynthetic eukaryotes, 5-15 µm in diameter, and yellow-brown in color (Freudenthal, 1962; Schoenberg and Trench, 1980). They have two life stages, the vegetative cyst and the motile zoospore (see Figure 1.3) (Freudenthal, 1962). The vegetative cyst has a coccoid shape and is the common form when endosymbiotic (Stat et al., 2006). It can divide to form two (sometimes three) equal daughter cells (Freudenthal, 1962). Following duplication of the nucleus, a furrow is formed, establishing an equator, along which the cell constricts to form 2 daughter cells, which often stay attached for some time (Freudenthal, 1962).

The coccoid vegetative cyst can also give rise to one or four motile zoospores (Freudenthal, 1962; Schoenberg and Trench, 1980). The motile zoospore has a thicker cell wall, consisting of cellulose plates termed thecal plates, and has one longitudinal and one transverse flagellum, which facilitate motility (Freudenthal, 1962; Schoenberg and Trench, 1980). No direct evidence was found for meiosis (Freudenthal, 1962; Schoenberg and Trench, 1980), but genetic studies suggest that sexual reproduction occurs in the Symbiodiniaceae, likely in the motile zoospores (Baillie et al., 1998; LaJeunesse, 2001).

1.3 Corals

1.3.1 Phylogenetic position of scleractinian corals

Coral reefs depend on the three-dimensional stony structures formed by hermatypic (reef-building) corals. Most hermatypic corals belong to Scleractinia (stony corals), which form exoskeletons out of limestone. Together with sea anemones (Actiniaria), Scleractinia are members of the subclass Hexacorallia (Figure 1.4) (Daly et al., 2007). Most Hexacorallia have hexameric symmetry, although exceptions exist (Daly et al., 2007). Together with Ceriantharia (tube anemones) and Octocorallia, Hexacorallia form the Anthozoa (from Greek *anthos* "flower" and *zoos* "animal") (Daly et al., 2007). Some anthozoans besides Scleractinia are also sometimes referred to as corals, e.g. the soft corals (Alcyonacea, formerly: gorgonians), which do not form a stony skeleton. Scleractinia are not the only hermatypic corals, however members of this class contribute the majority of the deposited limestone to reefs (Sheppard et al., 2018). Minor reef-building corals are the blue corals (Helioporaceae) and the organ pipe corals (Turbipora), both Octocorallia (Sheppard et al., 2018).

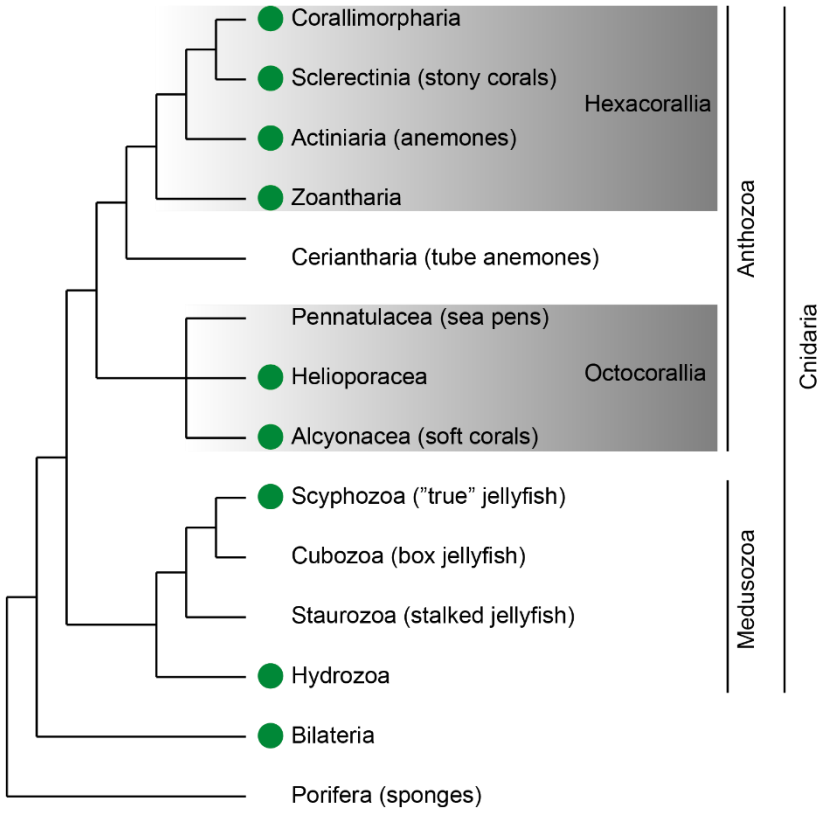

Figure 1.4. Phylogeny of Cnidaria. Branch lengths arbitrary. Green circles represent taxa that form symbiosis with Symbiodiniaceae. Adapted from (Kayal et al., 2018), presence of symbiosis within Octocorallia according to (Schubert et al., 2017).

Anthozoa and Medusozoa (Hydrozoa, Staurozoa, Cubozoa, and Scyphozoa) together form the phylum Cnidaria (Daly et al., 2007). The unifying feature of cnidarians are their cnidae, specialized organelles which contain harpoon-like structures, which are used for multiple purposes, including the capture of prey and defense against predators (Daly et al., 2007). Cnidarians are diploblastic animals with two tissue layers, the ectoderm and the endoderm, and are most likely sister to Bilateria (animals with embryonic bilateral symmetry) or potentially Placozoa (from Greek *placo* "flat" and *zoos* "animal") (Laumer et al., 2019). Basal to Cnidaria is Porifera (sponges).

1.3.2 Coral anatomy

Cnidarians have three life stages: medusae, planula larvae, and polyps (Daly et al., 2007). Medusae have an umbrella-shaped body fringed by stinging tentacles. They only occur in Medusozoa, not Anthozoa (including Scleractinia), which only have the planula larvae and polyp life stages (Daly et al., 2007). The planulae have a simple body plan and are ovoid (egg-shaped), usually with an oral opening on one end. The outside of the body and the tissue lining the oral opening is ectodermal. The tissue on the inside of the larvae lining the gastric cavity is endodermal. The ciliated planula larvae are usually free-swimming and eventually attach to a suitable substrate where they metamorphose into the polyp (Gleason and Hofmann, 2011).

Polyps consist of a hollow cylindrical body column that is roughly circular in cross-section (Figure 1.5). They are usually attached to a surface at the pedal disc. At the opposite end, the oral disc, they have a single opening, surrounded by symmetrically arranged tentacles, that are employed to catch prey using the nematocysts (a type of cnidae). The tentacles bring the captured prey to pharynx for digestion in the body column. After digestion, any undigested debris is expelled through the mouth. Like planula larvae, polyps also have two tissue layers, the endoderm and the ectoderm. The endoderm lines the inside of the body column and tentacles, while ectoderm comprises the outside of the body and the pharynx, a tube connecting the mouth opening to the gastrovascular cavity (coelenteron) (Daly et al., 2007). Between the ecto- and endodermal tissue is the mesoglea, a mostly acellular tissue, which functions as a hydrostatic skeleton and houses immune cells and muscle fibers (Slobodkin and Bossert, 2010). The gastrovascular cavity is divided into chambers by the mesenteries. These are radially arranged sheets of tissue protruding from the body wall into the gastrovascular cavity that run from the pedal to the oral disc (Khanna and Yadav, 2005) and house the gametogenic tissue as well as muscle cells involved in retraction of the polyp (Daly et al., 2007).

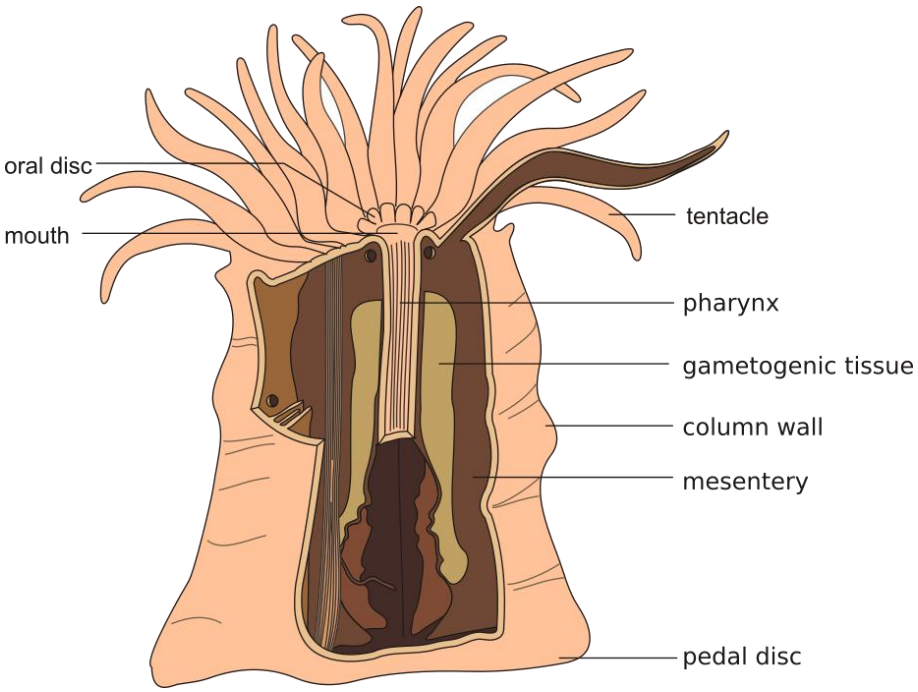

Figure 1.5. Polyp anatomy. © Hans Hillewaert / CC BY-SA 4.0.

1.3.3 Coral skeletons

Many Anthozoa, including most Scleractinia, are colonial, i.e. their polyps form large colonies consisting of many clonal polyps. In Scleractinia, these colonies produce stony skeletons made of limestone, which provide the polyps with shelter from predators and act as substrates for them to live on. The massive coral skeleton is dotted with small depressions at regular intervals termed 'corallites', in which individual polyps sit (Sheppard et al., 2018). The polyps are connected by living tissue, the 'coenosarc', which spreads over the skeletons (Sheppard et al., 2018). In most species, the polyps retract into the corallites by day to avoid predation and protrude from them at night to feed on passing plankton. The polyps, and in some species also the coenosarc, continually deposit limestone at their base, resulting in the growth of the skeleton. This is facilitated by specialized cells in the ectodermal tissue called 'calcyoblasts', which deposit limestone (calcium carbonate) extracellularly (Vandermeulen and Watabe, 1973). Over time, the coral colonies form elaborate skeletons with unique patterns, which are governed by both species-specific deposition patterns and environmental factors, such as exposure to waves (Todd, 2008) (see Figure 1.6).

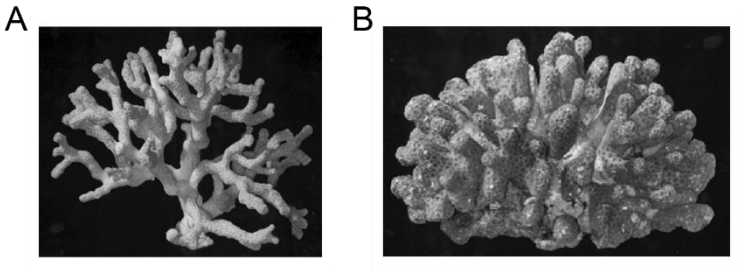

Figure 1.6 Growth form of scleractinian corals depends on environmental factors. A) Madracis mirabilis grown in a low-flow environment B) M. mirabilis grown in a high-flow environment. Reproduced from (Kaandorp, 2013) published under CC-BY 3.0.

1.3.4 Coral reproduction

Most coral species reproduce sexually once per year in the polyp stage, either as hermaphrodites (producing both sperm and eggs) or gonochorites (with separate sexes) (Harrison, 2011). There are two main strategies for sexual reproduction: broadcast spawning (in ~83% of species) and brooding (~14% of species), with both forms described for the remaining species (Harrison, 2011). In broadcast spawning, all conspecifics release their symbiont-free gametes synchronously with meticulous timing at a specific day of the year and time of the day, for external fertilization (Harrison, 2011). In brooding corals, fertilization and subsequent larval development occurs in the parent colonies (Harrison, 2011), which often results in vertical transmission of symbionts (Gleason and Hofmann, 2011). Planula larvae can survive up to 100 days in some species before settling and metamorphosing into a juvenile polyp (Davies et al., 2017). Symbionts are either acquired from the parental colony (for brooding corals) (Hirose et al., 2000), as planula larvae (Schwarz et al., 1999; Szmant-Froelich et al., 1985), or in the juvenile polyp stage (Hirose et al., 2008).

Following metamorphosis, skeleton formation begins, resulting in the formation of a new colony, which grows by budding off new polyps. Budding of polyps can occur via splitting of existing polyps (intratentacular budding) or generation of polyps from the coenosarc (extratentacular budding) (Harrison, 2011). In addition to budding during colony growth, asexual reproduction can also result in the formation of physically separate entities that can grow into new, genetically identical colonies (Harrison, 2011). The asexual reproductive capacity of corals is exploited in reef restoration, where coral colonies are fragmented and regrown in sheltered conditions before transplanting clonal colonies onto damaged reefs (Rinkevich, 2014).

1.4 Coral endosymbiosis

1.4.1 Coral symbiosis is driven by metabolic exchange

Coral reefs exist in the tropics, where the energy input from sunlight is particularly high. However, this location is also characterized by oligotrophic waters, i.e. waters with low concentrations of inorganic nutrients such as nitrates, phosphates, and carbon sources, which limits the productivity of phytoplankton (Hecky and Kilham, 1988). Such nutrient-poor environments typically do not support much life; however, in coral reefs, efficient recycling of inorganic nutrients leads to a thriving ecosystem. Recycling occurs both on a macroscopic level, the reef system as a whole (Furnas et al., 2011), and on a microscopic level, in symbiotic interactions of animals and phytoplankton, such as corals and Symbiodiniaceae (Wang and Douglas, 1998). Instead of releasing metabolic waste products such as nitrates, phosphates, and carbon dioxide into the surrounding water, corals can directly transfer them to their photosynthetic symbionts. The symbionts then use the inorganic nutrients in their metabolism, resulting in higher carbon fixation by photosynthesis. In doing so, they produce energy-rich compounds including lipids, sugars, and amino acids, of which they are estimated to transfer over 90% to their hosts (Davies, 1991; Davy et al., 1996; Muscatine et al., 1984; Steen and Muscatine, 1984). In this manner, the symbiont-provided nutrients can support 100% of their host's respiratory carbon needs under ideal conditions (Davies, 1991).

1.4.2 Corals harbor endosymbionts in the symbiosome

The efficient exchange of nutrients between host and symbiont without loss to the surrounding sea water is made possible by endosymbiosis (Greek *endon* "within", *syn* "together", and *biosis* "living") where the symbionts live within the coral cells. Symbiodiniaceae colonize juvenile corals and quickly spread throughout the coral endoderm (Wolfowicz et al., 2016). Within their host cells, they reside in specialized organelles termed symbiosomes, resulting from phagocytosis of symbionts (Schwarz et al., 1999). A host-derived membrane acts as a physical boundary between host and symbiont, through which nutrients are exchanged. How nutrients are exchanged over this membrane and which transporters are involved remains largely unknown. Additionally, it is unclear how symbionts are able to proliferate within their host organelle and spread throughout the host tissue.

1.4.3 Evolution of cnidarian-dinoflagellate symbiosis

Within Cnidaria, not only stony corals form a symbiosis with dinoflagellates of the family Symbiodiniaceae. Also, sea anemones and few jellyfish (Scyphozoa) form symbioses with Symbiodiniaceae, in some cases even with the same species (see Figure 1.4). Further, some cnidarians also form a symbiosis with other photosynthetic eukaryotes. For example, *Hydra viridis* (green hydra, also known as *H. viridissima*), forms a symbiosis with *Chlorella vulgaris*, a unicellular photosynthetic alga of the phylum Chlorophyta (Jolley and Smith, 1980). Like in the case of cnidarian-dinoflagellate

symbiosis, *H. viridis* harbor symbionts within symbiosomes of the endodermal cells (Habetha et al., 2003).

The wide-spread occurrence of intracellular symbiosis with photosynthetic eukaryotes within Cnidaria raises the question whether the common ancestor of cnidarians was symbiotic. However, ancestral state reconstruction has revealed that the common cnidarian ancestor was likely not symbiotic and that endosymbiosis evolved independently several times in the cnidarian lineage (Kayal et al., 2018). For example, the common ancestor of Hexacorallia (including stony corals and anemones) was likely symbiotic, but the common ancestor of Hexacorallia and Octocorallia was not and symbiosis arose in Octocorallia independently of Hexacorallia (Kayal et al., 2018).

1.4.4 Most corals produce aposymbiotic offspring

Most corals produce sexual offspring once annually in meticulously timed events to ensure cross-fertilization and sexual recombination. Despite the strict dependence of corals on their symbionts, in >70% of coral species (>80% of species with broadcast spawning) there is no vertical transmission of symbionts from parents to offspring (Baird et al., 2009). Therefore, symbionts must be taken up from the environment either in the larval stage or as juvenile polyps following metamorphosis. It remains unclear why symbionts are not vertically transmitted from parents to offspring, but a plausible hypothesis is that this allows the offspring to take up symbionts that are well-adapted to the environment where they establish a new colony. After all, corals produce copious amounts of larvae that can persist on maternally-provided yolk for extended periods of time in the open sea, making it possible for them to colonize locations far from their parent colonies with potentially different environmental conditions (Davies et al., 2017). Thus, not being associated with their parent's symbionts may allow them to more easily adapt to the environment where they settle by taking up native symbionts.

1.4.5 Specificity of coral symbiosis and establishment of coral symbiosis

Symbiosis establishment is a crucial process for corals, as they rely on the symbionts for nutrition. It occurs either at the larval stage or in juvenile polyps as well as following symbiont loss in bleaching. Symbionts are taken up via phagocytosis by endodermal cells, where they establish an intracellular niche in the symbiosome (Schwarz et al., 1999). The symbiosome is a host-derived vesicle in which the symbionts live, and from which they transfer nutrients to the host cell. In order to establish this host-niche, symbionts are thought to avoid the host's defense mechanisms, such as phagolysosomal digestion and the innate immune system, but the underlying mechanisms remain unclear (Davy et al., 2012).

Symbiosis establishment is a selective process, with corals associating with certain species of Symbiodiniaceae, but not others (see also Figure 1.2), and has a profound influence on coral physiology, as the type of symbionts can influence e.g. the growth rate (Little et al., 2004) and temperature

tolerance of the host (Jones and Berkelmans, 2010; Jones et al., 2008; Sampayo et al., 2008). However, the criteria important for symbiont selection are only beginning to be studied.

1.4.6 Breakdown of coral symbiosis – coral bleaching

The symbiosis between corals and Symbiodiniaceae requires stable environmental conditions for proper photosynthetic activity of the symbionts. These conditions are perturbed by increased temperature, light and altered concentrations of inorganic nutrients (C, N, P), leading to increased production of reactive oxygen species (ROS) as by-products of photosynthesis (Suggett and Smith, 2020; Weis, 2008). In an effort to eliminate the source of the toxic ROS, symbionts are removed from the coral tissue, leading to slower growth, vulnerability to disease, and often death of the coral (Brown, 1997; Hoegh-Guldberg, 1999; Hoegh-Guldberg et al., 2007). This process is known as coral bleaching due to the loss of symbionts and their photosynthetic pigments resulting in pale corals. Bleaching can occur via several mechanisms, including detachment of symbiotic host cells from the coral tissue, apoptosis or necrosis of symbiotic host cells, degradation of symbionts, or expulsion of symbionts (Bieri et al., 2016; Weis, 2008). However, the underlying pathways triggering these mechanisms, as well as which mechanisms contribute to bleaching under which environmental perturbations, remain largely unclear (Bieri et al., 2016; Suggett and Smith, 2020; Weis, 2008).

1.5 The *Aiptasia* model system

Despite the importance of coral reefs and the threats they face, little is known about the cellular and molecular mechanisms underlying coral symbiosis. Understanding these mechanisms is key to understanding how corals can cope with their changing environment. Open questions include the mechanisms of symbiont recognition and uptake, evasion of the host immune system, establishment of the intracellular niche, cross-talk between host and symbiont, nutrient-exchange, proliferation of symbiont within the host cell/tissue, and bleaching. This lack of understanding is in part because corals are difficult to study under laboratory conditions and in part because a model system approach to study coral symbiosis was only recently adopted (Weis et al., 2008).

Major advances in molecular, developmental, and cell biology have been made possible by focusing on few model systems (Davis, 2004). These model systems were chosen because they were accessible for experimental approaches and facilitated the reproducibility of experiments (Davis, 2004). This in turn allowed many researchers working on the same system, resulting in rapid progress, giving rise to synergistic effects in the development of tools and advancing research (Davis, 2004).

Unfortunately, corals lack important characteristics of model systems. They are generally slow-growing, often endangered (limiting access to specimen), difficult to maintain under laboratory conditions, and have a calcareous skeleton making them inaccessible for experiments. Additionally, they only spawn once annually, severely limiting access to offspring and resulting in long generation times. Given these difficulties with studying corals, the sea anemone *Exaiptasia pallida* (formerly *Aiptasia pallida* or *Exaiptasia diaphana*, commonly referred to as *Aiptasia*), has emerged as a model organism for coral symbiosis (Baumgarten et al., 2015; Bucher et al., 2016; Davis, 2004; Davy et al., 2012; Grawunder et al., 2015; Hambleton et al., 2019; Lehnert et al., 2012, 2014; Oakley et al., 2016; Sproles et al., 2019; Weis et al., 2008; Wolfowicz et al., 2016).

As a member of Actiniaria (sea anemones), *Aiptasia* is closely related to Scleractinia. Both are members of the subclass Hexacorallia in the subphylum Anthozoa (see Figure 1.4). The main differences between corals and sea anemones are that the former usually live in colonies on a limestone skeleton, while the latter are solitary and do not form a skeleton. Both corals and sea anemones occur in similar habitats (including coral reefs) and representatives of both form a symbiosis with Symbiodiniaceae. In fact, symbiosis with Symbiodiniaceae is thought to have originated in the common ancestor of Hexacorallia, preceding the emergence of Actiniaria and Scleractinia (Kayal et al., 2018). As such, it is likely that common molecular mechanisms underlie endosymbiosis in both taxa.

Aiptasia can be easily maintained under laboratory conditions and is considered a pest species by aquarists (Rhyne et al., 2004). It quickly reproduces asexually by pedal laceration. Here, a small part of the pedal disc is pinched off and develops into a new polyp. In the laboratory, this process is harnessed to generate and maintain clonal lines, a vital prerequisite for reproducible experimentation

based on the same genotype. Further, *Aiptasia* establishes symbiosis with similar species of Symbiodiniaceae as Scleractinia (Wolfowicz et al., 2016). Additionally, spawning can be artificially induced, allowing access to aposymbiotic (symbiont-free) offspring on a weekly basis (Grawunder et al., 2015). *Aiptasia* lends itself to comparative approaches as it can be rendered symbiont free (aposymbiotic) (Belda-Baillie et al., 2002; Matthews et al., 2016), allowing researchers to directly study the influence of symbiosis on host physiology in genetically identical animals. Further, it can establish symbiosis with various species of Symbiodiniaceae allowing researchers to study the influence of symbiont identity on the symbiosis.

1.5.1 Limitations of the *Aiptasia* model system

Despite its many advantages as a model system for cnidarian-dinoflagellate symbiosis, the *Aiptasia* system has some limitations. Most obvious, because *Aiptasia* do not possess limestone skeletons, the model system cannot be used to study the role of symbionts in coral skeleton formation (calcification) (Weis et al., 2008). This includes studies on the impact of projected sea water acidification on skeleton formation, which may pose a major threat to coral growth in the future.

Further, findings on the effects of symbiosis on growth in *Aiptasia* can only be transferred to corals to a certain degree, as colony growth is more complex than the growth of solitary polyps. For example, in Acroporid (staghorn) corals, nutrients are distributed among polyps through the coenosarc (Pearse and Muscatine, 1971) to ensure nutrient availability in newly formed, growing polyps at the branch tips, which are populated with less symbionts (Goreau and Goreau, 1959). However, given the close relation between *Aiptasia* and reef-building corals, as well as their evolution from a common, symbiotic ancestor, it is likely that common principles underlie symbiosis at the cell biological level.

1.5.2 Biology of *Aiptasia*

Aiptasia is a species of sea anemones within the family Aiptasiidae with global distribution (Grajales and Rodríguez, 2016), likely the result of a recent introduction, either via the aquarium trade or with ballast water (Thornhill et al., 2013). The genetic homogeneity of the species is likely facilitated its propensity for asexual reproduction via pedal laceration (Figure 1.7 left). Sexual reproduction of *Aiptasia* occurs by broadcast spawning, with different clonal lines being either male or female (Grawunder et al., 2015). Crucially, spawning can be induced by a blue light cue and elevated temperature allowing the production of larvae in the laboratory (Grawunder et al., 2015). Aposymbiotic planula larvae (Figure 1.7) fully develop by 48 hours post fertilization (hpf) and are able to acquire symbionts starting at this time (Bucher et al., 2016). The ability to acquire symbionts is maintained until ~14 days post fertilization (dpf) (Bucher et al., 2016). Larvae survive up to 40 dpf, however, settlement and metamorphosis into polyps has not been observed in cultured *Aiptasia* (Figure 1.7, right).

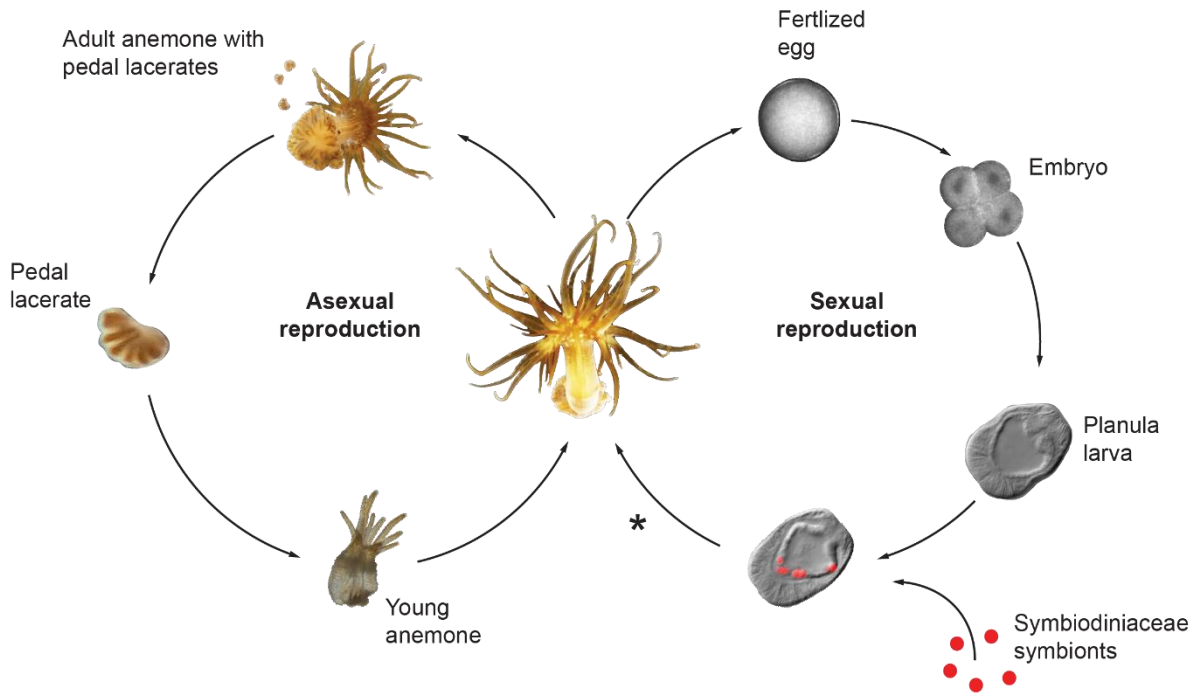

Figure 1.7. Life Cycle of Aiptasia. Aiptasia reproduce asexually by pedal laceration (left) and sexually by broadcast spawning (right). Asterisk (*) indicates incomplete sexual life cycle under laboratory conditions. This figure was adapted from Figure 1 in (Grawunder et al., 2015) published under CC-BY 4.0.

1.5.3 Available tools and resources in *Aiptasia*

Aiptasia polyps can be bleached, resulting in aposymbiotic individuals that can be used to assay uptake of Symbiodiniaceae in genetically identical animals (Belda-Baillie et al., 2002; Matthews et al., 2016). Because symbiosis is facultative for *Aiptasia* under laboratory conditions, aposymbiotic and symbiotic animals can be used to study symbiosis with a comparative approach.

Genetic resources for the *Aiptasia* model system are increasing, with a published genome (Baumgarten et al., 2015) and multiple transcriptome studies, e.g. comparing symbiotic and aposymbiotic animals (Lehnert et al., 2012, 2014; Matthews et al., 2017; Sunagawa et al., 2009; Wolfowicz et al., 2016). Similarly, other -omics approaches have yielded proteomic (Medrano et al., 2019; Oakley et al., 2016; Sproles et al., 2019) and lipidomic datasets (Garrett et al., 2013).

Aiptasia larvae are especially amenable to microscopy because of their transparency and small size, allowing imaging without the need for sectioning; this has been exploited for assessment of symbiont uptake, immunofluorescence imaging, and *in situ* hybridizations (Bucher et al., 2016; Hambleton et al., 2014, 2019; Wolfowicz et al., 2016). The use of gain of function and loss of function experiments genetic engineering is just emerging in the field, but has not yet been applied to biologically relevant questions (Jones et al., 2018).

1.6 Aims of this thesis

Symbiosis establishment is fundamentally important both for successful founding of new coral colonies and recovery of corals following bleaching events. However, little is known regarding the molecular mechanisms of the underlying processes. This includes basic information on when selection of symbionts occurs, how selection is mediated, and which cell biological processes are required for successful establishment of symbiosis.

To identify when during symbiosis establishment the selection of suitable symbionts occurs, I compared the uptake into the gastric cavity and phagocytosis of compatible and incompatible species of Symbiodiniaceae with each other and inert beads.

To characterize the cellular processes following the phagocytosis of symbionts, it was my aim to characterize the transcriptional response to symbiont uptake at the cellular level. To this end, I needed to develop a method to analyze the gene expression in symbiotic cells following uptake of symbionts.

Based on results from the gene expression analysis, I aimed to validate the involvement of identified candidate pathways in the cross-talk between host and symbiont and refine the model of the molecular events governing cnidarian-dinoflagellate endosymbiosis.

2 Symbiont uptake in *Aiptasia* larvae

2.1 Introduction

In all mutualisms, the symbiotic partners need to identify compatible species for symbiosis, while avoiding associations with other, potentially pathogenic organisms. In most corals, as well as *Aiptasia*, symbiosis is established after uptake of symbionts from the surrounding sea water (Baird et al., 2009; Bucher et al., 2016). This occurs at the beginning of the life cycle, i.e. in the larval stage or in the juvenile polyp, but may also occur after loss of symbionts by bleaching, so that hosts avoid starvation by re-acquiring their main source of nutrition.

Selecting appropriate symbionts is of great importance to the host, as different symbionts affect host physiology in different ways (Jones and Berkelmans, 2010; Jones et al., 2008; Little et al., 2004; Sampayo et al., 2008). For example, corals harbor different symbionts depending on their depth (Eckert et al., 2020), and symbiont identity can affect the host's growth rate (Little et al., 2004) or bleaching susceptibility, allowing the symbiosis to persist at higher temperatures (Jones and Berkelmans, 2010; Jones et al., 2008; Sampayo et al., 2008). The ability of corals to take up different types of symbionts which confer different benefits has led to the hypothesis that corals may be able to quickly adapt to environmental changes and local environments such as elevated sea temperatures and ocean acidification, by associating with symbionts that are uniquely adapted to the local environment (LaJeunesse et al., 2010; Rowan, 2004).

2.1.1 Specificity of cnidarian-dinoflagellate symbiosis

Members of the family Symbiodiniaceae establish symbiosis with various host species, including various cnidarians, sponges, molluscs and foraminifers (LaJeunesse et al., 2018); however, not all species of Symbiodiniaceae are symbiotic. Further, any given species of Symbiodiniaceae only appears to establish symbiosis with certain host species and *vice versa*, known as 'specificity.'

Interestingly, this specificity is not related to how closely related species are, as some hosts will establish symbiosis with species of Symbiodiniaceae belonging to two or more different genera of Symbiodiniaceae but not to all species within either of the genera. For example, the staghorn coral *Acropora digitifera* establishes symbiosis with *Breviolum minutum* and *Symbiodinium necroappetens* but not with *Symbiodinium linuchae*, despite being from the same genus (Wolfowicz et al., 2016).

2.1.2 Stages of symbiont selection in coral symbiosis

In other endosymbioses, symbiont selection does not occur based on a single criterion but rather on multiple criteria, which are all required, but not alone sufficient for symbiosis establishment (Cooper, 2007; Nyholm and McFall-Ngai, 2004). Given the importance of symbiont selection for the survival of

coral reefs, surprisingly little is known about how corals select compatible symbionts. Symbionts are taken up into coral cells in the endodermal tissue through phagocytosis (Schwarz et al., 1999).

Phagocytosis is initiated by cell-cell contact between the symbiont and the engulfing host cell, however, the interacting proteins have not been conclusively identified. Carbohydrate-binding lectins on the host cell surface have been implicated in recognition of glycans on the symbiont surface (Bay et al., 2011; Lin et al., 2000; Wood-Charlson et al., 2006). However, different studies found different results regarding their involvement and whether they activate or inhibit phagocytosis. Following phagocytosis, nascent canonically undergo a maturation process, in which they sequentially fuse with early endosomes, late endosomes, and lysosomes in a kiss-and-run manner (Gotthardt et al., 2002). Eventually, the phagosome matures into a phagolysosome, an acidic compartment (pH ~ 4.5) containing degradative enzymes that digest the phagocytosed particle (Levin et al., 2016). It has been proposed that the symbiosome resembles an early arrested phagosome, allowing symbionts to persist without being digested (Chen et al., 2004; Davy et al., 2012; Mohamed et al., 2016). However, which exact criteria allow symbionts to first enter their host cells and then persist there, is unclear (Davy et al., 2012).

To characterize when selection of symbionts occurs, I used a controlled symbiosis establishment assay in *Aiptasia* larvae to compare the uptake of two species of Symbiodiniaceae. These were the compatible *Breviolum minutum* and the free-living *Effrenium voratum*, as well as inert beads as a control. *B. minutum*, originally isolated from *Aiptasia*, is readily taken up and establishes symbiosis with *Aiptasia*, as well as the corals *A. tenuis* and *A. digitifera* (Hambleton et al., 2014; Wolfowicz et al., 2016). *E. voratum*, on the other hand, is a free-living species of Symbiodiniaceae and was originally isolated from sediment (Santos et al., 2002; Xiang et al., 2013).

2.2 Results

2.2.1 Uptake of non-symbiotic *Effrenium voratum* and inert beads

In order to characterize the mechanisms underlying the uptake of symbionts, a comparative approach was used to evaluate the uptake of clonal axenic strains of *B. minutum* (strain SSB01), the incompatible *Effrenium voratum* (strain SSE01), as well as inert beads of a similar size as *B. minutum*.

In previous experiments, *E. voratum* failed to be taken up by *Aiptasia* polyps or larvae (Hambleton et al., 2014; Xiang et al., 2013). However, these experiments used concentrations of only 10^4 algae/ml for durations between 2 – 31 days (Hambleton et al., 2014). Based on the increased infection with *B. minutum* at concentrations of 10^5 algae/ml after 4 days of exposure in a later publication (Bucher et al., 2016), *Aiptasia* larvae were infected with *E. voratum,* as well as beads, at this concentration. Indeed, after 4-5 days, 19% of larvae had taken up *E. voratum,* 65 % *B. minutum*, and 10 % inert beads (Figure 2.1 A).

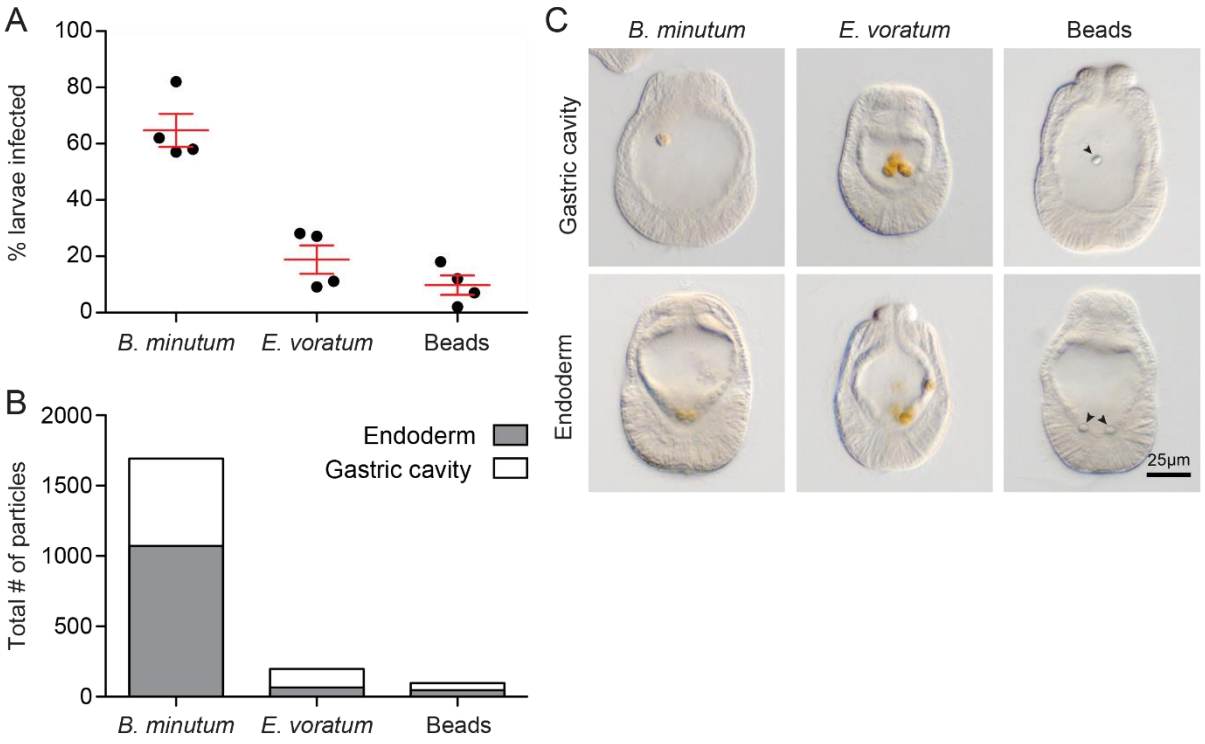

Figure 2.1. Preferential acquisition of compatible symbionts. A) Proportion of infected larvae 9 dpf after exposure to B. minutum, E. voratum, or beads for 4 or 5 days. Bar and whiskers represent mean and SEM of 4 replicate experiments. B) Total number of particles in the gastric cavity (GC) or endodermal tissue (EN) for larvae in A.C) Representative DIC images of larvae hosting particles in their gastric cavity or endodermal tissue used for analysis shown in A and B. This figure was rearranged from Figure 4 in (Wolfowicz et al., 2016) published under CC-BY 4.0.

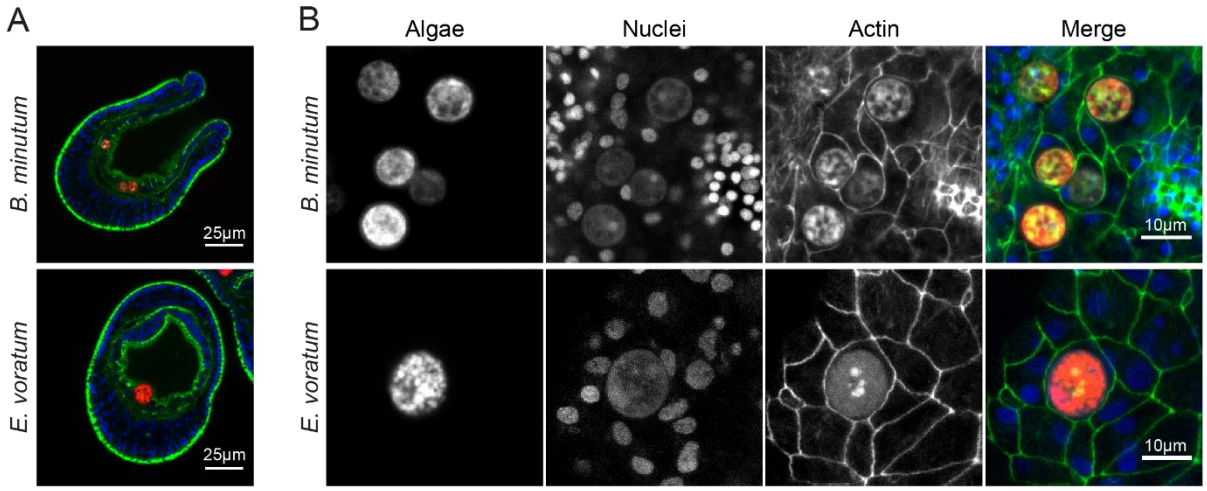

Figure 2.2. Intracellularization of B. minutum and E. voratum. Representative confocal images of B. minutum and E. voratum in the endodermal tissue of Aiptasia larvae. A) overview of whole larvae. Colors in merge are nuclei in blue (Hoechst33258), F-actin (detected with phalloidin-Alexa488) in green, and algal auto-fluorescence in red. Scale bars 25 µm. B) Confocal images of intracellular B. minutum (SSB01) and E. voratum (SSE01). Colors in merge are nuclei in blue (Hoechst33258), F-actin (detected with phalloidin-Alexa488) in green, and algal auto-fluorescence in red. Scale bars 10 µm. This figure was rearranged from Figure 4 in (Wolfowicz et al., 2016) published under CC-BY 4.0.

Inspection of infected larvae with differential interference contrast (DIC) microscopy revealed that both algae and beads were located, at least in part, within the endodermal tissue (Figure 2.1 B). Quantification of the location of the particles using DIC microscopy revealed that in the case of *B. minutum*, 63 % of algae (1072/1693) were located in the endodermal tissue, while only 33 % of *E. voratum* (65/198) were localized to the endoderm. Interestingly, 49 % of beads (48/98) were located in the endodermal tissue, intermediate between the compatible *B. minutum* and incompatible *E. voratum* (Figure 2.1 C). Confocal microscopy confirmed that *E. voratum* were localized within endodermal cells of *Aiptasia* larvae, just like *B. minutum* (Figure 2.2).

2.2.2 Size selection in the uptake of incompatible *Effrenium voratum*

A notable difference between *B. minutum* and *E. voratum* is the larger size of the latter. Phagocytosis efficiency varies with the size and shape of the phagocytosed particle and is higher for smaller particles (Champion et al., 2008). To test whether lower uptake of *E. voratum* could be the result of particle size, we measured the size of algae located in the gastric cavity (GC) or within the endodermal tissue (EN). Indeed, *E. voratum* in the endodermal tissue were significantly smaller than those in the gastric cavity (8.5 vs. 11 µm, Figure 2.3), while *B. minutum* in the gastric cavity and endodermal tissue were of the same size (Figure 2.3).

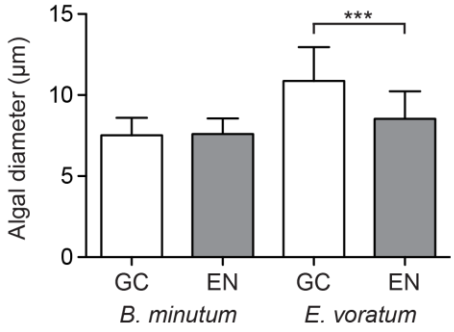

Figure 2.3. Size selection in uptake of E. voratum. B. minutum in the gastric cavity (GC) and endodermal tissue (EN) were of the same size, while E. voratum in the EN were significantly smaller than their counterparts in the GC (8.5 µm vs 11 µm mean diameter; Student's unpaired t-test, p<0.0001). This figure was rearranged from Figure 4 in (Wolfowicz et al., 2016) published under CC-BY 4.0.

2.3 Discussion

The results presented here suggest that selection of symbionts occurs at three stages during symbiont uptake in *Aiptasia* larvae: uptake from the medium into the gastric cavity, during phagocytosis by endodermal cells, and following phagocytosis.

2.3.1 Preferential uptake of compatible algae into the gastric cavity

For the compatible symbiont *B. minutum*, both the proportion of infected larvae, as well as the total number of particles per larva (in the gastric cavity or in the endodermal tissue) was by far the highest. This suggests that there is selection for *B. minutum* in the gastric cavity. Whether this is mediated by the preferential uptake of *B. minutum* into the gastric cavity or elevated retention of symbionts there remains unclear. In either case, it suggests that there is a step in symbiont selection that precedes their phagocytosis. Whether this step is mediated by action of the larvae (e.g. by active seeking of symbionts or preferential retention of symbionts in the gastric cavity) or by the symbionts remains unclear. It is possible that symbionts use phototactic or chemotactic behavior to enter the larval mouth, as has been shown for symbionts infecting juvenile polyps of the coral *A. tenuis* (Aihara et al., 2019; Takeuchi et al., 2017; Yamashita et al., 2014). Another explanation is that larvae could be more likely to meet *B. minutum* than *E. voratum* or beads because of different local densities of the different particles. *B. minutum* and *E. voratum* swim actively, while beads do not and lie on the bottom of the container, which could result in a lower probability of the swimming larvae encountering the beads than the Symbiodiniaceae. Additionally, the swimming behavior might be different between *E. voratum* and *B. minutum*, which could (at least in part) explain differences in numbers of particles in the gastric cavity of the larvae. To test the influence of local densities of the particles on uptake into the gastric cavity, future studies could keep all particles suspended by rotating the container.

2.3.2 Selection during phagocytosis

It has been suggested that symbiosis specificity is in part mediated by interactions between surface markers on the symbionts and pattern recognition receptors (PRRs) on the host cells, which lead to the initiation of phagocytosis, e.g. by lectin-glycan interactions (Bay et al., 2011; Lin et al., 2000; Wood-Charlson et al., 2006). However, the uptake of beads suggests that, as in mammalian phagocytes, phagocytosis does not necessarily require initiation by PRRs and can be induced by mere physical contact (Flannagan et al., 2012). This suggests that PRR interactions do not act as an all-or-nothing switch to regulate uptake of specific algae, but rather as one factor which guides phagocytosis of particles. In fact, different studies have revealed both activating and inhibiting effects of lectin-glycan interactions on phagocytosis of symbionts in different species, suggesting that these interactions could be species specific (Bay et al., 2011; Lin et al., 2000; Wood-Charlson et al., 2006).

Interestingly, *E. voratum* in the endodermal tissue were significantly smaller than those in the gastric cavity. Because phagocytosis efficiency and rate depends on particle size, with higher efficiency for

phagocytosis of smaller particles (Champion et al., 2008), this is likely the result of different rates of phagocytosis for different-sized particles. Indeed, a later study corroborated the role of symbiont size in uptake, and showed that larger beads or species of Symbiodiniaceae are taken up at lower rates than smaller particles (Biquand et al., 2017). This selection against larger particles during phagocytosis could at least partly explain the lower proportion of endodermal *E. voratum* compared to *B. minutum* or the beads.

2.3.3 Post-phagocytic selection of symbionts

Both species of Symbiodiniaceae, as well as beads, were taken up into endodermal cells. The uptake of inert beads and incompatible *E. voratum* suggests that phagocytosis is to some degree unspecific. This implies that further symbiont selection occurs following phagocytosis, e.g. through intracellular sorting, as in the *Hydra-Chlorella* symbiosis (Davy et al., 2012). If this were not the case, pathogens could easily persist and easily infect corals and *Aiptasia* via phagocytosis, leading to detrimental effects.

The proportion of particles in the endodermal tissue was highest for the compatible *B. minutum* (63%), followed by beads (49%) and *E. voratum* (33%). This suggests selection for the compatible *B. minutum*, however, it is unclear by which mechanism this selection is facilitated. If could be the result of either preferential phagocytosis or preferential retention of *B. minutum* by the endodermal cells, or a combination of both. To elucidate this mechanism, a higher temporal resolution would be necessary, for example to study the fate of phagocytosed particles. Since publication of these results (Wolfowicz et al., 2016), a method for live imaging of *Aiptasia* larvae has been developed and used to study the fate of non-symbiotic algae (Jacobovitz et al., 2019). We challenged *Aiptasia* larvae with various non-symbiotic algae, and found that they are phagocytosed, just like *E. voratum*, corroborating our results that phagocytosis is to some degree unspecific (Jacobovitz et al., 2019). Monitoring the fate of phagocytosed *B. minutum* and non-symbiotic algae revealed that symbionts are retained in the host cells and proliferate, while the non-symbiotic algae are eliminated from the host cells by non-lytic expulsion (Jacobovitz et al., 2019). Interestingly, expulsion occurred at different time points for different algae, suggesting that the host response varies with the type of algae (Jacobovitz et al., 2019).

Further investigating the events following phagocytosis, we found that persistence of symbionts appeared to be linked to quickly (≤ 6h) establishing a LAMP1-positive niche in the host cell while incompatible algae failed to do so or did so at a much slower rate, resulting in their expulsion from host cells (Jacobovitz et al., 2019). Further, symbiont persistence was accompanied by a suppression of host immunity, while stimulation of host immunity resulted in the expulsion even of newly taken up compatible *B. minutum* (Jacobovitz et al., 2019). Together, these findings suggest a complex interplay of vesicular trafficking and innate immunity to be involved in symbiosis establishment.

2.3.4 Outlook

The results presented here lay the groundwork for further inquiries about symbiont selection in cnidarian-dinoflagellate symbiosis. They show that selection of suitable symbionts occurs at three steps in symbiosis establishment: 1) the uptake or retention of algae into the gastric cavity, 2) size selection during phagocytosis, and 3) during post-phagocytic processes.

How the overall selection process works and how the individual steps are involved in symbiont selection remains unclear and could be further elucidated using live imaging of larvae. This would allow to assess the retention times of the phagocytosed particles which would make it possible to determine the contributions of each of the steps to the overall selection process. Further it could be used to examine the fate of phagocytosed incompatible algae.

In order to identify the underlying molecular and cellular mechanisms of symbiont selection, hypothesis-generating experiments will be crucial to identify candidate genes involved in the both the initial host-symbiont contact and the maturation of phagosomes into symbiosomes.

3 Nutrient-dependent mTORC1 signaling in cnidarian-dinoflagellate symbiosis

3.1 Exchange of nutrients fuels cnidarian-dinoflagellate symbiosis

The symbiosis between Cnidaria and Symbiodiniaceae revolves around the exchange of nutrients between host and symbiont. Symbionts provide photosynthetically fixed carbon to fuel the host's energy requirements and receive end products of the host's metabolism, in return. These inorganic nutrients are limiting to the growth of photosynthetic organisms in the coral reef environment. Thus, the efficient recycling of nutrients is to the benefit of both host and symbionts and gives both the ability to thrive in their nutrient-poor environment (Muscatine, 1990; Yellowlees et al., 2008). The efficient use of their partner's metabolic products is made possible by the close association of the two with the symbionts living inside the host's cells in symbiosomes.

3.1.1 Importance of symbiont-derived lipids for host nutrition

It remains largely unclear how fixed carbon and inorganic nutrients are exchanged between the host and symbiont (Davy et al., 2012). Symbionts receive nitrogen, in the form of ammonium (NH_4^+) and nitrate (NO_3^-) and phosphorus, mostly in the form of phosphate (PO_4^{3-}) from their host (Davy et al., 2012). Nutrients transferred from the symbiont to the host include carbohydrates, amino acids and lipids (Lewis and Smith, 1971; Peng et al., 2011; Whitehead and Douglas, 2003). While their precise respective proportions remain unclear, there is consensus that lipids constitute the major component of symbiont-derived nutrients (Battey and Patton, 1984; Crossland et al., 1980; Revel et al., 2016). In fact, the formation of lipid droplets in corals depends on the symbionts (Chen et al., 2012; Muscatine et al., 1994) and lipid droplets serve as a source of energy to endure times of low nutrient availability (Stimson, 1987), Additionally, corals also provide their larvae with lipid reserves to fuel early development, like many other marine invertebrates (Marlow and Martindale, 2007).

Among lipids, sterols have emerged as an important nutrient, as both corals and anemones are sterol-auxotroph, and rely on sterols derived from either food or symbionts (Baumgarten et al., 2015; Goad L. J., 1981; Hambleton et al., 2019). Indeed, both *Aiptasia* and Scleractinia have expanded repertoires of sterol-binding NPC2 proteins, likely to be able to use symbiont-derived sterols (Hambleton et al., 2019; Lehnert et al., 2014).

Despite the reliance of hosts on the nutritional input from their symbionts, how symbiont-derived nutrients are integrated into host cell metabolism and functions remains largely unclear. To address this, we performed a series of experiments to characterize the nutritional status of aposymbiotic *Aiptasia* larvae and how it changes upon symbiont acquisition.

3.1.2 mTOR as a master regulator of growth and proliferation in response to nutrient availability

For all organisms, nutrient availability limits their ability to grow and reproduce. Therefore, mechanisms have evolved to regulate growth based on nutrient availability. From yeast to vertebrates, regulation of growth and cell proliferation is coordinated by the conserved protein kinase mTOR, which translates growth signals and nutrient abundance into cellular activity necessary for cell growth and proliferation. When nutrient levels are high, anabolic processes and cell proliferation are activated, and when they are low, catabolic processes such as autophagy are activated to make nutrients available. In animals, this is mediated by two distinct protein complexes, mTOR complex 1 (mTORC1) and mTORC2. mTORC1 is responsible for regulating cell growth and anabolism, while mTORC2 regulates cell survival and proliferation by activating Akt, a key effector of insulin/PI3K signaling (Saxton and Sabatini, 2017). Unfortunately, the molecular mechanisms of mTOR regulation are only known in detail in mammals. Therefore, the following description of mTORC1 regulation is based on mammalian research.

Activation of mTORC1

mTORC1 is active only when both cellular nutrient levels and growth signals allow it. This is achieved by separate regulation of mTORC1 recruitment to the lysosomal surface and activation (Figure 3.1A). Recruitment of mTORC1 depends on nutrient availability, while mTORC1 activation depends on growth signaling (Saxton and Sabatini, 2017). When nutrients are available, the Rag GTPases associated with the Ragulator complex on the lysosomal surface are activated, triggering the assembly of mTORC1 on the lysosomal surface (Sancak et al., 2008, 2010). Sensed nutrients include cytosolic levels of amino acids sensed via Sestrin and CASTOR1 (cytosolic arginine sensor for mTORC1 protein 1) (Chantranupong et al., 2014; Parmigiani et al., 2014; Wolfson et al., 2016). Further, the production of nutrients in catabolic processes is assessed by monitoring lysosomal nutrient levels. Both lysosomal cholesterol and amino acids are sensed by the amino acid transporter SLC38A9 and result in mTORC1 assembly at the lysosome in a H^+-ATPase-dependent manner (Castellano et al., 2017; Rebsamen et al., 2015; Wang et al., 2015).

The assembled mTORC1 is activated by its activator Rheb only when growth signaling via the insulin, Wnt, or TNFα pathways results in the inhibition of its negative regulator TSC (tuberous sclerosis complex) (Saxton and Sabatini, 2017). As a further control of mTORC1 activity, the stress regulator AMPK (AMP-activated protein kinase) is activated in the absence of ATP, which can inhibit mTORC1 directly by phosphorylation of the mTORC1 component Raptor as well as indirectly by activation of TSC (Inoki et al., 2003).

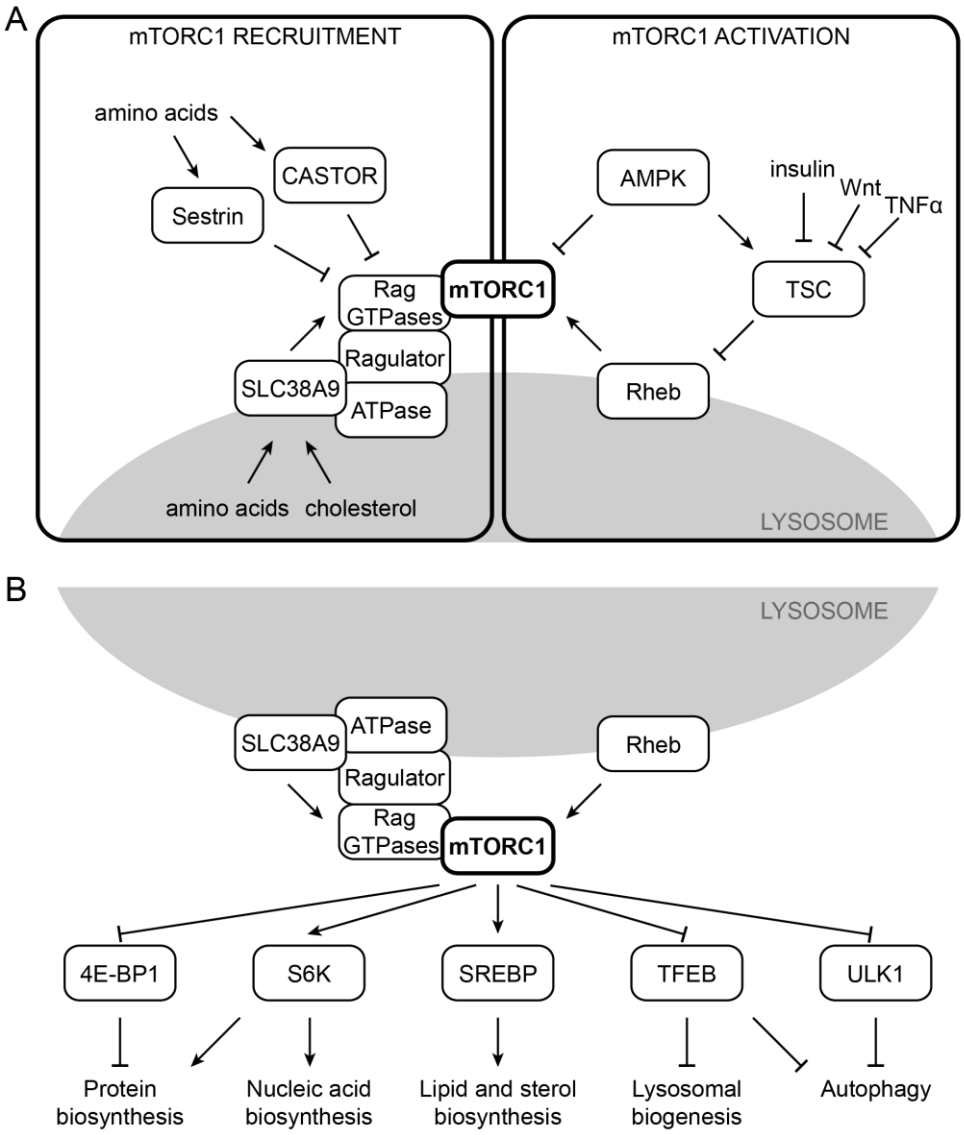

Figure 3.1. Upstream and downstream of mTORC1 in mammals. A) Regulation of mTORC1 requires both nutrient-dependent mTORC1 recruitment to the lysosome and growth signaling-dependent activation. B) Activated mTORC1 stimulates protein, nucleic acid, lipid and sterol biosynthesis while inhibiting lysosomal biogenesis and autophagy.

mTORC1 activation of protein, nucleotide and lipid synthesis

Following recruitment of mTORC1 to the lysosomal surface and its activation by Rheb, mTOR kinase activity results in the switch from catabolic to anabolic activity by altering the activity of several target proteins, thereby promoting protein, nucleotide, and lipid synthesis (Figure 3.1B).

Protein synthesis is promoted by mTORC1 through inhibition of the negative regulator 4-EBP1 as well as phosphorylation of the positive regulator S6 kinase (S6K). S6K further activates the carbamoyl-phosphate synthetase (CAD), a critical component in *de novo* pyrimidine synthesis. Purine synthesis is similarly promoted through increased activity of Atf4 (activating transcription factor 4) (Ben-Sahra

et al., 2016). Lipid synthesis is activated via phosphorylation of SREBP (sterol responsive element binding protein) transcription factors, which regulate the expression of various genes involved in sterol and lipid biosynthesis (Porstmann et al., 2008).

mTORC1-mediated regulation of autophagy

In addition to activation of cellular anabolism, mTORC1 also regulates protein turnover by inhibition of autophagy (Figure 3.1B). In autophagy, autophagic vesicles are formed around misfolded proteins and organelles, which are then degraded following fusion of the vesicles with lysosomes (Kaur and Debnath, 2015). mTORC1 regulates autophagy directly by phosphorylation and inhibition of ULK1, which initiates autophagic vesicle formation (Ganley et al., 2009).

Additionally, mTORC1 controls autophagy at the transcriptional level via inhibition of the transcription factor EB (TFEB) (Perera and Zoncu, 2016). TFEB promotes expression of the CLEAR network (Coordinated Lysosomal Expression And Regulation), a gene regulatory network of autophagy and lysosomal biogenesis by binding to E-box motifs (CANNTG) in the promoters of CLEAR genes (Bouché et al., 2016; Sardiello, 2016). TFEB is itself a CLEAR network gene, promoting its own expression in an auto-regulatory feedback loop via an E-box motif in its own promoter (Sardiello et al., 2009; Settembre et al., 2013). Phosphorylation of TFEB by mTORC1 results in cytosolic retention, and thus inhibition of CLEAR network expression (Martina et al., 2012; Roczniak-Ferguson et al., 2012; Settembre et al., 2012).

3.1.3 Need for cellular resolution in analyses of the cellular mechanisms of symbiosis

In order to understand how the cellular functions of host and symbiont are integrated to allow for coordination of their metabolisms, we studied the role of symbiont-derived nutrients in symbiont establishment after phagocytosis of symbionts, by performing a transcriptome experiment. Previous gene expression experiments have compared gene expression of aposymbiotic and symbiotic whole anemones or corals (Lehnert et al., 2014; Matthews et al., 2017; Mohamed et al., 2016; Wolfowicz et al., 2016; Yuyama et al., 2018). While this approach has significantly improved our understanding of cnidarian-dinoflagellate symbiosis in general, it has limited capacity to identify the processes that occur at the cellular level, a prerequisite to understanding the underlying mechanism of the interactions between the dinoflagellate symbionts and their host cells. Whole-organism transcriptomes cannot identify the source of differences in gene expression, and unfortunately often attribute observed changes to the symbiotic cells, while they could have occurred in other cells of the organism. Further, using whole-organism transcriptome approaches it is particularly difficult to identify the responses to symbiosis in circumstances when comparatively few cells are symbiotic, like e.g. during symbiosis establishment. Here, any signal from the few symbiotic cells is “diluted” by that from the more abundant non-symbiotic cells.

To circumvent these issues, we aimed to perform a transcriptome study that compared the gene expression in symbiotic cells to that in non-symbiotic cells. Planula larvae are comprised of relatively few cell types, making them a good model for such an approach. They consist of only four differentiated broader cell types: epitheliomuscular cells, cnidocytes (stinging cells), gland cells, and nerve cells; additionally, they have stem cells (Frank and Bleakney, 1976; Sebé-Pedrós et al., 2018; Siebert et al., 2019). The cnidocytes only occur in the ectodermal tissue, making the endodermal tissue comprised of only 3 differentiated cell types, of which the epitheliomuscular cells, which take up the symbionts, are the predominant one (Plickert et al., 1988). Thus, in this study we sought to develop a protocol to isolate symbiotic epitheliomuscular cells as well as non-symbiotic cells for comparison of their transcriptional profiles.

3.2 Results

3.2.1 Aposymbiotic larvae quickly deplete maternally-deposited nutrients

Corals store large amounts of lipids to endure times of low nutrient availability (Stimson, 1987), and also provide their larvae with lipid reserves to fuel early development, just like other marine invertebrates (Marlow and Martindale, 2007). To be aware of possible interference of nutrient-signaling from maternally-deposited nutrients with that of symbiont-derived nutrients, we first assessed the nutritional state of aposymbiotic *Aiptasia* larvae.

Aposymbiotic larvae 2 dpf had large amounts of lipids, especially in the endodermal tissue (Figure 3.2 A, left panels). By 6dpf, stored lipids were mostly used and by 10 dpf, they were effectively depleted (Figure 3.2 A). We then measured cell proliferation in larvae as a proxy for the presence of other nutrients (e.g. carbohydrates) which could fuel larval metabolism (Figure 3.2B). Cell proliferation dropped from occurring in 44% of cells 1 dpf to less than 10 % of cells 3dpf and then stayed below 4 % from 6 – 9 dpf in aposymbiotic larvae (Figure 3.2 C). This is in line with the development of *Aiptasia* larvae. Larvae are fully formed including the oral opening by 48 hpf (Bucher et al., 2016). This suggests that *Aiptasia* larvae deplete maternally-provided nutrients in early development and depend on an alternative energy source for survival and metamorphosis into polyps.

Together, these results suggest that lipid stores and other energy sources are depleted by 6 dpf, making larvae of this age or older suitable to study the effects of symbiont derived nutrients with minimal interference from stored nutrients.

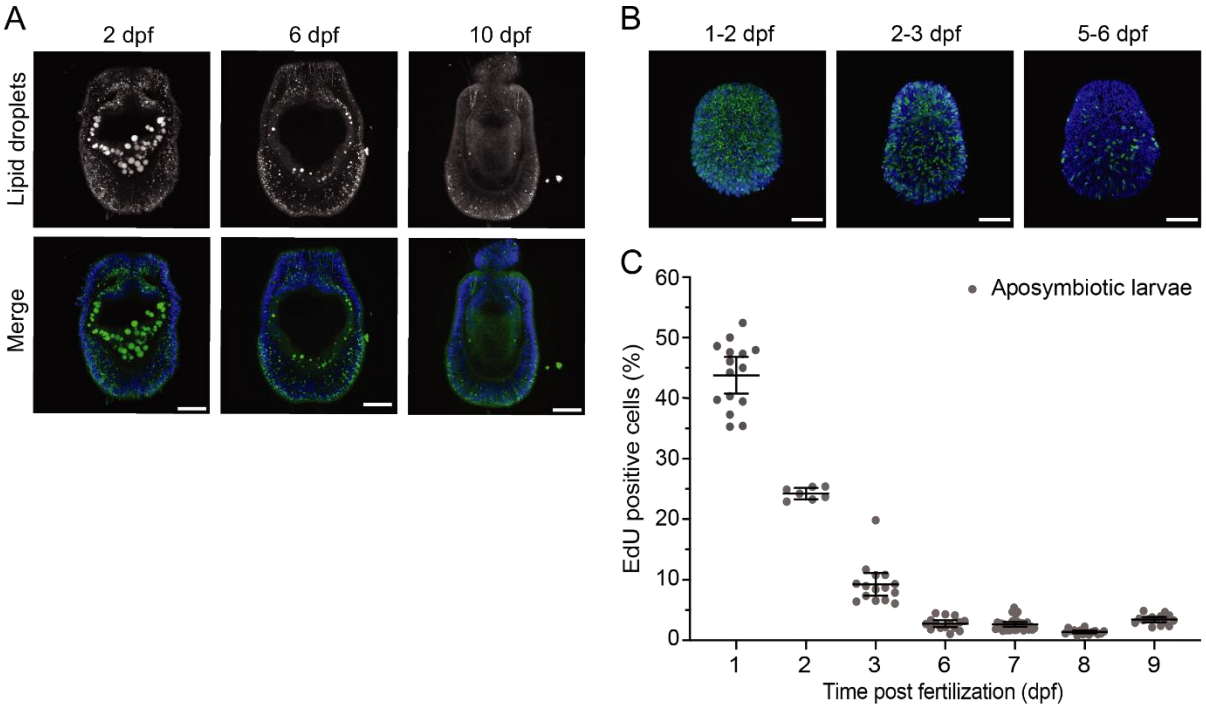

Figure 3.2: Depletion of maternally-provided nutrients in aposymbiotic larvae. A) Representative confocal images of lipid content in Aiptasia larvae 2, 6, and 10 dpf. Images are maximum projections of 30 µm thick larval mid-sections. Colors in merge are: nuclei in blue (Hoechst33258) and lipid droplets in green (Nile Red). Scale bar 25 µm. B) Representative images (maximum projections of whole larvae) of EdU incorporation in Aiptasia larvae used for analysis in C. Colors in merge are: nuclei in blue (Hoechst33258) and nuclei of proliferating cells in green (EdU). Scale bars 25 µm. C) Proportion of proliferating cells in aposymbiotic larvae, measured by EdU incorporation in the previous 18 h (1dpf) or 24 h (2-9 dpf). Each data point represents one larvae (n = 9 – 13). This figure was reproduced from Figure 1 A-C in (Voss et al., 2019) published under CC-BY-NC-ND 4.0.

3.2.2 Symbiosis establishment results in increased lipid stores and cell proliferation

Symbiodiniaceae provide corals with the majority of their nutrients and the formation of lipid droplets in corals depends on the symbionts (Chen et al., 2012; Muscatine et al., 1994). To characterize how quickly after symbiosis establishment symbionts transfer nutrients to their host, we compared the lipid stores of symbiotic and aposymbiotic *Aiptasia* larvae of the same age (Figure 3.3 A and B). Lipid stores were significantly increased in symbiotic larvae 2 and 8 dpi compared to aposymbiotic larvae, suggesting that symbionts transfer lipids quickly after uptake (Figure 3.3 B). In line with this, symbiont uptake resulted in significantly increased cell proliferation in symbiotic larvae (adjusted p-value < 0.001) compared to aposymbiotic larvae of the same age 3 days after symbiont uptake (Figure 3.3 C). Together, this suggest that symbiont-derived nutrients are transferred to the host early after symbiosis establishment, leading to an improved nutritional status in symbiotic larvae. This is in line with a previous study in the coral *Pocillopora damicornis*, which found that symbionts transfer nutrients early after symbiosis establishment, albeit at lower rates than in older larvae or polyps (Kopp

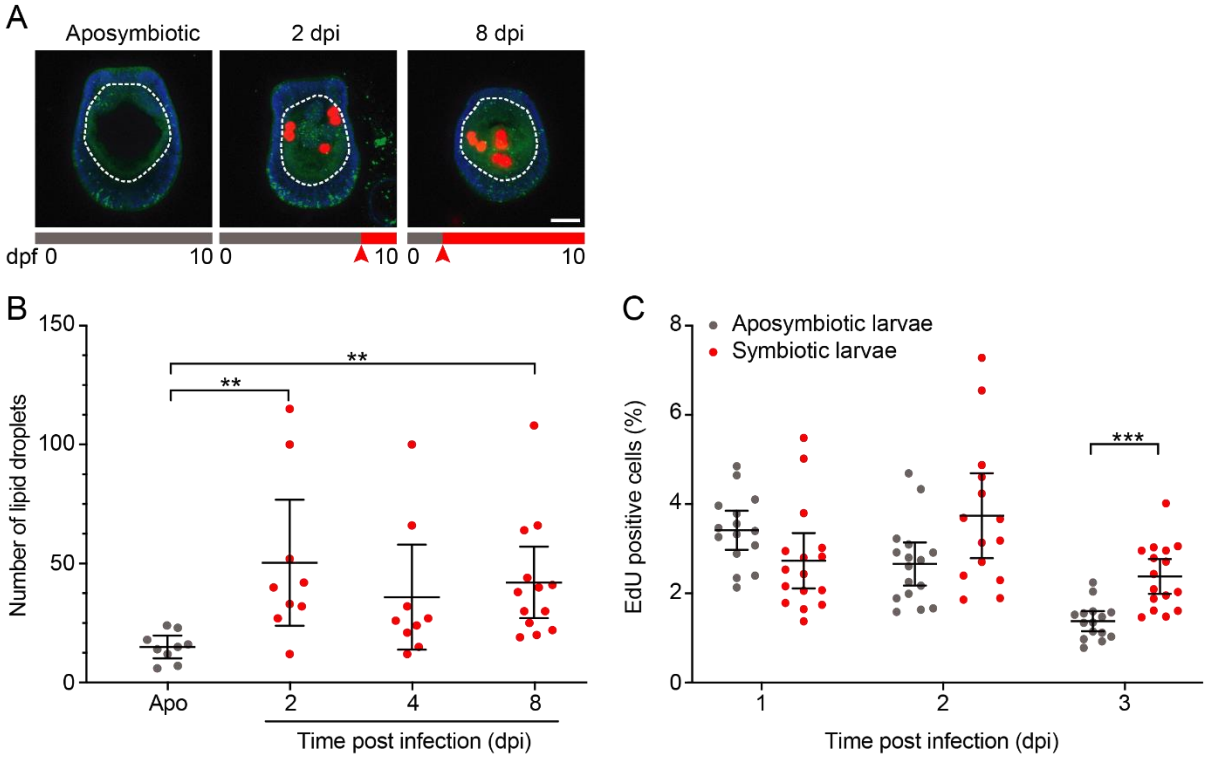

Figure 3.3. Symbiosis establishment improves nutritional status of Aiptasia larvae. A) Representative confocal images of aposymbiotic and symbiotic Aiptasia larvae 2 and 8 dpi, used in B). Colors in merge are nuclei in blue (Hoechst33258), lipid droplets in green (Nile Red), and symbionts in red (symbiont autofluorescence). Dashed lines outline the endodermal tissue. Scale bar 25 µm. B) Lipid droplets in the endodermal tissue of aposymbiotic (gray) and symbiotic (red) larvae 2, 4, and 8 dpi. Each data point represents one larva (n = 9 – 13). Error bars represent mean and 95% confidence interval. For ImageJ macros used for quantification, see Source Code 5.1 and Source Code 5.2. C) Cell proliferation in aposymbiotic (gray) vs. symbiotic (red) larvae 1, 2, and 3 dpi. Each data point represents one larvae (n = 15 – 16). Error bars represent mean and 95% confidence interval. This figure was reproduced from Figure 1 D-F in (Voss et al., 2019) published under CC-BY-NC-ND 4.0.

et al., 2016). These results show that symbiotic *Aiptasia* larvae are a suitable model to study how symbiont-derived nutrients are sensed and affect host metabolism and physiology at the cellular and molecular levels.

3.2.3 Development of a method to isolate symbiotic and aposymbiotic endodermal cells

To identify the changes in gene expression which occur upon uptake of symbionts, I developed a protocol to isolate symbiotic and aposymbiotic endodermal cells from *Aiptasia* larvae (Figure 3.4 A and B). The dissociation procedure consists of two steps. First, larvae are incubated in a mixture of sodium thio glycolate, which reduces disulfide bonds in extracellular matrix proteins, and Pronase, a mixture of peptidases, to cleave extracellular matrix proteins to facilitate cell dissociation. This leads to the selective removal of ectodermal tissue from the larvae, while the endodermal tissue remains intact within a transparent membrane, likely the mesoglea (Figure 3.4 A and B). In a second step, the washed

endodermal tissue was mechanically dissociated by pressing it on a cover slip, resulting in a mixture of single endodermal cells and clumps of few cells. From this endodermal cell suspension, symbiotic and aposymbiotic endodermal cells can be isolated using micropipetting with especially produced microcapillary needles that had a diameter slightly larger than the symbiotic endodermal cells, ~10 µm.

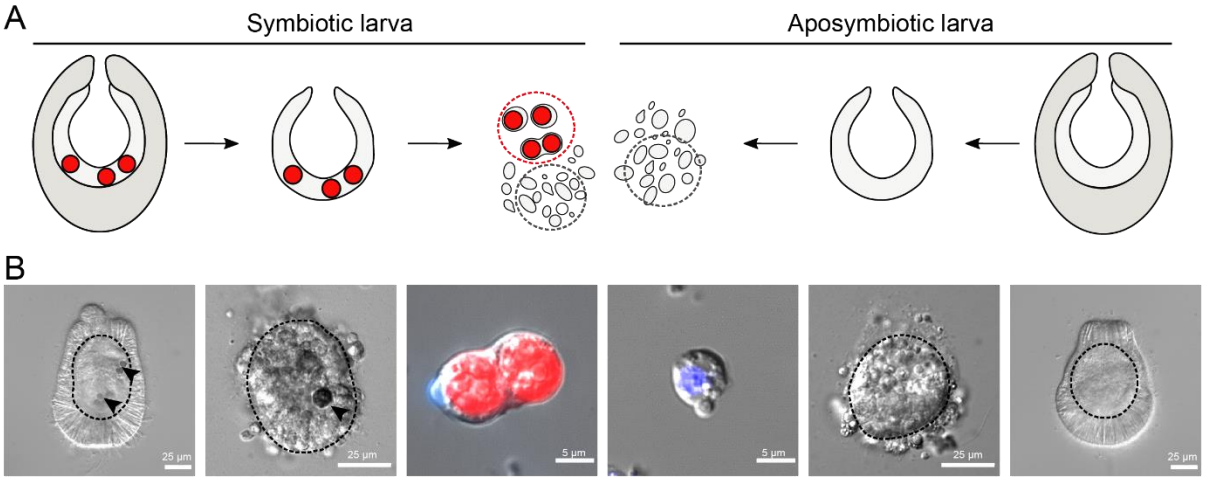

Figure 3.4: Isolation of symbiotic and aposymbiotic endodermal cells from Aiptasia larvae. A) Schematic of the cell isolation procedure. Following dissociation with Pronase, endodermal was macerated to obtain dissociated cells. Pools of either symbiotic (red circle) or aposymbiotic (gray circles) were collected for RNAseq experiment. B) Representative images of the steps displayed in A). Colors in merge are nuclei in blue (Hoechst33258) and symbionts in red (symbiont autofluorescence). This figure was reproduced from Figure 2 A and B in (Voss et al., 2019) published under CC-BY-NC-ND 4.0.

3.2.4 Transcriptional response to symbiont uptake is mostly restricted to symbiotic cells

Larvae 6 or 7 dpf that had been infected with symbionts for 24 or 48 h, as well as aposymbiotic larvae of the same age as a control were dissociated with the developed method for cell isolation. Pools of 7 to 20 either symbiotic or aposymbiotic endodermal cells (Figure 3.4 B, center panels) were collected by micropipetting and directly lysed before snap-freezing in liquid nitrogen. Samples were prepared for RNA-sequencing using the SmartSeq2 method, which allows sequencing of full-length transcripts from only picograms of RNA (Picelli et al., 2014).

Sequenced reads were mapped to the *Aiptasia* genome to filter out transcripts derived from the symbionts or contaminating RNA from e.g. bacteria in the medium. Filtered reads were then mapped to the *Aiptasia* transcriptome (GCA_001417965.1) to quantify gene expression.

Overall mapping rates of transcripts from aposymbiotic cells (56.9 - 71.7%) were high (Supplemental Table 5.1). Mapping rates for symbiotic cells were lower and more variable than in aposymbiotic cells (4.6 – 44%), likely due to the presence of symbiont transcripts. This was partially compensated by

deeper sequencing of symbiotic cells (24 – 54 M reads vs. 11 – 28 M reads). Variability of mapping rates in symbiotic cells likely stemmed from differences in the lysis efficiency of symbionts.

Principal component analysis comparing the expression of all genes showed differences in gene expression between symbiotic (red) and aposymbiotic (gray) cells, indicating that gene expression is drastically altered following uptake of symbionts (Figure 3.5). However, whether aposymbiotic cells originated from symbiotic (+) or aposymbiotic (x) larvae was indistinguishable in principal components 1 and 2. This suggests that at 24 - 48 hpi, differences in gene expression due to symbiont presence are mostly restricted to symbiotic cells, while gene expression in aposymbiotic endodermal cells of the same larvae remains largely unchanged. This underlines the importance of a cell-type-specific approach to identify differences in gene expression resulting from symbiont uptake, especially to identify where these changes occur – in the symbiotic cells or in other cells of the organism. As symbiotic cells are only a small proportion of the entire larva, the restriction of gene expression changes to symbiotic cells we observe here could also explain why previous studies comparing gene expression in symbiotic and aposymbiotic larvae only find minor differences shortly after symbiont uptake (Mohamed et al., 2016; Wolfowicz et al., 2016).

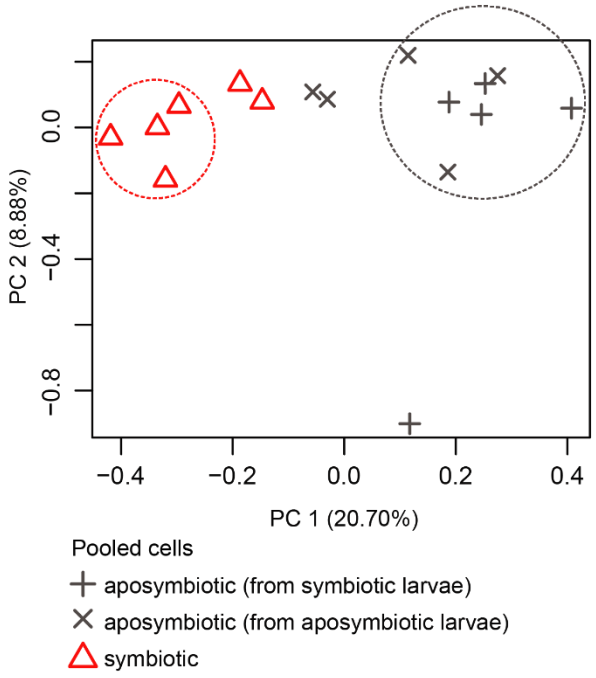

Figure 3.5: Principle component analysis of gene expression in host cells in all replicates. Circled replicates were used for differential gene expression analysis. For total read counts and mapping statistics of individual replicates, see Supplemental Table 5.1. This figure was reproduced from Figure 2C in (Voss et al., 2019) published under CC-BY-NC-ND 4.0.

3.2.5 Down regulation of gene expression in symbiotic cells

To identify the most drastic changes in gene expression upon symbiont uptake, we compared gene expression of the samples with the largest differences in Principle component analysis (Figure 3.5 , red and gray circles). Using DESeq2 (log2-fold change > 2; false-discovery-rate < 0.01), we found 4,456 differentially expressed genes (DEGs), with the majority (>99%) down regulated in the symbiotic cells (4,421/4,456), and only 35 genes upregulated in the symbiotic cells (Figure 3.6 and Supplemental File 5.5).

A higher proportion of down-regulated genes in the symbiotic condition has been reported in previous studies (Matthews et al., 2017; Mohamed et al., 2016; Wolfowicz et al., 2016), albeit to a lesser extent than in our data set. We hypothesize that it could be detected due to the improved signal-to-noise ratio of our approach over the previous whole-organism approaches.

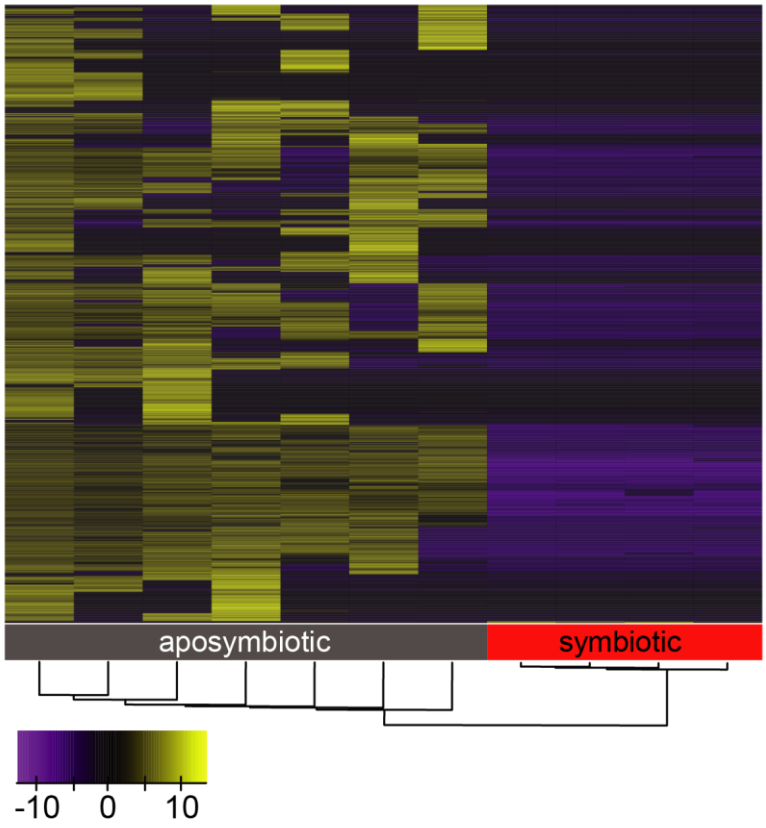

Figure 3.6. Heat map of differentially expressed genes (DEGs) between symbiotic and non-symbiotic cells. 4,456 out of 27,334 genes were differentially expressed; 4,421 genes were down-regulated in the symbiotic condition and 35 genes were up-regulated (log2-fold change > 2; false-discovery-rate < 0.01). For a complete list of differentially expressed genes, see Supplemental File 5.4. For results of KEGG enrichment analysis, see Table 3.1 and Supplemental File 5.5. For a schematic summarizing gene expression of core metabolic pathways, see Supplemental Figure 5.1. This figure was reproduced from Figure 2D in (Voss et al., 2019) published under CC-BY-NC-ND 4.0.

3.2.6 Host cell metabolism and autophagy are down regulated upon symbiosis uptake.

In order to interpret the DEGs in the context of the biological processes occurring in the cells, we performed KEGG pathway enrichment analysis. This revealed that several pathways in the categories Metabolism, Cellular Processes, Genetic Information Processing, and Environmental Information Processing were significantly enriched among the down-regulated genes in symbiotic cells (Table 3.1, Supplemental File 5.5).

Table 3.1. Overview of enriched KEGG pathways among the down-regulated DEGs in symbiotic cells (p-value ≤ 0.15). For a complete list of DEGs in each KEGG pathway, see Supplemental File 5.5. This table was reproduced from Table 1 in (Voss et al., 2019) published under CC-BY-NC-ND 4.0.

Pathway	KEGG Pathway ID
Metabolism	
Synthesis and degradation of ketone bodies	[PATH:ko00072]
Terpenoid backbone biosynthesis	[PATH:ko00900]
Arginine biosynthesis	[PATH:ko00220]
Starch and sucrose metabolism	[PATH:ko00500]
Galactose metabolism	[PATH:ko00052]
N−Glycan biosynthesis	[PATH:ko00510]
Fructose and mannose metabolism	[PATH:ko00051]
Pyrimidine metabolism	[PATH:ko00240]
Glycosylphosphatidylinositol (GPI)−anchor biosynthesis	[PATH:ko00563]
Cellular Processes	
Autophagy - yeast	[PATH:ko04138]
Peroxisome	[PATH:ko04146]
Endocytosis	[PATH:ko04144]
Genetic Information Processing	
Basal transcription factors	[PATH:ko03022]
RNA polymerase	[PATH:ko03020]
RNA degradation	[PATH:ko03018]
Protein export	[PATH:ko03060]
RNA transport	[PATH:ko03013]
Non−homologous end−joining	[PATH:ko03450]
Spliceosome	[PATH:ko03040]
Ribosome biogenesis in eukaryotes	[PATH:ko03008]
Environmental Information Processing	
Phosphatidylinositol signaling system	[PATH:ko04070]

In the category Genetic Information Processing, several pathways related to transcription and protein translation were enriched, suggesting a general down regulation of these processes in symbiotic cells. In the category Cellular Processes, the pathways endocytosis and autophagy were enriched. Symbiont uptake occurs via phagocytosis (Schwarz et al., 1999). In mammalian phagocytic cells (e.g. macrophages), following engulfment and uptake into the cell, nascent phagosomes fuse with endosomal vesicles, first with early and then with late endosomes, before eventually fusing with lysosomes to form phagolysosomes, in which the phagocytosed particle is digested. It has been hypothesized that phagosomal maturation is arrested after fusion of the phagosome with early endosomes in cnidarian-dinoflagellate symbiosis, for symbionts to avoid digestion (Chen et al., 2004; Mohamed et al., 2016). In line with this hypothesis, gene expression of several genes associated with late endosomes are down regulated in symbiotic cells. However, also many early endosomal genes are down regulated, making it difficult to draw conclusions regarding the arrest of phagosomal maturation based on the gene expression data in this study.

In the autophagy pathway, > 20% of DEGs (17/83) are down regulated in symbiotic cells, including the key players ATG2, ATG4, ATG9, ATG13, ATG18, HIF1α, TSC1, PKCδ and RagC/D. Additionally, genes of the endocytosis pathway are down regulated in symbiotic cells (Supplemental File 5.5). Based on this, together with our finding that maternal nutrients are depleted in aposymbiotic larvae 6 dpf, we hypothesized that aposymbiotic larvae meet their energy requirements with autophagy. Upon uptake of symbionts, autophagy is then shut down, as symbiont-derived nutrients become available to the host cell.

In line with this hypothesis, various catabolic pathways (i.e. pathways involved in the degradation of energy-rich compounds) including autophagy, peroxisomes, and metabolic pathways such as starch and sucrose metabolism are suppressed in symbiotic cells (Table 3.1). A detailed analysis of core metabolic pathways shows the down regulation of key enzymes in the pathways glycolysis/gluconeogenesis, fatty acid biosynthesis and degradation, as well as oxidative phosphorylation, and the TCA cycle, most of which are catabolic pathways (Supplemental Figure 5.1). Indeed, the expression of several genes encoding some of the key enzymes in these pathways was below the detection limit, indicating drastic down regulation of primary metabolic pathways shortly after symbiont uptake.

These results support that aposymbiotic larvae engage in autophagy and other catabolic processes to maintain cellular functions, including gene expression and protein synthesis, as well as cell proliferation. Upon uptake of symbionts, however, cellular metabolism is altered, possibly due to the availability of symbiont-derived nutrients.

3.2.7 Regulation of autophagy by MITF-like transcription factors is evolutionarily conserved.

How cells maintain a balance between autophagy and other catabolic processes and anabolism is well understood in mammals, and depends on the nutritional state of the cell (Perera and Zoncu, 2016). It is transcriptionally regulated in the CLEAR network (Coordinated Lysosomal Expression And Regulation). The CLEAR network is transcriptionally activated when cellular nutrient levels are low, and leads to autophagy, the consumption of cellular components, to maintain cellular homeostasis (Settembre et al., 2011). The CLEAR network is under the control of transcription factor EB (TFEB), which activates gene expression of CLEAR network genes by binding to E-box motifs (CANNTG) in their promoters (Bouché et al., 2016; Sardiello, 2016). TFEB is itself a CLEAR network gene, regulating its own expression in an auto-regulatory feedback loop via an E-box motif in its own promoter (Sardiello et al., 2009; Settembre et al., 2013).

TFEB belongs to the MITF family of transcription factors, which expanded from one homolog in invertebrate Bilateria to four homologs in vertebrates, one of which is TFEB (Bouché et al., 2016; Sardiello, 2016). The single MITF-family proteins in *Drosophila melanogaster* and in *Caenorhabditis elegans* both regulate expression of autophagy and lysosome related genes via E-box motif binding (Bouché et al., 2016; Lapierre et al., 2013; O'Rourke and Ruvkun, 2013; Settembre et al., 2013), suggesting that this is the ancestral function of MITF-family transcription factors. The function of MITF-family transcription factors in non-bilaterian animals, however, is unknown.

To see whether autophagy could be regulated in a similar manner in Cnidaria, we conducted a phylogenetic analysis of MITF-family transcription factors in vertebrate and invertebrate animals, including Cnidaria. The resulting phylogeny recapitulates the expansion of the MITF-family in vertebrates from one invertebrate ancestor that was already present in Cnidaria (Figure 3.7A). This suggests that the coordinated regulation of autophagy in a CLEAR-like network is the ancestral function of MITF-like genes in invertebrates including Cnidaria.

In line with MITF-like regulating the expression of CLEAR-network genes, for 16 out of 17 homologs of mammalian CLEAR network genes, including MITF-like itself, E-box motifs were significantly enriched in their promoter regions (Figure 3.7 B and C). Additionally, 12 out of 17 of these genes were significantly down regulated in symbiotic cells (Figure 3.7 B). Together, these results indicate that the regulation of autophagy via a CLEAR network in response to nutrient availability is conserved in *Aiptasia* and could be the mechanism by which autophagy is down regulated upon symbiont uptake.

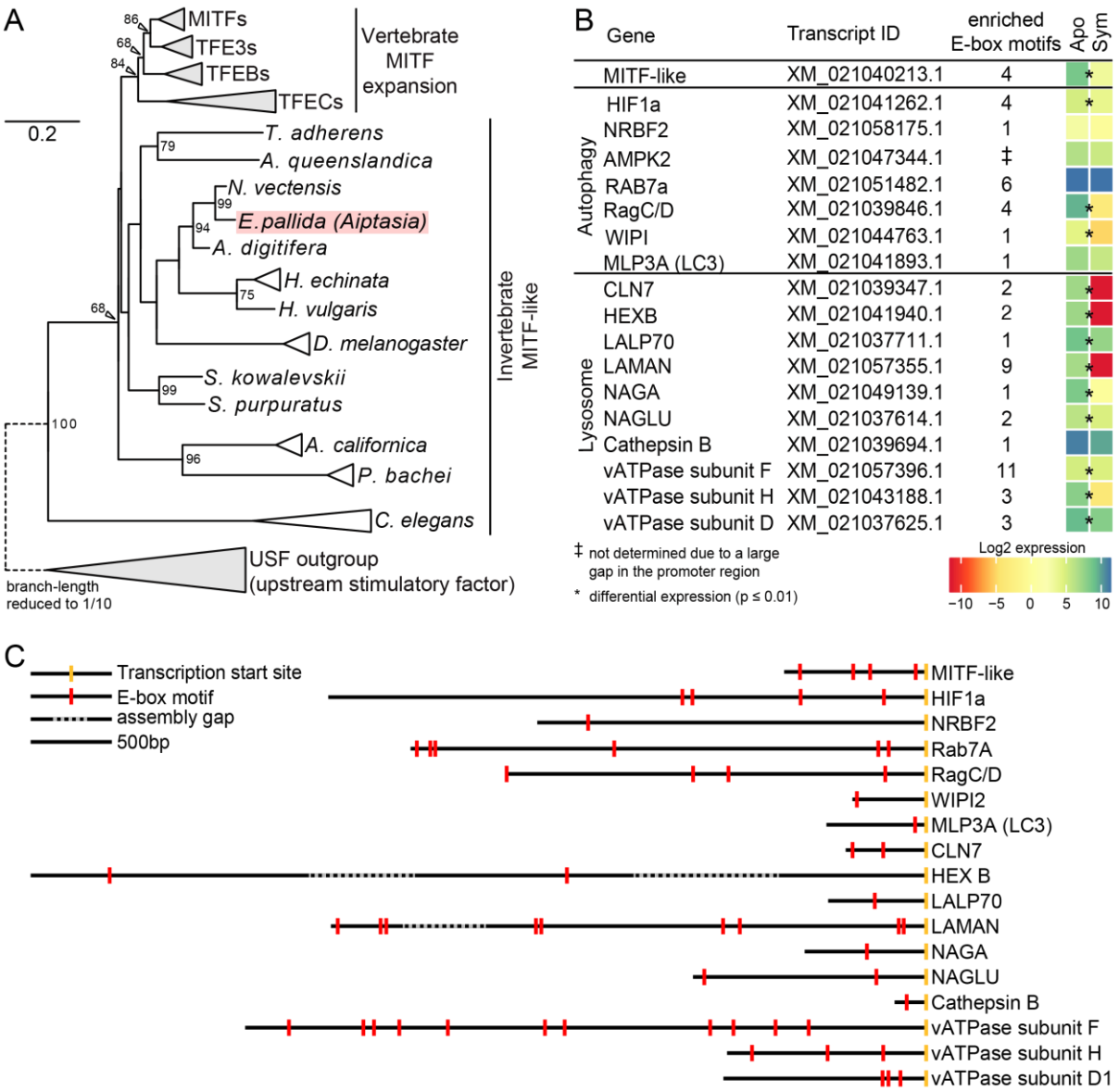

Figure 3.7: Conservation of transcriptional regulation of autophagy. A) Maximum Likelihood phylogeny (PhyML) of MITF-family transcription factors in vertebrates and invertebrates. Bootstrap values ≥50 are indicated next to nodes. Upstream stimulatory factors were used as an outgroup. Species names are italized; triangles represent collapsed branches; position of Aiptasia MITF-like is highlighted in red. For raw sequences, trimmed alignments and tree information see Supplemental File 5.6. B) Overview of gene expression of Aiptasia homologs of mammalian TFEB target genes including number of significantly enriched E-box elements in their promoter regions. Significantly differentially expressed genes (log2-fold change >2; false-discovery-rate < 0.01) indicated by asterisks (*). C) Visualization of positions of significantly enriched E-box motifs in the promoters of CLEAR network homologs in Aiptasia. Figure 3.7 A was reproduced from Figure 3A in (Voss et al., 2019) published under CC-BY-NC-ND 4.0. Figure 3.7 B was adapted from Figure BA in (Voss et al., 2019) published under CC-BY-NC-ND 4.0 with friendly permission by the authors.

3.2.8 Conservation of MITF-like phosphorylation sites

In mammals, the activity of TFEB is regulated via post-translational modification by the master growth regulator mTOR. When nutrients are available, mTOR kinase activity leads to the phosphorylation of TFEB at conserved binding sites (Martina et al., 2012; Roczniak-Ferguson et al., 2012; Settembre et al., 2012). This phosphorylation results in the cytosolic retention of TFEB, inhibiting its function as a transcriptional activator of the CLEAR network. Conversely, under starvation conditions (in the absence of mTOR activity) TFEB is dephosphorylated by calcineurin (activated by lysosomal calcium release) resulting in a positive feedback loop of TFEB expression and expression of CLEAR network genes (Napolitano et al., 2018).

Alignment of *Aiptasia* MITF-like with *H. sapiens* TFEB reveals the conservation of the mTOR phosphorylation sites at S142 and S211, further suggesting conservation of the regulation of autophagy in *Aiptasia* by MITF-like (Figure 3.8).

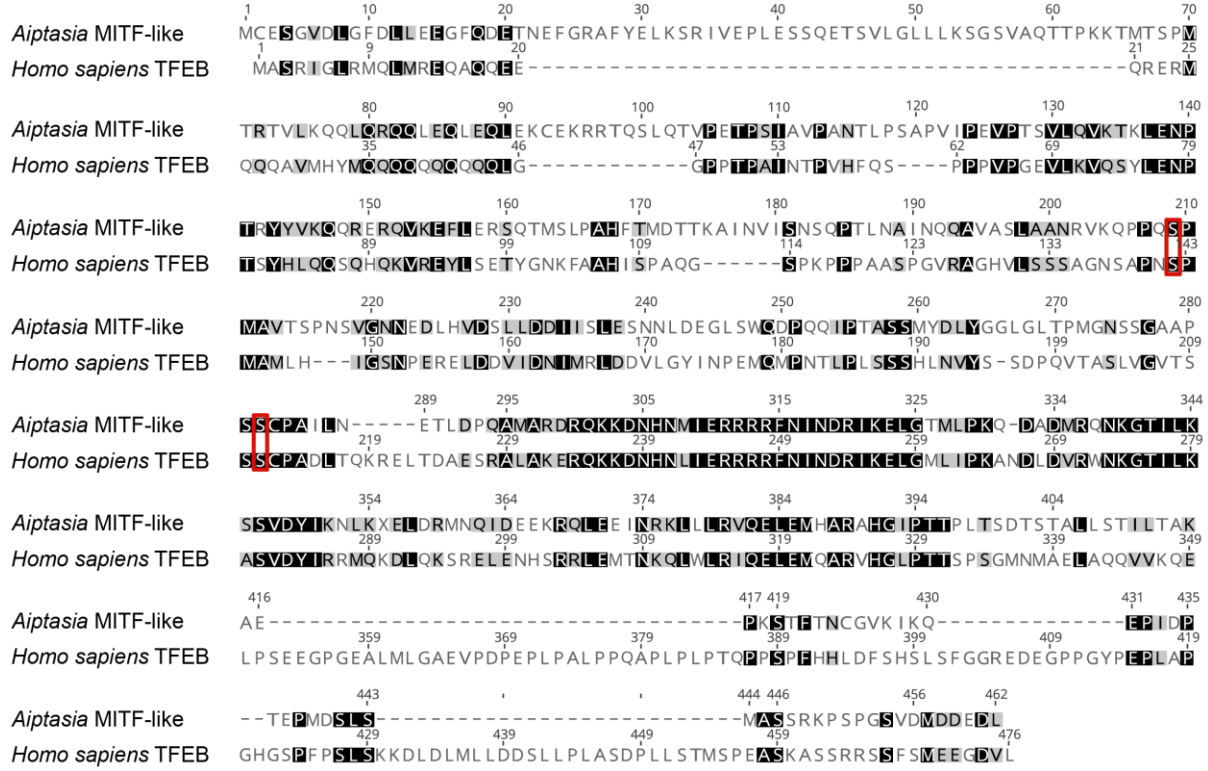

Figure 3.8. Alignment of amino acid sequences of Aiptasia MITF-like (XM_020895872.1) with H. sapiens TFEB (P19484). Conserved mTOR-specific phosphorylation sites framed in red. This figure was reproduced from Figure S2A in (Voss et al., 2019) published under CC-BY-NC-ND 4.0.

3.2.9 Symbiosis activates mTORC1 signaling.

When nutrients are available, mTOR kinase is activated in the mTOR complex 1 (mTORC1). Homologs of all major mTORC1 components, including mTOR, raptor, deptor, mLST8, and Rheb, with the

exception of PRAS40, are encoded in the *Aiptasia* genome (Kanehisa and Goto, 2000) and not differentially expressed between symbiotic and aposymbiotic cells (Supplemental File 5.4). Similarly, various effector proteins of mTORC1, including eukaryotic translation initiation factor 4E (eIF4E)-binding protein 1 (4E-BP1) and ribosomal protein S6, are encoded in the *Aiptasia* genome (Kanehisa and Goto, 2000) and not differentially expressed between symbiotic and aposymbiotic cells (Supplemental File 5.4).

To test whether mTORC1 signaling is conserved in *Aiptasia*, we tested the effect of mTOR inhibition on mTORC1-specific phosphorylation of the mTOR targets 4E-BP1 and S6. For both proteins, levels of phosphorylated protein in *Aiptasia* polyps decreased with increasing concentrations of the mTOR kinase inhibitor AZD8055 (AZD) (Figure 3.9). This indicates that mammalian mTOR-specific phospho-sites are conserved in the *Aiptasia* homologs of both 4E-BP1 and S6.

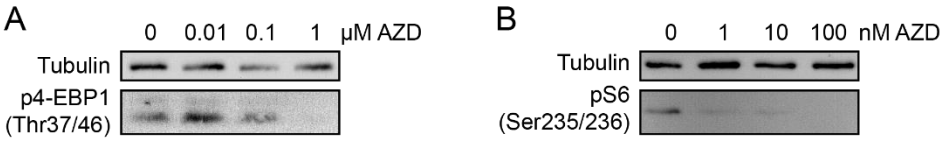

Figure 3.9. Conservation of mTOR signaling in Aiptasia. A) Decreasing levels of p4E-BP1 with increasing concentration of mTOR kinase inhibitor AZD. B) Decreasing levels of pS6 with increasing concentration of mTOR kinase inhibitor AZD.

We then tested whether mTOR kinase is active in symbiotic *Aiptasia* by Western blot using the antibody against phosphorylated 4E-BP1 (p4E-BP1). We find that symbiotic starved polyps have similar levels of p4-EBP1 as aposymbiotic and symbiotic polyps which had been fed 1 day prior, while starved aposymbiotic polyps have low levels of p4-EBP1 (Figure 3.10 A). This indicates that symbiont-derived nutrients can activate mTORC1 signaling in the same way as food-derived nutrients. However, mTORC1 activation in the presence of symbionts is continuous, while mTORC1 activation from feeding is lost 3 days after feeding in aposymbiotic animals (Figure 3.10 A, right panels).

No differences in mTORC1 activation could be detected when comparing symbiotic and aposymbiotic larvae, likely due to the low proportion of symbionts per larva in the larval stage (Supplemental Figure 5.2).

Consistent with mTORC1 activation promoting anabolic processes (Perera and Zoncu, 2016), lipid droplet formation was elevated in starved symbiotic polyps compared to starved aposymbiotic polyps (Figure 3.10 B). Corroborating the Western Blot results that feeding only has a temporary effect on mTORC1 activation, fed aposymbiotic polyps had less lipids than starved symbiotic animals, albeit more than starved aposymbiotic animals (Figure 3.10 B). The highest levels of lipids were detected in fed symbiotic animals, in line with previous work showing the positive effect of symbiosis on growth and asexual reproduction under starvation conditions in polyps of *Aiptasia* (Clayton and Lasker, 1985).

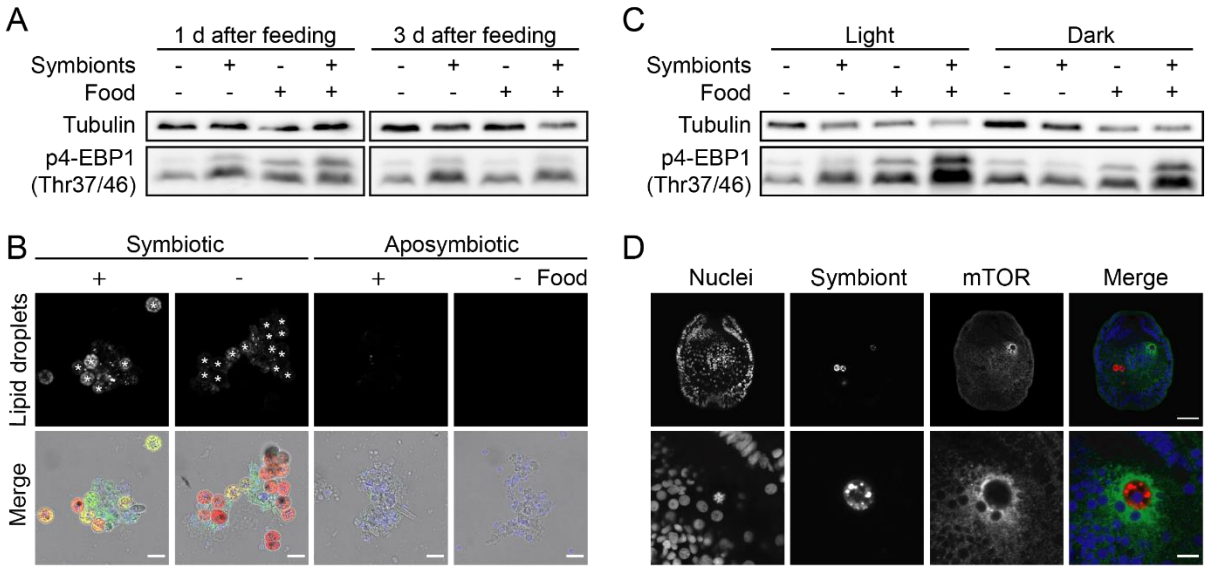

Figure 3.10. Symbiont-derived nutrients activate mTOR signaling. A) Representative Western Blots comparing p4-EBP1 levels in aposymbiotic and symbiotic Aiptasia polyps. Anemones were either fed (3 times per week for > 3weeks) or starved (for ≥ 3 weeks). B) Representative confocal images of lipid content of cells from starved (for 9 days) and fed (3 times per week for 10 days), symbiotic and aposymbiotic Aiptasia polyps. Colors in merge are nuclei in blue (Hoechst33258), lipid droplets in green (Nile Red), and symbionts in red (symbiont autofluorescence). Scale bar 25 µm. Asterisks (*) indicate interference of symbiont autofluorescence. C) Representative Western Blots comparing p4-EBP1 levels in fed (3 times per week for ≥13 days) and starved (for 13 days) aposymbiotic and symbiotic Aiptasia polyps under normal light conditions (12L:12D, sampled 6h into the light period) or darkness (66h prior to experiment) to block photosynthesis. D) Representative confocal microscopy images of mTOR localization in Aiptasia larvae. Colors in merge are nuclei in blue (Hoechst33258), mTOR (detected with Alexa488-anti-rabbit-IgG) in green, and symbiont in red (symbiont autofluorescence. Scale bars 25 µm (upper panel) and 5 µm (lower panel). Figure 3.10 A and D were reproduced from Figures 3C and 3E, respectively in (Voss et al., 2019) published under CC-BY-NC-ND 4.0. Figure 3.10 B was rearranged from Figure S2B in (Voss et al., 2019) published under CC-BY-NC-ND 4.0 with friendly permission from the authors.

To verify that symbiont-derived nutrients, and not another factor released by the symbionts activates mTORC1 signaling, we blocked photosynthesis in the symbiont using a dark treatment (Figure 3.10 C). In starved symbiotic anemones under dark conditions, levels of p4-EBP1 dropped to similar levels as in aposymbiotic anemones. In well-fed anemones, p4-EBP1 levels were higher in the symbiotic condition than in the aposymbiotic condition, likely due to larger nutrient reserves in that condition (Figure 3.10 B and C).

All these results support that mTORC1 signaling is stimulated by symbiont-derived nutrients, raising the question whether mTOR is localized in the vicinity of symbionts. Immunofluorescence using an mTOR-specific antibody revealed the presence of mTOR in the vicinity of symbionts (Figure 3.10 D). Interestingly, mTOR was not localized exclusively in direct vicinity of the symbionts, but throughout the symbiotic cell and possibly also neighboring cells (Figure 3.10 D), potentially due to trafficking of

symbiont-derived nutrients to neighboring cells. Further, mTOR localized in the vicinity of symbionts only in 53% of larvae (Supplemental Table 5.2), suggesting that mTOR recruitment could be dynamically regulated, e.g. in response to changing nutrient transfer rates or hormonal signaling.

3.3 Discussion

The endosymbiosis between Cnidaria and dinoflagellates is driven by a mutually beneficial nutrient exchange. The host provides the dinoflagellate with inorganic nutrients, which are scarce in the oligotrophic reef environment, in exchange for fixed carbon, mostly in the form of lipids and carbohydrates. Despite the reliance of hosts on the nutritional input from their symbionts, how symbiont-derived nutrients are integrated into host cell metabolism and functions remained largely unclear. To address this, we performed a series of experiments characterizing the nutritional status of aposymbiotic *Aiptasia* larvae and their gene expression response to symbiont acquisition. This revealed the conservation of a gene regulatory network involved in the switch between autophagy and anabolism, which is regulated by the master regulator of the nutritional response, mTOR. mTOR likely acts as the activator of cell proliferation in response to symbiont-derived nutrients and may be activated by symbiont derived sterols, sensed by the lysosomal transmembrane protein SLC38A9.

3.3.1 Nutritional benefit of symbionts on *Aiptasia* larvae

Our results indicate that aposymbiotic *Aiptasia* larvae quickly depleted maternally deposited energy reserves, leading to their reliance on autophagy to fuel cellular functions. In this situation, symbiont uptake quickly had positive effects, as already 2 days after the uptake of symbionts, larval lipid stores began to be replenished. The availability of nutrients not only led to an increase in the lipid stores, but also resulted in increased cell proliferation, highlighting the importance of symbiosis establishment for *Aiptasia* larvae. Interestingly, lipid stores were significantly increased 2 and 8 dpi, but not 4dpi (Figure 3.3). This is just 1 day after the increase in cell proliferation and could be the result of quick use of the symbiont-derived lipids as an energy source for proliferation.

The nutritional input from symbionts thus appears to have considerable effects on host metabolism in *Aiptasia* larvae. In contrast, the contribution of symbiont-derived nutrients to host nutrition has been shown to be low in young larvae (1d) of the brooding coral *Pocillopora damicornis*, partly because of the low symbiont density and partly because symbionts transferred less nutrients than in adults (Kopp et al., 2016). However, these larvae still relied on maternally-deposited nutrients (Kopp et al., 2016) and in older larvae of *P. damicornis* (22-27d), transfer of nutrients was similar to that in adults (Gaither and Rowan, 2010). Thus, the contribution of symbiont-derived nutrients to planula nutrition likely varies from species to species with the amount of maternally-deposited nutrients, symbiont density, and duration of the symbiosis.

In the case of *Aiptasia* larvae, where maternally-deposited nutrients are quickly depleted, the input of symbiont-derived nutrients may be a crucial to meet the energy demands of metamorphosis into juvenile polyps. Thus, future experiments with the aim to close the life cycle of *Aiptasia* should try to trigger metamorphosis in symbiotic, and not aposymbiotic larvae.

3.3.2 New insights from symbiotic-cell specific transcriptome

To our knowledge, this is the first transcriptome study in cnidarian-dinoflagellate symbiosis comparing gene expression at a level below the whole organism. To this end, non-symbiotic and symbiotic endodermal epitheliomuscular cells were isolated based on morphology 24-48 hpi.

This has two distinct advantages over previous whole-organism approaches: 1) it allows to detect smaller differences in gene expression in response to symbiosis, as symbiosis-specific gene expression changes are not "diluted" by non-symbiotic cells. 2) it allows the identification of where in the organism gene expression changes occur in response to symbiosis.

This approach allowed insights into the gene expression changes at the level of the cell state – comparing gene expression between symbiotic and non-symbiotic epitheliomuscular endodermal cells. This has two distinct advantages over previous whole-organism approaches: 1) it allows to detect smaller differences in gene expression in response to symbiosis, as symbiosis-specific gene expression changes are not "diluted" by non-symbiotic cells. 2) it allows the identification of where in the organism gene expression changes in response to symbiosis occur. Previous whole-organism studies assumed that changes in gene expression in response to symbiosis occurred in cells containing symbionts, but some changes could have been the result of changes in non-symbiotic cells affected e.g. by transfer of nutrients. We show that 24-48 hpi, the majority of changes do occur in the symbiotic cells. However, we expect that gene expression changes also occur in non-symbiotic cells in later stages of symbiosis, especially once nutrient transfer between host and symbiont is fully established.

The time point of sampling in this study was chosen to reflect an intermediate time point during symbiosis establishment, which appears to take at least several days. The transfer of lipids started to be detectable 2 days after symbiosis establishment. Similarly, previous studies have shown that nutrient transfer takes time to be fully established and is low shortly after symbiosis establishment (Kopp et al., 2016). In line with this, the symbiosomal NPC2 proteins, which are involved in transfer of symbiont-derived sterols, can only be detected at symbiosomes after several days, as symbiosomes mature (Hambleton et al., 2019). Therefore, the results presented here represent one time point in symbiosis establishment and it is to be expected that different time points yield different results, as in previous studies (Mohamed et al., 2016). For these reasons, the transcriptome data was analyzed at the level of KEGG pathways and used for hypothesis generation rather than detailed analysis of gene expression.

This revealed a major down regulation of gene expression in symbiotic cells as well as a down-regulation of autophagy and several other catabolic pathways. Combined with the observed depletion of maternal nutrient deposits and drop in cell proliferation, this led to the hypothesis that aposymbiotic larvae quickly deplete their lipid reserves and resort to autophagy to meet their energy requirements.

Upon uptake of symbionts, transferred nutrients can be used to fuel host cell metabolism, resulting in a shut-down of autophagy in the symbiotic cells.

3.3.3 Conserved regulation of autophagy in Cnidaria

Corroborating this hypothesis, we identified a homolog of the mammalian transcriptional regulator of autophagy TFEB. Phylogenetic analysis revealed that the invertebrate ancestor of vertebrate MITF-family transcription was already present in Cnidaria. The invertebrate MITF-family TFs have been shown to regulate autophagy in *C. elegans* and *D. melanogaster* (Bouché et al., 2016; Lapierre et al., 2013; O'Rourke and Ruvkun, 2013; Settembre et al., 2013) suggesting that regulation of autophagy via the CLEAR network is the ancestral function of all invertebrate MITF-family TFs, including those in Cnidaria. Corroborating this, we found an enrichment of E-box motifs in the promoters of *Aiptasia* homologs of mammalian CLEAR network genes. Further, mTOR-specific phosphorylation sites important for the regulation of mammalian TFEB were found to be conserved in *Aiptasia* MITF-like. However, the data regarding the conservation of CLEAR network in Cnidaria is based on *in silico* analysis.

To prove conservation of MITF-like as a transcriptional regulator of autophagy, further validation is necessary. This could for example be done using qPCR experiments to monitor the expression of MITF-like and CLEAR network homologs in response to symbiosis in *Aiptasia* larvae or in response to feeding of *Aiptasia* polyps. If regulation of MITF-like and the CLEAR network is conserved, their expression is expected to drop in symbiotic or fed animals and increase in aposymbiotic or starved animals. Similarly, expression of MITF-like and CLEAR network homologs is expected to increase in animals treated with an mTOR inhibitor if *Aiptasia* MITF-like is under the control of mTOR, as in Bilateria. Binding of MITF-like to E-boxes in promoters of CLEAR network homologs could be tested using ChIP-seq experiments. Unfortunately, no commercially available antibodies likely to be specific for the *Aiptasia* homolog were available at the time of this study.

3.3.4 Role of mTORC1 in sensing of symbiont-derived nutrients

Similarly, nutrient-dependent mTOR signaling appears to be conserved in *Aiptasia*. The activation of mTORC1 in response to food or symbiont presence shows the conservation of this pathway in Cnidaria (Figure 3.9 and Figure 3.10) and suggests that it was co-opted to integrate input of symbiont-derived nutrients and host cellular processes in cnidarian-dinoflagellate symbiosis.

Immunolocalization showed mTOR in symbiotic cells and near symbiosomes (Figure 3.10 D). This raises the question where exactly mTOR is localized. mTORC1 activity in symbiotic animals (Figure 3.10) suggests that mTOR is in the mTORC1 complex, which is formed on the lysosomal surface. However, mTORC1 could also be assembled directly on symbiosomes, which could facilitate direct sensing of symbiosomal nutrient levels, without shuttling of nutrients to other cellular compartments. Direct sensing of transferred nutrients at the symbiosome could then allow host cells to quickly adapt

their own functions, in particular their own metabolism, to the availability of nutrients. In line with this hypothesis, two proteins involved in mTORC1 regulation in response to lysosomal nutrient levels have been shown to localize to the symbiosome: the lysosomal H^+-ATPase and the cholesterol transporter NPC1 (Barott et al., 2015; Dani et al., 2017). Sensing of lysosomal amino acids is dependent on interaction of the lysosomal H^+-ATPase with Rag proteins, activators of mTORC1 (Zoncu et al., 2011), while NPC1 acts as an inhibitor of mTORC1 when lysosomal cholesterol levels are low (Castellano et al., 2017).

To test this hypothesis, the subcellular localization of mTORC1 needs to be identified. To do so, a double-staining using e.g. an mTOR antibody and a symbiosomal marker such as LAMP1 (this study), Rab5 (Chen et al., 2004), or H^+-ATPase (Barott et al., 2015) would be necessary. Unfortunately, all of these antibodies were raised in rabbits, just as the mTOR antibody. The mTOR antibody used in this study was selected because of the high sequence homology between the immunogen used for its generation and *Aiptasia* mTOR, and other commercial mTOR antibodies are less likely to work in *Aiptasia* due to lower sequence homology. Unfortunately, double staining with mTOR and LAMP1 antibodies using a directly-labeled LAMP1 antibody was unsuccessful, likely due to lacking signal amplification from secondary antibody binding. In the future, it would be interesting to identify the precise subcellular localization of mTOR in symbiotic cells as new antibodies become available.

3.3.5 Symbiont-derived sterols as a candidate mTORC1 activator

Which symbiont-derived nutrients trigger mTORC1 activity? Previous studies suggest that lipids are the major component of symbiont-derived nutrients (Battey and Patton, 1984; Crossland et al., 1980; Revel et al., 2016). In particular, sterols have emerged as an important nutrient transferred to the cnidarian host, as corals and anemones are sterol-auxotroph, and rely on sterols derived from either food or symbionts (Baumgarten et al., 2015; Goad L. J., 1981; Hambleton et al., 2019). Indeed, both *Aiptasia* and Scleractinia have expanded repertoires of NPC2 proteins, which bind sterols in the lysosomal lumen for transfer into the cytoplasm (Hambleton et al., 2019; Lehnert et al., 2014). This makes sterols a likely candidate to be sensed in symbiotic cnidarians by mTORC1. In line with this, NPC2 proteins and NPC1 have been found to be localized to the symbiosome (Dani et al., 2017; Hambleton et al., 2019). NPC2 functions by handing off cholesterol to the lysosomal membrane protein NPC1 for transport to the cytoplasm (Kwon et al., 2009; Pfeffer, 2019; Subramanian and Balch, 2008). In addition to NPC1, the more abundant lysosome-associated membrane proteins (LAMPs) have been shown to interact with NPC2 in the export of cholesterol from the lysosome (Li and Pfeffer, 2016). Consistent with export of symbiont-derived sterols, immunofluorescence with an *Aiptasia*-LAMP1-specific antibody (Supplemental Figure 5.3) shows localization of LAMP1 on symbiosomes (Figure 3.11 A).

In mammals, mTORC1 is activated in response to elevated lysosomal cholesterol levels by the amino acid transporter SLC38A9 (Castellano et al., 2017). SLC38A9 acts as an antagonist to NPC1, which inhibits mTORC1 activation in the absence of cholesterol (Castellano et al., 2017). We found a homolog of SLC38A9 in *Aiptasia* (XM_021036759.2), which contains the conserved cholesterol binding CRAC (cholesterol recognition amino acid consensus) and CARC motifs in transmembrane domain 8 (Figure 3.11 B). This makes SLC38A9 a promising candidate as a symbiosomal nutrient-sensor, involved in the detection of symbiont-derived sterols to activate the mTORC1 pathway. To test its involvement in activation of mTORC1 in response to symbiont-derived nutrients, immunolocalization of SLC38A9 could be performed.

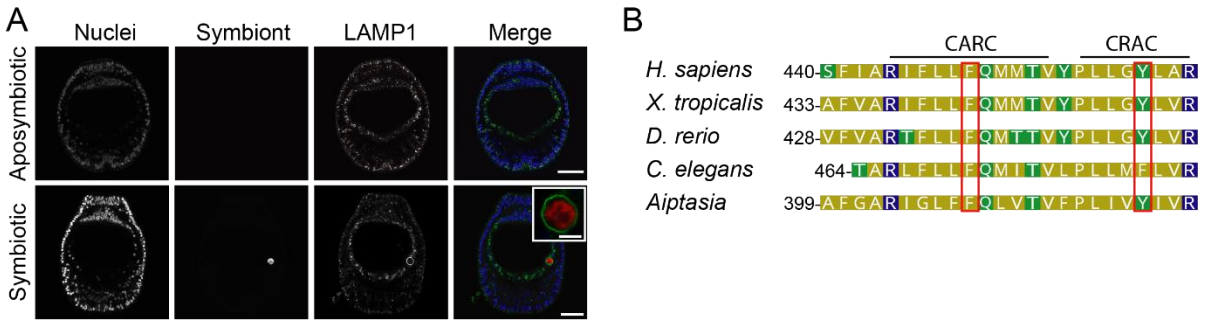

Figure 3.11. Possible nutrient sensing at the symbiosome. A) Representative confocal images of LAMP1 localization in aposymbiotic and symbiotic Aiptasia larvae. Colors in merge are nuclei in blue (Hoechst33258), LAMP1 (detected with Alexa488-anti-rabbit-IgG) in green, and symbiont in red (symbiont autofluorescence. Scale bars 25 µm (larval overviews) and 5 µm (inset). B) Protein sequence alignment of transmembrane domain 8 of SLC38A9 homologs. Conserved phenylalanine (F) and tyrosine (Y) residues in the CARC and CRAC cholesterol-binding domains are framed in red. Figures A and B were reproduced from Figures 3D and F, respectively, in (Voss et al., 2019) published under CC-BY-NC-ND 4.0.

3.3.6 The symbiosome as a lysosome-related organelle

The possibility that the symbiosome is the site of mTORC1 activation raises questions regarding the nature of the symbiosome. It has been proposed to resemble an arrested early phagosome (Chen et al., 2004; Davy et al., 2012; Mohamed et al., 2016). This hypothesis is based on the presence of the early endodermal marker Rab5 on symbiosomes, which is switched to the late endosomal marker Rab7 under stress conditions (Chen et al., 2003, 2004; Downs et al., 2009). Additionally, the guanosine nucleotide exchange factors (GEFs) ALS2 and rabenosyn-5 associated with the early endosomal marker Rab5 (Hadano et al., 2007; Jovic et al., 2010) were found to be transiently upregulated in symbiotic *Acropora millepora* 4 hpi (but not 12 or 48 hpi) which led to the conclusion that phagosome maturation is arrested (Mohamed et al., 2016). However, this data should be interpreted with caution, as the up regulation of ALS2 and rabenosyn-5 was transient and observed in a whole-animal transcriptome, which does not allow conclusions about where it occurred. In fact, no other whole-organism transcriptome study found the GEFs to be differentially regulated between aposymbiotic and symbiotic animals (Lehnert et al.,

2014; Matthews et al., 2017; Wolfowicz et al., 2016; Yuyama et al., 2018), and rabenosyn-5 was actually down regulated in symbiotic cells in this study (Supplemental File 5.4).

Several studies have identified features of the symbiosome inconsistent with it being an early arrested phagosome and some characteristics of the symbiosome more closely resemble those of lysosomes. Symbiosomes are acidified by the vacuolar H^+-ATPase to ~pH 4 to facilitate symbiont photosynthesis (Barott et al., 2015), while early phagosomes have pH > 6 and lysosomes have pH ~4.5 (Flannagan et al., 2012). Symbiosomes harbor the lysosomal Niemann-Pick Type C2 (NPC2) and NPC1 sterol-binding proteins, for transport of symbiont-derived sterols to the host (Dani et al., 2017; Hambleton et al., 2019). and are positive for LAMP1, which mainly associates with late endosomes and lysosomes (Figure 3.11 B). While LAMP1 can be trafficked through early endosomes (Cook et al., 2004), which would make a weak association of LAMP1 with symbiosomes possible if phagosomal maturation was arrested. However, symbiosomes are strongly associated with LAMP1 without exception, and appear to have an even stronger signal than other LAMP1-positive vesicles (Figure 3.11 B). Additionally, symbiosomes are associated with LAMP1 as early as 6 h after uptake, while other phagocytosed algae are not decorated with LAMP1 (Jacobovitz et al., 2019).

Based on these data, it seems unlikely that phagosomal maturation is arrested; however, it appears similarly unlikely that it proceeds in the canonical sequence of phagolysosomal maturation, as this would lead to symbiont digestion. To reconcile existing data on the symbiosome, I propose describing the symbiosome as a lysosome-related organelle (LRO) resulting from altered phagosomal maturation. LROs are described as cell-type specific organelles derived from the early or late endosomal/lysosomal systems, and around thirty have been described so far in various organisms (Delevoye et al., 2019).

In line with altered phagosomal maturation, we find several genes involved in lysosomal biogenesis, as well as several lysosomal acid hydrolases to be significantly down regulated in symbiotic cells (Supplemental File 5.4 and Supplemental File 5.5). Similarly, down-regulation of lysosomal acid hydrolases has previously been reported in symbiotic *Acropora tenuis* (Yuyama et al., 2018) and could be a way in which phagosomal maturation is altered to avoid the degradation of symbionts.

Given the somewhat contradicting data regarding the nature of the symbiosome, we encourage future studies to further characterize its physiology and protein composition to better understand how it is regulated to adapt symbiosome function to endosymbiotic associations in cnidarians.

3.3.7 Working model

Based on the findings presented in this thesis, we propose a working model for nutrient sensing in cnidarian-dinoflagellate symbiosis: Symbionts transfer nutrient to their hosts, resulting in the activation of mTORC1. This results in the activation of anabolic pathways and cell proliferation. At the same time, mTORC1 activity leads to inhibition of autophagy, which is regulated in a gene regulatory network under the control of MITF-like, which has a similar function as the CLEAR network in mammals.

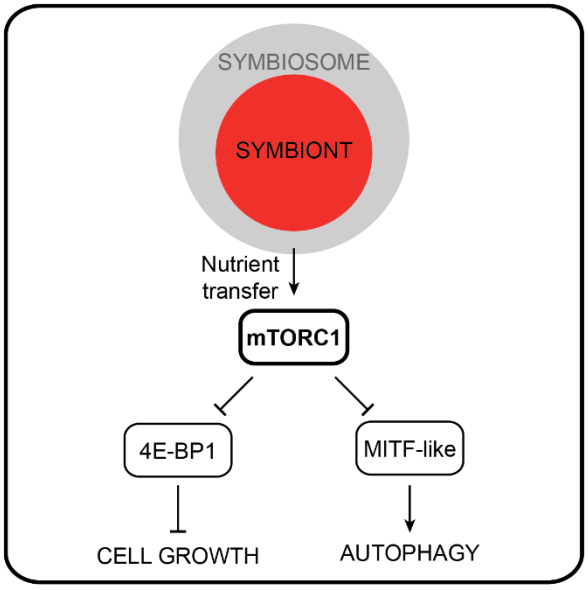

Figure 3.12. Model of mTORC1 activation in response to symbiont-derived nutrient transfer in cnidarian-dinoflagellate symbiosis.

4 General Discussion

Corals need to be associated with beneficial symbionts in order to persist. In coral bleaching, symbionts which are beneficial under normal circumstances become detrimental to the holobiont (i.e. the combined unit of host and symbionts) because they produce toxic ROS and are thus eliminated to ensure host survival. Similar to coral bleaching as a mechanism to select against ROS-producing, 'defective' symbionts during heat stress, corals must have evolved other mechanisms to select beneficial symbionts under normal conditions. Otherwise, parasitic symbionts which transfer few or no nutrients could easily populate corals. In this light, sensing of symbiont-derived nutrients via mTORC1 as identified in this thesis emerges as a possible mechanism for the selection of suitable or beneficial symbionts.

Symbionts which transfer nutrients inadvertently activate mTORC1, leading to cellular growth and proliferation and the maintenance of these symbionts. Conversely, parasitic Symbiodiniaceae which do not share nutrients would fail to activate mTORC1, leading to the activation of autophagy and potentially their digestion. In fact, autophagy is one mechanism by which symbionts are lost in bleaching and mTOR inhibition in *Aiptasia* has been shown to result in the digestion of symbionts (Dunn et al., 2007; Hanes and Kempf, 2013). Thus, nutrient-dependent mTORC1 signaling emerges as a mechanism for both positive and negative selection of symbionts at the cellular level. Additionally, the positive selection could emerge as a mechanism leading to the preferential colonization of a host with the most beneficial symbionts. Even slightly increased growth and proliferation of host cells harbouring 'generous' symbionts would favour their proliferation in the host organism. This would lead to a positive selection for beneficial symbionts at the organismal level, and preferential colonization of the host with these symbionts.

Selection of symbionts based on the amount of shared nutrients has been observed in the *Hydra-Chlorella* symbiosis. Here, strains of *Chlorella* which release large amounts of maltose were better able to spread in the host than strains that share little or no maltose (Hohman et al., 1982; McAuley and Smith, 1982). Interestingly, persistence of symbionts was reduced when nutrient transfer was inhibited by either darkness or photosynthesis inhibition. However, no mechanism of selection of beneficial symbionts was proposed. mTORC1-mediated sensing of symbiont-derived nutrients could be a mechanism by which this selection is mediated.

Selection of nutritionally beneficial symbionts has profound implications on coral adaptation to their changing environment. By associating with different symbionts corals may quickly adapt to changing environmental conditions due to climate change

Coral adaptation by association with different types of symbionts is best studied in heat tolerance/bleaching tolerance. Following bleaching events, surviving corals are often predominantly

associated with heat-tolerant Symbiodiniaceae of the genus Durusdinium (Grottoli et al., 2014; Kennedy et al., 2015). Interestingly, these symbionts are usually lost in favor of the less heat-tolerant strains that are usually associated with the corals under ‘normal conditions (LaJeunesse et al., 2009; Thornhill et al., 2006).

So far, the mechanisms underlying the loss of heat-tolerant symbionts remains unknown. Researchers have speculated that Durusdinium, which transfers less nutrients under normal temperatures is replaced by other, more nutritionally beneficial symbionts (LaJeunesse et al., 2009). My model that mTORC1-mediated nutrient sensing is involved in selection of nutritionally beneficial symbionts can explain this observation, as it favors symbionts which transfer more nutrients.

Furthermore, the model could help guide efforts to generate strains of symbionts that allow corals to adapt to environmental change more rapidly. For example, there are efforts to generate strains of symbionts that are adapted to higher temperatures, by directed or experimental evolution (Buerger et al., 2020; Chakravarti and van Oppen, 2018; Chakravarti et al., 2017). To ensure that the resulting strains are beneficial even under normal conditions and form a lasting symbiosis that equips corals for future stress conditions, it should be taken into account that they need to transfer stable levels of nutrients to the host even under changing environmental conditions. This shows that understanding the molecular mechanisms is crucial to guide efforts aiming at coral adaptation to climate change.

5 Supplemental Information

5.1 Supplemental Figures

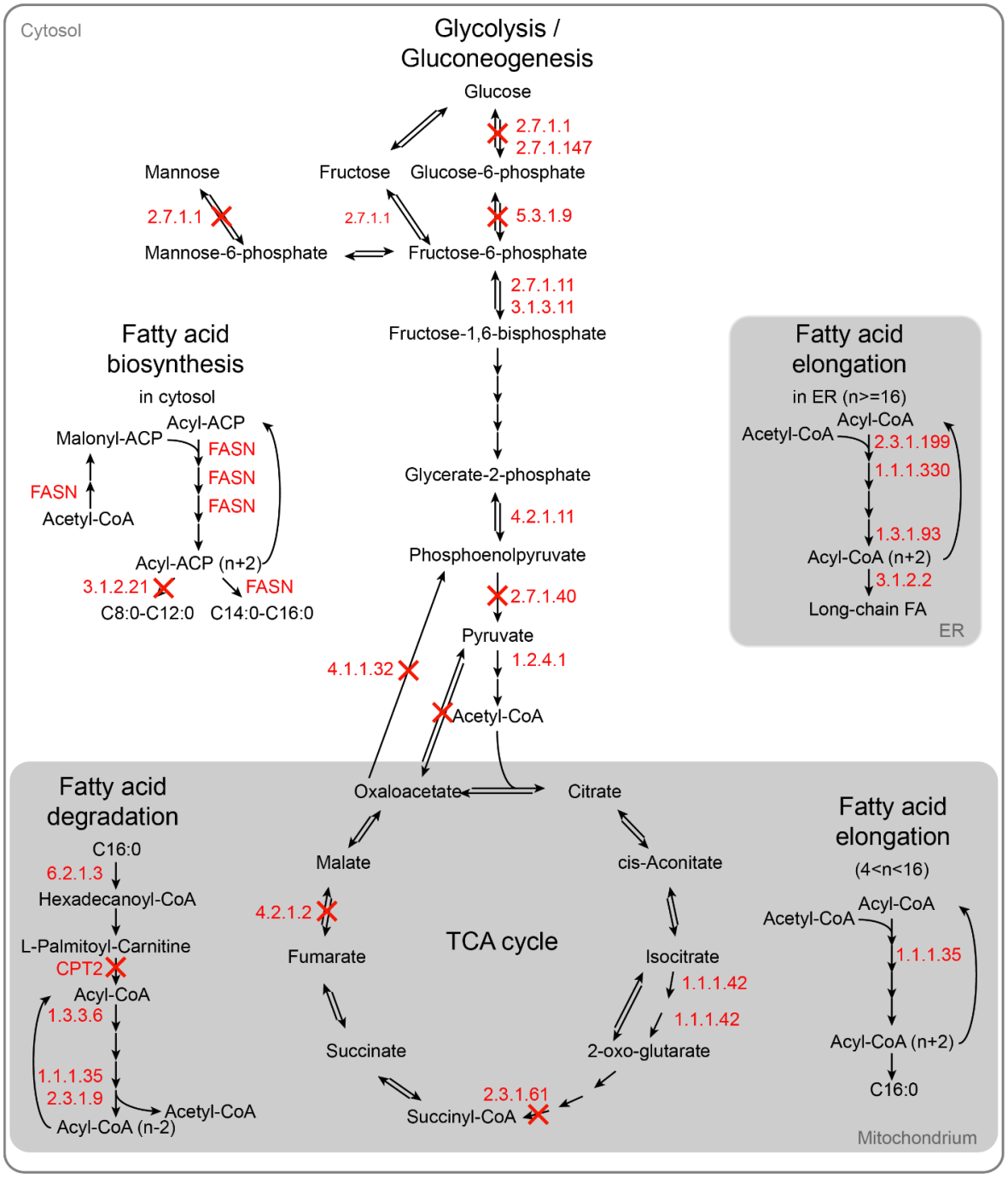

Enzyme significantly down regulated in symbiotic cells

✕ Gene expression below detection limit

Supplemental Figure 5.1 Changes in gene expression in major metabolic pathways based on KEGG pathways. Down-regulated genes are indicated by their Enzyme Commission (EC) number in red. Where no expression was detected for any gene coding for an enzyme, the corresponding reaction is crossed out in red. This figure was reproduced from Figures S1 in (Voss et al., 2019) published under CC-BY-NC-ND 4.0.

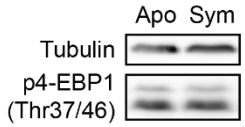

Supplemental Figure 5.2. mTORC1 activity in Aiptasia larvae. Representative Western Blot comparing p4-EBP1 levels in aposymbiotic (Apo) and symbiotic (Sym) Aiptasia larvae. No differences in p4E-BP1 levels were detected in larvae.

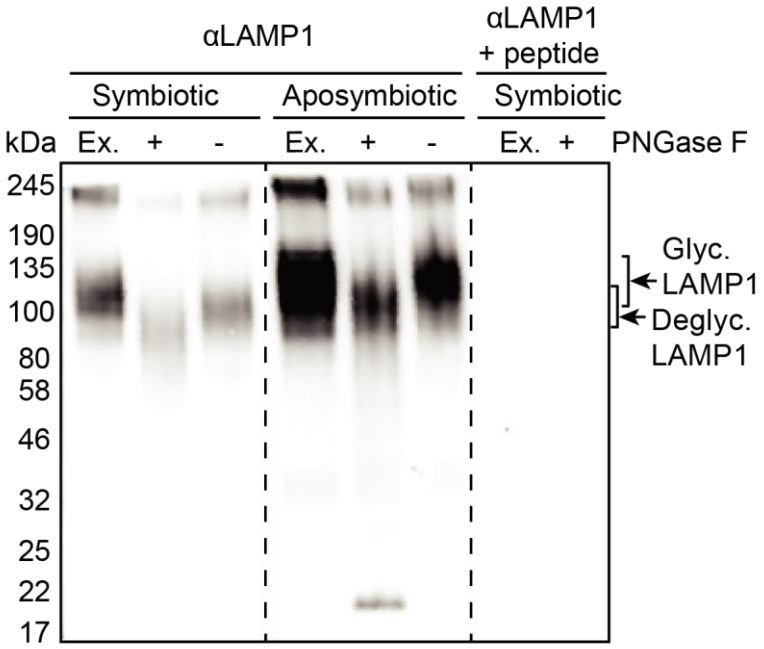

Supplemental Figure 5.3. Verification of Aiptasia-specific LAMP1-antibody. LAMP1 is a heavily glycosylated protein, which runs at a higher than predicted (38 kDa) molecular weight (Winchester, 2001). In line with this, deglycosylation of homogenates of both symbiotic and aposymbiotic Aiptasia polyps with the glycosidase PNGase F resulted in a shift of the detected protein to lower molecular weight. Detection using antibody pre-absorbed to the antigenic peptide resulted in loss of detection, indicating specificity of the raised LAMP1-antibody. This figure was reproduced from Figure S2C in (Voss et al., 2019) published under CC-BY-NC-ND 4.0.

5.2 Supplemental Tables

Supplemental Table 5.1 Mapping statistics of RNAseq experiment. Samples used for DEG analysis are highlighted in gray (aposymbiotic cells) and red (symbiotic cells).

		sample	total number of paired reads	paired reads mapped to *Aiptasia* genome	% mapped to *Aiptasia* genome	paired reads mapped concordantly 1x to *Aiptasia* genome	% paired reads mapped concordantly 1x to *Aiptasia* genome
aposymbiotic larvae	aposymbiotic cells	1	20,087,830	12,399,278	61.7	6,912,518	34.4
		2	20,877,749	11,886,311	56.9	6,431,597	30.8
		3	11,171,715	6,389,709	57.2	4,316,128	38.6
		4	22,872,259	15,128,631	66.1	10,614,751	46.4
		5	18,697,844	12,246,128	65.5	8,530,464	45.6
symbiotic larvae	aposymbiotic cells	1	18,957,950	13,592,731	71.7	7,761,680	40.9
		2	28,482,747	19,324,494	67.9	10,635,619	37.3
		3	16,926,849	12,030,290	71.1	8,200,187	48.4
		4	18,564,553	13,107,033	70.6	9,217,977	49.7
		5	21,428,035	12,643,721	59.0	12,014,891	56.1
	symbiotic cells	1	30,039,492	1,378,905	4.6	815,133	2.7
		2	25,755,436	1,720,285	6.7	960,229	3.7
		3	24,421,642	4,677,767	19.2	2,555,674	10.5
		4	38,799,982	10,780,550	27.8	7,059,110	18.2
		5	49,034,909	14,759,837	30.1	10,348,880	21.1
		6	54,295,092	23,885,879	44.0	16,739,833	30.8

Supplemental Table 5.2. Localization of mTOR. Raw data of proportion of larvae where mTOR was localized near symbionts.

Larvae with mTOR near symbionts	Total number of larvae	% mTOR-positive larvae	Mean % mTOR-positive larvae
22	50	44.0	53.3
29	50	58.0	
29	50	58.0	

5.3 Supplemental Files provided in digital format only

Supplemental File 5.1. Related to Figure 3.2 C. Excel file (.xlsx) containing raw data for quantification of cell proliferation in aposymbiotic larvae.

Supplemental File 5.2. Related to Figure 3.3 B. Excel file (.xlsx) containing raw data for quantification of number of lipid droplets per endoderm.

Supplemental File 5.3. Related to Figure 3.3 C. Excel file (.xlsx) containing raw data and statistical tests for comparison of cell proliferation in aposymbiotic and symbiotic larvae. Tukey's multiple comparisons test was used to determine significant differences in cell proliferation between either aposymbiotic or symbiotic larvae over time.

Supplemental File 5.4. Related to Figure 3.6. Excel file (.xlsx) containing different data sets in different tabs: one contains raw read counts for each gene per replicate, one contains normalized expression values (TMM) for all genes and replicates, one contains log2-fold changes and normalized expression values of significantly down regulated genes in symbiotic cells, and one contains log2-fold changes and normalized expression values of significantly down regulated genes in symbiotic cells. This file was reproduced from Table S1 in (Voss et al., 2019) published under CC-BY-NC-ND 4.0 and expanded by adding additional tabs containing raw read counts for each gene and replicate.

Supplemental File 5.5. Related to Table 3.1. Excel file (.xlsx) containing lists of DEGs of KEGG pathways that were significantly enriched among the down-regulated genes. This file was reproduced from Table S2 in (Voss et al., 2019) published under CC-BY-NC-ND 4.0.

Supplemental File 5.6. Related to Figure 3.7A. Nexus file (.nex) containing raw sequences of MITF-family genes, trimmed alignments, and tree information for maximum likelihood phylogeny. This file was reproduced from File S3 in (Voss et al., 2019) published under CC-BY-NC-ND 4.0.

Supplemental File 5.7. Related to Figure 3.7B and C. Text file (.txt) containing a library of 9 transcription factor binding patterns including a manually generated E-box motif and several MITF and USF TF binding motifs used in CLOVER analysis of overrepresented E-box motifs.

Supplemental File 5.8. Related to Figure 3.7B and C. Fasta file (.fasta) containing promoter sequences of 10 randomly chosen genes used as a control in CLOVER analysis of overrepresented E-box motifs.

5.4 Source Code

Source Code 5.1. ImageJ macro used for analysis shown in Figure 3.3 B to make maximum projections of center 30 µm of Z-stacks.

```
path = File.openDialog("Select a lif File");
output = File.openDialog("Select a output location")
setBatchMode(true);
run("Bio-Formats Macro Extensions");
Ext.setId(path);
Ext.getCurrentFile(file);
Ext.getSeriesCount(seriesCount);


for (i=1; i<=seriesCount; i++) {
      //open file and get info
      run("Bio-Formats Importer", "open=&path autoscale color_mode=Composite view=Hyperstack stack_order=XYCZT series_"+i);
      getDimensions(width, height, channels, slices, frames);
      name = getTitle();
      //specify range (30 µm around the center of the larva)
      start = slices/2-15;
      stop = slices/2+15;
      // (images of symbiotic larvae have 3 channels, images of aposymbiotic larvae have 2 channels
      if (channels == 3){ // for symbiotic larvae
      name = getTitle();
      run("Split Channels");
      selectWindow("C3-"+name+""); //C3 nile red channel
      run("Smooth", "stack");  //smooth to enhance removing of symbionts
      selectWindow("C2-"+name+""); //C2 symbiont channel
      run("Smooth", "stack"); //smooth to enhance removing of symbionts
      imageCalculator("Subtract create stack", "C3-"+name+"","C2-"+name+""); //substract symbionts
      run("Merge Channels...", "c1=[C2-"+name+"] c2=[Result of C3-"+name+"] c3=[C1-"+name+"] create ignore"); // combine channels to stack
      run("Z Project...", "start="+start+" stop="+stop+" projection=[Max Intensity]"); // do projection of 30 µm in the middle
      saveAs("Tiff", output+name+"_proj.tif");
      run("Stack to RGB"); // convert to RGB
      saveAs("Tiff", output+name+"_proj_RGB.tif");
      close();
```

```
      close();
}
else { // for aposymbiotic larvae
      name = getTitle();
      run("Split Channels");
      selectWindow("C2-"+name+""); //C2 nile red channel
      run("Smooth", "stack");  //smooth for consistency with treatment of images
of symbiotic larvae
      run("Merge  Channels...",  "c2=[C2-"+name+"]  c3=[C1-"+name+"]  create
ignore"); // combine channels to stack
      run("Z  Project...",  "start="+start+"  stop="+stop+"  projection=[Max
Intensity]");// do projection of 30 µm in the middle
      saveAs("Tiff", output+name+"_proj.tif");
      run("Stack to RGB");// convert to RGB
      saveAs("Tiff", output+name+"_proj_RGB.tif");
      close();
      close();
}}
```

Source Code 5.2. ImageJ macro used for analysis shown in Figure 3.3 B to count the number of lipid droplets per larval endoderm.

```
// 1. select endoderm, then run script
output = File.openDialog("Select an output location")
name = getTitle();
run("Set Scale...", "distance=3.3231 known=1 pixel=1 unit=micron global"); //
make sure scale is set correctly (sometimes got lost with previous script)
// make duplicate of endoderm and select duplicate
run("Copy");
run("Internal Clipboard");
selectWindow("Clipboard");
//Auto-detect vesicles
setAutoThreshold("MaxEntropy dark");
setOption("BlackBackground", true);
run("Convert to Mask");
saveAs("Tiff", ""+output+name+"_endo_specles.tif");
//Count vesicles
run("Set  Measurements...",  "area  mean  modal  centroid  integrated  display
redirect=None decimal=3");
run("Analyze Particles...", "display clear");
```

```
saveAs("Results", ""+output+name+"_endo_speces.csv");
//Measure endoderm size
selectWindow(name);
run("Internal Clipboard");
selectWindow("Clipboard");
saveAs("Tiff", ""+output+name+"_endo.tif");
setThreshold(1, 255);
run("Convert to Mask");
run("Analyze Particles...", "display clear");
saveAs("Results", ""+output+name+"_endo_size.csv");
// Measure endoderm intensitiy
selectWindow(name);
run("Measure");
saveAs("Results", ""+output+name+"_endo_channel.csv");
selectWindow(name);
run("Draw", "slice");
Stack.setActiveChannels("111");
run("Stack to RGB");
saveAs("Tiff", ""+output+name+"_merge.tif");
run("Clear Results");
close();
close();
close();
close();
```

6 Methods

6.1 Live Organism Culture and Maintenance

6.1.1 Algal culture maintenance

For infection of aposymbiotic *Aiptasia* larvae, clonal axenic cultures of *B. minutum* (strain SSB01), originally isolated from *Aiptasia* strain H2, and *E. voratum* (strain SSE01), originally isolated from sea water off the coast of New Zealand (Xiang et al., 2013) were used. Cultures were grown in cell culture flasks in 0.22 µm filter-sterilized 1X Daigo's IMK medium (398-01333, Nihon Pharmaceutical Co. Ltd., Tokyo, Japan) on a 12h light:12h dark (12L:12D) cycle under 20–25 µmol m−2 s−1 of photosynthetically active radiation (PAR) at 26 °C.

6.1.2 *Aiptasia* culture conditions and spawning induction

Aiptasia clonal lines CC7 (hosting *Symbiodinium linuchae*, (Sunagawa et al., 2009)) and F003 (hosting a mixture of *B. minutum*, a variant of *B. minutum,* and *S. linuchae* (Grawunder et al., 2015)) were maintained at 26 °C in a 12L:12D cycle. Animals were induced to spawn following the previously described protocol (Grawunder et al., 2015). *Aiptasia* larvae were maintained at ~300 larvae per ml in glass beakers in 0.22 µm filter-sterilized artificial sea water (FASW) at 26ºC and exposed to a 12L:12D cycle.

6.1.3 Infection experiments

Larvae 6 or 7 dpf at a concentration of ~300 larvae per ml were exposed to *B. minutum*, *E. voratum* or inert beads (#C36950, Thermo Fisher Scientific) at 10^5 particles per ml for 4 or 5 days at 26ºC and exposed to a 12L:12D cycle. At this time, algae or beads were washed out and larvae were fixed in 4 % formaldehyde for 30 min at room temperature followed by 3 washes in PBS.

For assessment of proportion of infected larvae and localization of algae or beads (Figure 2.1) and size comparisons (Figure 2.3), larvae were mounted in 87% glycerol in PBS. Microscopic analysis was carried out with a Nikon Eclipse Eclipse 80i microscope using Differential Interference Contrast (DIC). Representative images were captured using a Digital Sight DS-U1 color camera (Nikon Instruments). Four replicates (separate infections from distinct spawning events) were counted, with a minimum of 85 larvae per replicate. Sizes of *B. minutum* and *E. voratum* were measured from images using the Measure tool in ImageJ software (Schindelin et al., 2012, 2015).

6.2 Transcriptome sample preparation

Aiptasia larvae (~300 per ml) were infected 5 or 6 dpf with 10^5 *B. minutum* cells per ml for 24 or 48 hours or left aposymbiotic. Three to five infected larvae were transferred in 2 µl FASW to 5 ml of Calcium- and Magnesium-free artificial sea water (CMF-SW, doi:10.1101/pdb.rec12053). After

incubation for 5 min, larvae were transferred to a 70 µl drop of Pronase (0.5 % in CMF-SW; 10165921001, Sigma-Aldrich Co. LLC, St. Louis, MO, USA) and sodium thio glycolate (STG, 1 % in CMF-SW; T0632, Sigma-Aldrich Co. LLC) on a glass microscopy slide. After mixing larvae by pipetting up and down in 20 µl 3 to 5 times, larvae were incubated for ca. 2 min until ectodermal cells began to be released from the larval body. The endoderm was transferred to a drop of 70 µl FASW and remaining ectodermal cells were washed off by pipetting up and down five to 10 times in 20 µl. Endodermal tissue was transferred to a 70 µl drop of FASW on a cover slip and crushed using the tip of tweezers to yield single cells. The total time from beginning of dissociation of larvae to lysis was 30 min.

Pools of 7 to 20, either non-symbiotic (five pools, each) or symbiotic (6 pools) cells were picked using special microcapillary needles with openings of 8 to 12 µm diameter pulled with a P-97 Flaming/Brown Micropipette puller from glass capillaries (GB100T-8P, Science Products, Hofheim, Germany). Glass capillaries were pre-loaded with 4.3 µl of lysis buffer (0.2 % TritonX-100, 1U/µl Protector RNase inhibitor (3335399001, Sigma-Aldrich Co. LLC), 1.25 µM oligo-dT_{30}VN, and 2.5 mM dNTP mix) and collected cells were flushed out of the capillary with the lysis buffer into a PCR tube before flash-freezing in liquid nitrogen. After cell capture and lysis as described above, sequencing libraries were prepared as previously described (Picelli et al., 2014). Briefly, full-length polyA+ mRNA was reverse transcribed using SuperScript II Reverse Transcriptase (18064014, Sigma-Aldrich Co. LLC), followed by pre-amplification of cDNA over 21 PCR cycles using KAPA HiFi Hotstart Ready Mix (07958935001, Roche Diagnostics International AG, Rotkreuz, Switzerland). cDNA libraries were then prepared for Illumina sequencing using the Nextera XT sequencing kit (FC-131-1096, Illumina, Inc., San Diego, CA, USA) and sequenced on NextSeq500 with 75 bp paired-end sequencing.

6.3 Computational Methods

6.3.1 Differential gene expression analysis

To exclude reads derived from the symbiont or bacteria in the medium, paired-end reads were mapped to the *Aiptasia* genome version GCF_001417965.1 using HISAT2 version 2.1.0 at default settings, except -X 2000 --no-discordant --no-unal --no-mixed. Host-derived transcripts were quantified in Trinity v2.5.1 using salmon v0.10.2 at default settings. Principal component analysis of gene expression across all samples was conducted using the perl script PtR supplied with Trinity based on raw expression counts. Differentially expressed transcripts between clustered symbiotic and non-symbiotic samples (circled in Figure 2C) were detected using DESeq2 (log2-fold change > 2; false-discovery-rate < 0.01) from raw read counts using default settings.

6.3.2 KEGG pathway enrichment analysis

Differentially expressed genes were examined for enrichment of KEGG pathway terms in R v3.4.1 using the 'enricher' function from the R package 'clusterProfiler' (Yu et al., 2012) at standard settings

(with p-value ≤0.15). clusterProfiler adjusted the estimated significance level to account for multiple hyphothesis testing and q-values were calculated for FDR control (Gu et al., 2016).

6.3.3 Phylogeny of MITF-family

For MITF phylogenies, metazoan MITF and USF (upstream stimulatory factor) homologs were identified from public databases. Alignments were generated using ClustalW v2.0 (Larkin et al., 2007) and manually corrected in Geneious v10.2.6 (Biomatters). Ambiguous sites and poorly aligned regions were removed automatically using trimAI set to '-automated1' (Capella-Gutiérrez et al., 2009). We then determined the best-fitting substitution model using ModelFinder (set to '-m MF -msub nuclear') within iqTree 1.6.10 and PROTTEST3 (set to '-JTT -LG -DCMut -Dayhoff -WAG -G -I -F -AIC -BIC') (Darriba et al., 2011; Kalyaanamoorthy et al., 2017; Nguyen et al., 2014). Maximum-likelihood phylogenies were inferred with iqTree using a JTT+I+G4 substitution matrix with USF sequences as outgroups with the following settings: '-m JTT+I+G4 -bb 10000 –bnni –nt AUTO -alrt 10000 -abayes'. The resulting tree was finalized using FigTree v1.4.4 (Morariu et al., 2008) and Adobe Illustrator CC 2018.

6.3.4 Alignment of *Homo sapiens* TFEB and *Aiptasia* MITF-like

Amino acid sequences of *Homo sapiens* TFEB (P19484) and *Aiptasia* MITF-like (XM_020895872.1) were aligned using ClustalW v2.0 (Larkin et al., 2007) in Geneious v10.2.6 (Biomatters).

6.3.5 Search for E-box motifs

Aiptasia homologs of human CLEAR network genes (Palmieri et al., 2011) were identified using reciprocal BLAST. Promoter sequences (defined as intergenic sequences upstream of each CLEAR gene transcription start site) were then searched for statistically overrepresented motifs using Clover (Frith, 2004) and a library of 9 transcription factor binding patterns (Figure 3 – Source Data 2), including a manually generated E-box motif and several MITF and USF TF binding motifs from JASPAR at standard settings. An approx. 6Mbp *Aiptasia* genomic scaffold (Genbank Accession NW_018384103.1) was used as a background sequence. Promoters of 10 randomly chosen genes from genomic scaffold NW_018384103.1, which are not CLEAR homologs, were also tested as control (Figure 3 – Source Data 3).

6.3.6 Alignment of SLC38A9 transmembrane domain 8

Amino acid sequences of SLC38A9 homologs in *Homo sapiens* (Q8NBW4), *Danio rerio* (NP_001073468.1), *Xenopus tropicalis* (NP_001011337.1), *Caenorhabditis elegans* (NP_001076680.1), and *Aiptasia* (XP_020892418.1) were analyzed using SMART protein prediction v8.0 (Letunic and Bork, 2017) to identify transmembrane domain 8 (TM8). TM8 sequences were aligned using ClustalW v2.0 (Larkin et al., 2007) in Geneious v10.2.6 (Biomatters, Auckland, New Zealand).

6.4 Staining procedures in *Aiptasia* larvae

6.4.1 Phalloidin staining and confocal imaging

Larvae 6 dpf were infected with 10^5 algae (*B. minutum* or *E. voratum*) per ml for 4 days and fixed for 30 min in 4% formaldehyde at room temperature (RT), followed by 3 washes in 0.2% Triton X-100 in PBS (PBT). Larvae were then permeabilized in 0.01 mg/ml Proteinase K(#03115879001, Roche Diagnostics International AG, Rotkreuz, Switzerland) in PBS for 8 min. Permeabilization was stopped by washing larvae in 2 mg/ml glycine in PBT twice for 15 min each. Larvae were post-fixed in 4% formaldehyde in PBT for 20 min and then washed twice in PBT and twice in PBS, for 15 min each. Larvae were stained with Phalloidin-Atto 565 (#94072, Sigma-Aldrich Co. LLC) diluted 1:200 in PBS for 60 min at 20 rpm.

Larvae were washed twice in PBT, followed by a 15-minute incubation with 10 µg/ml Hoechst 33258 (B2883, Sigma-Aldrich Co. LLC) in buffer (Tris-buffered saline, pH 7.4; 0.1% Triton X-100; 2% bovine serum albumin; 0.1% sodium azide). After three washes in PBT for 15 min, each, larvae were mounted in 87% glycerol in PBS containing 2.5 mg/ml DABCO (1,4-Diazabicyclo[2.2.2]octan, #D27802, Sigma-Aldrich Co. LLC). Confocal images were acquired using a Nikon A1R confocal microscope with a Nikon Plan Apo 60x oil immersion objective (NA 0 1.4) and Nikon Elements Software. Image processing and maximum projections of Z-stacks were performed in ImageJ software (Schindelin et al., 2012, 2015).

6.4.2 Lipid droplet staining with Nile Red

For assessment of maternal lipids in *Aiptasia* larvae, aposymbiotic larvae were fixed 2, 6, and 10 dpf in 4 % formaldehyde for 20 min at room temperature followed by 3 washes in PBS. For assessment of lipid contribution by symbionts, larvae were infected with 10^5 SSB01 per ml at various time points (2-5 dpf, 6-7 dpf, 8-9 dpf) or left aposymbiotic and fixed 10 dpf in 4 % formaldehyde for 20 min at RT, followed by 3 washes in PBS. Larvae were stained with Nile Red (final concentration 5 µg/ml in 1x PBS from 0.5 mg/ml stock in acetone; N3013, Sigma-Aldrich Co. LLC) for 15 min, followed by staining with Hoechst 33258 (final conc. 10 µg/ml in 1x PBS; B2883, Sigma-Aldrich Co. LLC) for 15 min and 2 washes in 1x PBS before mounting in 87% glycerol in PBS. Images were acquired on a Leica TCS SP8 confocal laser scanning microscope using a 63x glycerol immersion lens (NA 1.30) and Leica LAS X software. Hoechst 33258 and symbiont autofluorescence were excited with the 405 nm laser line, and Nile Red autofluorescence was excited with the 488 nm laser. Fluorescence emission was detected at 405 – 480 nm for Hoechst 33258, 540 – 620 nm for Nile Red and 700 – 740 nm for symbiont autofluorescence.

For assessment of lipid contribution by symbionts, the number of lipid droplets in the endodermal tissue was counted. To this end, stacks of whole larvae with a step size of 1 µm were acquired with confocal microscopy. Maximum projections of the center 30 µm were made in FIJI (Schindelin et al., 2012, 2015) using a custom macro (Source Code 1), followed by manual selection of the endodermal tissue. In order to measure only signal from host tissue, the signal from symbionts was subtracted from

the Nile Red signal. The number of lipid droplets was determined using a custom ImageJ macro (Source Code 2).

6.4.3 Lipid droplet staining in polyp macerates

For assessing the abundance of lipids in *Aiptasia* polyps depending on their symbiotic state, aposymbiotic and symbiotic polyps that either had been starved (for 9 days) or fed (3 times per week for 10 days) were macerated and stained with Nile Red. Small polyps (~2 mm oral disc) in 100 µl FASW were pulled through hypodermic needles of decreasing sizes five times each (gauges 23 and 25). The resulting suspension was fixed in 4 % formaldehyde for 20 min and washed in PBS twice before resuspension in 20 µl PBS. 15 µl of tissue suspension was pipetted onto a well of a 10-well PTFE diagnostic slide (631-1371, VWR International GmbH, Radnor, PA, USA) and left to dry completely. Tissue was rehydrated with 15 µl of MilliQ water before staining with Nile Red (final concentration 5 µg/ml in 1x PBS) for 15 min, followed by staining with Hoechst 33258 (final conc. 10 µg/ml in 1x PBS) for 15 min and 1 wash in PBS before mounting in 4 µl of 87% glycerol in PBS. Images were acquired on a Leica TCS SP8 confocal laser scanning microscope using a 63x glycerol immersion lens (NA 1.30) and Leica LAS X software. Hoechst 33258 and symbiont autofluorescence were excited with the 405 nm laser line, and Nile Red autofluorescence was excited with 488 nm laser. Fluorescence emission was detected at 405 – 480 nm for Hoechst 33258, 540 – 620 nm for Nile Red and 700 – 740 nm for symbiont autofluorescence. Transmitted light from the 488 nm laser was also detected.

6.4.4 Cell proliferation assay with EdU

Cell proliferation was determined using the 5-ethynyl-2'-deoxyuridine (EdU)-Click 488 kit (BCK-EDU488, Sigma-Aldrich Co. LLC). Larvae were washed and resuspended in FASW to a density of ~500 larvae per ml. For assessment of cell proliferation in aposymbiotic *Aiptasia* larvae over time, larvae were incubated in 10 µM EdU for 18 h (6 – 24 hpf) or 24 h (24-48 hpf, 48-72 hpf, 120-144 hpf, 144-168 hpf, 168-192 hpf, and 192-216 hpf). To assess the effect of symbiosis on cell proliferation, larvae that had been symbiotic for different durations were compared to aposymbiotic larvae of the same age. Symbiotic larvae were infected at 5 dpf with 105 SSB01 per ml for 24 hours before wash-out. Larvae were incubated with EdU for 24 h periods prior to fixation in 3.7 % formaldehyde for 15 min at 6, 7, and 8 dpf, respectively. Following 3 washes in 0.05 % PBS-Tween 20 (PBS-T), larvae were stained with Hoechst 33258 (final conc. 10 µg/ml) for 40 min. Larvae were washed twice in PBS-T and mounted in ~100 % glycerol. Stacks of whole larvae were acquired on a Leica TCS SP8 confocal laser scanning microscope using a 63x glycerol immersion lens (NA 1.30) and Leica LAS X software. Hoechst 33258 and EdU were excited with 405 and 488 nm laser lines, respectively. Fluorescence emission was detected at 410-501 nm for Hoechst 33258 and 501 – 556 nm, for EdU. For enumeration of nuclei and EdU-positive nuclei, pixel classification was performed in ilastik (Sommer et al., 2011) followed by

nuclei identification and enumeration in “vision 4d” software (arivis AG, Munich, Germany) using the blob finder tool.

6.4.5 *Aiptasia*-specific anti-LAMP1 antibody purification

An antibody against the *Aiptasia* LAMP1 homolog (KXJ16564.1) was raised using the peptide IIGRRKSQRGYEKV coupled to the adjuvant keyhole limpet hemocyanin in rabbit (DJ-Diagnostik BioScience, Göttingen, Germany). The antibody was affinity purified from the third bleed using the synthetic peptide coupled to N-hydroxysuccinimide esters (NHS)-activated sepharose (17090601, GE Health Care Life Sciences, Chicago, IL, USA) according to manufacturer’s protocols.

6.4.6 Immunofluorescence of LAMP1 and mTOR

Larvae (5 dpf, 24 hpi for LAMP1, and 6dpf, infected 2 – 5 dpf, for mTOR) were fixed for 45 minutes in 4% formaldehyde at room temperature (RT), followed by 3 washes in 0.2% Triton X-100 in PBS (PBT) and one wash in PBS. Larvae were then permeabilized in PBT for 1.5 hours at RT, followed by blocking in 5% normal goat serum and 1% BSA in PBT for 1 hour. Primary antibody was diluted in blocking buffer (rabbit-α-LAMP1: 1:100; rabbit-α-mTOR (HPA071227, Sigma-Aldrich Co. LLC): 1:12.5, final concentration 4 µg/ml) and incubated overnight at 4°C. After 3 washes in PBT, the secondary antibody (goat-α-rabbit Alexa 488, ab150089, Abcam plc., Cambridge, United Kingdom) diluted 1:500 in blocking buffer was added and incubated for 1.5 hours at RT. Larvae were washed 2 times in PBT, followed by a 15-minute incubation with 10 µg/ml Hoechst 33258 protected from light at RT, and 2 final washes in PBT and 1 in PBS before mounting in 87 % glycerol. Larvae were imaged on a Leica TCS SP8 confocal laser scanning microscope using a 63x glycerol immersion lens (NA 1.30) and Leica LAS X software. Hoechst 33258, Alexa 488, and symbiont autofluorescence were excited with 405, 496, and 633 nm laser lines, respectively. Fluorescence emission was detected at 410-501 nm for Hoechst 33258, 501-541 nm goat-α-rabbit Alexa 488, and 645-741 for symbiont autofluorescence.

6.5 Western blots

6.5.1 Western blot analysis of LAMP1 antibody and LAMP1 deglycosylation assay

Two aposymbiotic or symbiotic adult *Aiptasia* were homogenized in 50 mM Tris-HCl pH 7.5, 200 mM NaCl, and 1% NP-40 with 2X Halt Protease Inhibitor Cocktail (78430, Thermo Fisher Scientific, Waltham, MA, USA) and then sonicated on ice (Sonifier 250, Branson Ultrasonics, Danbury, CT, USA) with two rounds of 25 pulses at duty cycle 40%, output control 1.8. The homogenate was centrifuged at maximum speed at 4°C for 10 minutes and the supernatant was transferred to a new tube. Deglycosylation assay using PNGase F (P0704S, New England BioLabs Inc., Ipswich, MA, USA) was performed according to manufacturer’s protocol with the exception of incubating the reaction for 3 hours at 37°C followed by overnight at RT. 0.5 mg/ml of LAMP1 antibody was pre-adsorbed with 1 mg/ml of LAMP1 peptide in 4% milk in 0.1% PBT overnight at 4ºC. Untreated and treated extracts

were diluted 1:1 in 5X loading dye and heated to 100°C or 60°C, respectively, for 5 minutes. Samples were loaded into a 4-20% precast gel (4561095, Bio-Rad Laboratories Inc., Hercules, CA, USA), which was run at 90 V for 15 minutes then at 200 V for 1 hour at room temperature in 1X SDS running buffer. The proteins were transferred onto a nitrocellulose membrane at 0.37 A for 1 hour and 15 minutes at RT in 1X transfer buffer (20% v/v methanol, 200 mM glycine, 25 mM Trizma in water). The membrane was blocked for 1 hour at room temperature in 4% milk in 0.1% Triton X-100 in PBS. The blot was divided in two and incubated in either LAMP1 antibody diluted 1:2000 in blocking buffer or pre-adsorbed LAMP1 overnight at 4°C. The following day the blots were washed in 0.1% Triton X-100 in PBS 3 x 15 minutes at RT. The secondary antibody, goat-α-rabbit-HRP (Jackson ImmunoResearch, West Grove, PA, USA), was added at a dilution of 1:5000 for 1 hour at RT, protected from light, followed by 3 x 15 minute washes in either 0.1% Triton X-100 in PBS and one final wash in 1X PBS. The blot was developed using 1:1 ECL (GERPN2232, Sigma-Aldrich Co. LLC) and imaging on ECL Imager (ChemoCam, Intas Science Imaging Instruments GmbH, Göttingen, Germany).

6.5.2 Western blot analysis of phospho-4E-BP1 (p4E-BP1) and phospho-S6

Phosphorylation levels of 4E-BP1 and ribosomal protein S6 (S6) were analyzed by Western blotting in symbiotic *Aiptasia* polyps that had been exposed for 12h to various concentrations of the mTOR kinase inhibitor AZD8055 (Chresta et al., 2010) in DMSO or an equal concentration of DMSO as a control (Figure 3.9). Phosphorylation levels of 4E-BP1 were analyzed by Western blotting in symbiotic and aposymbiotic *Aiptasia* that were either fed (3 times per week) for > 13 days or starved for ≥ 13 days (Figure 3.10A). Animals were either kept under a regular light regime (12L:12D) or at constant darkness for 66h before analysis. Phosphorylation levels of 4E-BP1 in dependence on light were analyzed in symbiotic and aposymbiotic polyps that were either fed (3 times per week for ≥13 days) or starved (for 13 days) under normal light conditions (12L:12D, sampled 6h into the light period) or darkness (66h prior to experiment) to block photosynthesis (Figure 3.10C).

In all of these experiments, animals were harvested 6h into the light period, dried on tissue paper and resuspended in 75 µl of 2x loading dye (120 mM Tris-HCl pH 6.8, 20 % glycerol, 2 % SDS, 40 mM dithiothreitol) and incubated at 95 °C for 10 min. Lysed samples were then put on ice, and sonicated (Sonifier 250, Branson Ultrasonics), with two rounds of 30 and 20 pulses, respectively, at duty cycle 40% and output control 1.8), followed by incubation at 95 °C for 5 min. Samples were then pelleted by centrifugation at 2000 rcf for 30 s at room temperature and total protein concentrations of the supernatant were determined via Bradford Assay, masking SDS interference with 125 mg/ml α-cyclodextrin (Rabilloud, 2018). Samples were stored at room temperature until loading on gels. 30 µg (fed 1 d before sampling) or 45 µg (fed 3 d before sampling) of total protein were loaded per sample. Samples were run on 12 % SDS gels at 90 V (stacking gel) and then 150 V (resolving gel) in SDS running buffer (25 mM Tris, 192 mM glycine, 0.1% SDS). Proteins were transferred onto a nitrocellulose membrane at 0.35 A for 1 hour at RT in 1x transfer buffer (25 mM Tris, 200 mM glycine,

20% methanol). The membrane was blocked for 1 hour at room temperature in 5% milk in 0.1% Tween 20 in TBS. The blot was cut at the 25 kDa marker band. The top was incubated with α-tubulin antibody (1:3000; T9026, Sigma-Aldrich Co., LLC), the lower half incubated with the p4E-BP1 primary antibody (1:1000; 2855T, Cell Signaling Technology, Danvers, MA, USA) overnight at 4°C. The following day the blots were washed in 0.1% Tween 20 in TBS 3 x 5 minutes at RT. The secondary antibody, goat-α-rabbit-HRP (115-035-144, Jackson ImmunoResearch) for p4E-BP1 and goat-α-mouse-HRP (115-035-044, Jackson ImmunoResearch) for α-tubulin, was added at a dilution of 1:10000 for 1 hour at RT, followed by 3 x 5 minute washes in 0.1% Tween 20 in TBS. The blot was developed using ECL (GERPN2232, Sigma-Aldrich) and imaging on ECL Imager (ChemoCam, Intas).

6.6 Statistical Information

Biological replicates are defined as individual animals, either larvae or polyps, except for Western blot of larvae, in Supplemental Figure 5.2, where biological replicates refer to pools of larvae from separate spawning events. Technical replicates are defined as repetitions of the same experiment. Shown in Figure 3.2A are representative images of n = 7 biological replicates for 2dpf and 6dpf larvae, and n = 5 biological replicates for 10dpf larvae. In the timeline of cell proliferation in aposymbiotic larvae shown in Figure 3.2C, $n \geq 15$ biological replicates were used, with the exception of 2dpf, where n = 7 biological replicates were measured. In the comparison of number of lipid droplets in Figure 3.3 B, n = 10 biological replicates were used for aposymbiotic larvae, larvae 4dpi, and larvae 2dpi. n=14 biological replicates were measured for larvae 8dpi. For each condition, one outlier was removed, because noise was erroneously detected as lipid droplets in those samples with low signal. In the comparison of cell proliferation between aposymbiotic and symbiotic larvae in Figure 3.3 C, $15 \leq n \leq 16$ biological replicates were used.

For gene expression analysis, n = 5 biological replicates (pools of cells) were collected for non-symbiotic cells from aposymbiotic and symbiotic larvae, each, and n = 6 biological replicates were collected for symbiotic cells. For differential gene expression analysis, the replicates most representative of gene expression in non-symbiotic cells (n = 7) and symbiotic cells (n = 4) were used.

Western blots shown in Figure 3.9, Supplemental Figure 5.2, and Supplemental Figure 5.3 are representative of n = 2, and Western blots shown in Figure 3.10 are representative of n = 3 biological replicates, each. Immunofluorescence comparing lipid content in aposymbiotic and symbiotic, fed and starved *Aiptasia* polyps in Figure 3.10C is representative of n = 10 replicates for the aposymbiotic condition, and n = 12, or 13 for the starved and fed symbiotic condition, respectively. Immunofluorescence of mTOR in *Aiptasia* larvae shown in Figure 3.10D is a representative image of an mTOR positive larva (three technical replicates with n = 50 biological replicates, each). Immunofluorescence of LAMP1 in *Aiptasia* larvae shown in Figure 3.11 A are representative images of >15 biological replicates, each.

7 References

Aihara, Y., Maruyama, S., Baird, A.H., Iguchi, A., Takahashi, S., and Minagawa, J. (2019). Green fluorescence from cnidarian hosts attracts symbiotic algae. Proceedings of the National Academy of Sciences *116*, 2118–2123.

Baillie, B.K., Monje, V., Silvestre, V., Sison, M., and Belda-Baillie, C.A. (1998). Allozyme electrophoresis as a tool for distinguishing different zooxanthellae symbiotic with giant clams. Proceedings of the Royal Society of London. Series B: Biological Sciences *265*, 1949–1956.

Baird, A.H., Guest, J.R., and Willis, B.L. (2009). Systematic and Biogeographical Patterns in the Reproductive Biology of Scleractinian Corals. Annual Review of Ecology, Evolution, and Systematics *40*, 551–571.

Barneah, O., Brickner, I., Hooge, M., Weis, V.M., LaJeunesse, T.C., and Benayahu, Y. (2007). Three party symbiosis: acoelomorph worms, corals and unicellular algal symbionts in Eilat (Red Sea). Marine Biology *151*, 1215–1223.

Barott, K.L., Venn, A.A., Perez, S.O., Tambutté, S., and Tresguerres, M. (2015). Coral host cells acidify symbiotic algal microenvironment to promote photosynthesis. Proceedings of the National Academy of Sciences *112*, 607–612.

Battey, J.F., and Patton, J.S. (1984). A reevaluation of the role of glycerol in carbon translocation in zooxanthellae-coelenterate symbiosis. Marine Biology *79*, 27–38.

Baumgarten, S., Simakov, O., Esherick, L.Y., Liew, Y.J., Lehnert, E.M., Michell, C.T., Li, Y., Hambleton, E.A., Guse, A., Oates, M.E., et al. (2015). The genome of *Aiptasia*, a sea anemone model for coral symbiosis. Proceedings of the National Academy of Sciences *112*, 11893–11898.

Bay, L.K., Cumbo, V.R., Abrego, D., Kool, J.T., Ainsworth, T.D., and Willis, B.L. (2011). Infection Dynamics Vary between Symbiodinium Types and Cell Surface Treatments during Establishment of Endosymbiosis with Coral Larvae. Diversity *3*, 356–374.

Belda-Baillie, C.A., Baillie, B.K., and Maruyama, T. (2002). Specificity of a Model Cnidarian-Dinoflagellate Symbiosis. The Biological Bulletin *202*, 74–85.

Ben-Sahra, I., Hoxhaj, G., Ricoult, S.J.H., Asara, J.M., and Manning, B.D. (2016). mTORC1 induces purine synthesis through control of the mitochondrial tetrahydrofolate cycle. Science *351*, 728.

Bhattacharya, D., Yoon, H.S., and Hackett, J.D. (2004). Photosynthetic eukaryotes unite: endosymbiosis connects the dots. BioEssays *26*, 50–60.

Bieri, T., Onishi, M., Xiang, T., Grossman, A.R., and Pringle, J.R. (2016). Relative Contributions of Various Cellular Mechanisms to Loss of Algae during Cnidarian Bleaching. PLOS ONE *11*, e0152693.

Biquand, E., Okubo, N., Aihara, Y., Rolland, V., Hayward, D.C., Hatta, M., Minagawa, J., Maruyama, T., and Takahashi, S. (2017). Acceptable symbiont cell size differs among cnidarian species and may limit symbiont diversity. The ISME Journal *11*, 1702–1712.

Boschma, H. (1925). The Nature of the Association between Anthozoa and Zooxanthellae. Proc Natl Acad Sci U S A *11*, 65–67.

Bouché, V., Espinosa, A.P., Leone, L., Sardiello, M., Ballabio, A., and Botas, J. (2016). *Drosophila* Mitf regulates the V-ATPase and the lysosomal-autophagic pathway. Autophagy *12*, 484–498.

Brandt, K. (1881). Ueber das Zusammenleben von Thieren und Algen. Arch. Anat. Physiol. *1881*, 570–574.

Brown, B. (1997). Coral bleaching: causes and consequences. Coral Reefs *16*, S129–S138.

Brown, M.W., Heiss, A.A., Kamikawa, R., Inagaki, Y., Yabuki, A., Tice, A.K., Shiratori, T., Ishida, K.-I., Hashimoto, T., Simpson, A.G.B., et al. (2018). Phylogenomics Places Orphan Protistan Lineages in a Novel Eukaryotic Super-Group. Genome Biology and Evolution *10*, 427–433.

Bucher, M., Wolfowicz, I., Voss, P.A., Hambleton, E.A., and Guse, A. (2016). Development and Symbiosis Establishment in the Cnidarian Endosymbiosis Model *Aiptasia sp.* Scientific Reports *6*, 19867.

Buerger, P., Alvarez-Roa, C., Coppin, C.W., Pearce, S.L., Chakravarti, L.J., Oakeshott, J.G., Edwards, O.R., and van Oppen, M.J.H. (2020). Heat-evolved microalgal symbionts increase coral bleaching tolerance. Science Advances *6*, eaba2498.

Capella-Gutiérrez, S., Silla-Martínez, J.M., and Gabaldón, T. (2009). trimAl: a tool for automated alignment trimming in large-scale phylogenetic analyses. Bioinformatics *25*, 1972–1973.

Carlos, A.A., Baillie, B.K., Kawachi, M., and Maruyama, T. (1999). Phylogenetic position of Symbiodinium (Dinophyceae) isolates from Tridacnids (Bivalvia), Cardiids (Bivalvia), a sponge (Porifera), a soft coral (Anthozoa), and a free-living strain. Journal of Phycology *35*, 1054–1062.

Castellano, B.M., Thelen, A.M., Moldavski, O., Feltes, M., van der Welle, R.E.N., Mydock-McGrane, L., Jiang, X., van Eijkeren, R.J., Davis, O.B., Louie, S.M., et al. (2017). Lysosomal cholesterol activates mTORC1 via an SLC38A9–Niemann-Pick C1 signaling complex. Science *355*, 1306–1311.

Chakravarti, L.J., and van Oppen, M.J.H. (2018). Experimental Evolution in Coral Photosymbionts as a Tool to Increase Thermal Tolerance. Frontiers in Marine Science *5*.

Chakravarti, L.J., Beltran, V.H., and van Oppen, M.J.H. (2017). Rapid thermal adaptation in photosymbionts of reef-building corals. Global Change Biology *23*, 4675–4688.

Champion, J.A., Walker, A., and Mitragotri, S. (2008). Role of particle size in phagocytosis of polymeric microspheres. Pharmaceutical Research *25*, 1815–1821.

Chantranupong, L., Wolfson, R.L., Orozco, J.M., Saxton, R.A., Scaria, S.M., Bar-Peled, L., Spooner, E., Isasa, M., Gygi, S.P., and Sabatini, D.M. (2014). The Sestrins Interact with GATOR2 to Negatively Regulate the Amino-Acid-Sensing Pathway Upstream of mTORC1. Cell Reports *9*, 1–8.

Chen, M.-C., Cheng, Y.-M., Sung, P.-J., Kuo, C.-E., and Fang, L.-S. (2003). Molecular identification of Rab7 (ApRab7) in *Aiptasia pulchella* and its exclusion from phagosomes harboring zooxanthellae. Biochemical and Biophysical Research Communications *308*, 586–595.

Chen, M.-C., Cheng, Y.-M., Hong, M.-C., and Fang, L.-S. (2004). Molecular cloning of Rab5 (ApRab5) in *Aiptasia pulchella* and its retention in phagosomes harboring live zooxanthellae. Biochemical and Biophysical Research Communications *324*, 1024–1033.

Chen, W.-N.U., Kang, H.-J., Weis, V.M., Mayfield, A.B., Jiang, P.-L., Fang, L.-S., and Chen, C.-S. (2012). Diel rhythmicity of lipid-body formation in a coral-Symbiodinium endosymbiosis. Coral Reefs *31*, 521–534.

Chresta, C.M., Davies, B.R., Hickson, I., Harding, T., Cosulich, S., Critchlow, S.E., Vincent, J.P., Ellston, R., Jones, D., Sini, P., et al. (2010). AZD8055 Is a Potent, Selective, and Orally Bioavailable ATP-Competitive Mammalian Target of Rapamycin Kinase Inhibitor with In vitro and In vivo Antitumor Activity. Cancer Res *70*, 288.

Clayton, W.S., and Lasker, H.R. (1985). Individual and population growth in the asexually reproducing anemone *Aiptasia pallida* Verrill. Journal of Experimental Marine Biology and Ecology *90*, 249–258.

Cook, N.R., Row, P.E., and Davidson, H.W. (2004). Lysosome Associated Membrane Protein 1 (Lamp1) Traffics Directly from the TGN to Early Endosomes. Traffic *5*, 685–699.

Cooper, J.E. (2007). Early interactions between legumes and rhizobia: disclosing complexity in a molecular dialogue: Early legume-rhizobia interactions. Journal of Applied Microbiology *103*, 1355–1365.

Costanza, R., de Groot, R., Sutton, P., van der Ploeg, S., Anderson, S.J., Kubiszewski, I., Farber, S., and Turner, R.K. (2014). Changes in the global value of ecosystem services. Global Environmental Change *26*, 152–158.

Crossland, C.J., Barnes, D.J., and Borowitzka, M.A. (1980). Diurnal lipid and mucus production in the staghorn coral *Acropora acuminata*. Marine Biology *60*, 81–90.

Daly, M., Brugler, M.R., Cartwright, P., Collins, A.G., Dawson, M.N., Fautin, D.G., France, S.C., Mcfadden, C.S., Opresko, D.M., and Rodriguez, E. (2007). The phylum Cnidaria: a review of phylogenetic patterns and diversity 300 years after Linnaeus. Zootaxa *1668*, 127–182.

Dani, V., Priouzeau, F., Mertz, M., Mondin, M., Pagnotta, S., Lacas-Gervais, S., Davy, S.K., and Sabourault, C. (2017). Expression patterns of sterol transporters NPC1 and NPC2 in the cnidarian–dinoflagellate symbiosis. Cellular Microbiology *19*, e12753.

Darriba, D., Taboada, G.L., Doallo, R., and Posada, D. (2011). ProtTest 3: fast selection of best-fit models of protein evolution. Bioinformatics *27*, 1164–1165.

Davies, P.S. (1991). Effect of daylight variations on the energy budgets of shallow-water corals. Marine Biology *108*, 137–144.

Davies, S.W., Strader, M.E., Kool, J.T., Kenkel, C.D., and Matz, M.V. (2017). Modeled differences of coral life-history traits influence the refugium potential of a remote Caribbean reef. Coral Reefs *36*, 913–925.

Davis, R.H. (2004). The age of model organisms. Nature Reviews Genetics *5*, 69–76.

Davy, S., Lucas, I., and Turner, J. (1996). Carbon budgets in temperate anthozoan-dinoflagellate symbioses. Marine Biology *126*, 773–783.

Davy, S.K., Allemand, D., and Weis, V.M. (2012). Cell Biology of Cnidarian-Dinoflagellate Symbiosis. Microbiology and Molecular Biology Reviews *76*, 229–261.

Delevoye, C., Marks, M.S., and Raposo, G. (2019). Lysosome-related organelles as functional adaptations of the endolysosomal system. Current Opinion in Cell Biology *59*, 147–158.

Downs, C.A., Kramarsky-Winter, E., Martinez, J., Kushmaro, A., Woodley, C.M., Loya, Y., and Ostrander, G.K. (2009). Symbiophagy as a cellular mechanism for coral bleaching. Autophagy *5*, 211–216.

Dubinsky, Z. (1990). Coral reefs (Amsterdam; New York: Elsevier).

Dunn, S.R., Schnitzler, C.E., and Weis, V.M. (2007). Apoptosis and autophagy as mechanisms of dinoflagellate symbiont release during cnidarian bleaching: every which way you lose. Proceedings of the Royal Society B: Biological Sciences *274*, 3079–3085.

Eakin, C.M., Sweatman, H.P.A., and Brainard, R.E. (2019). The 2014–2017 global-scale coral bleaching event: insights and impacts. Coral Reefs *38*, 539–545.

Eckert, R.J., Reaume, A.M., Sturm, A.B., Studivan, M.S., and Voss, J.D. (2020). Depth Influences Symbiodiniaceae Associations Among Montastraea cavernosa Corals on the Belize Barrier Reef. Frontiers in Microbiology *11*, 518.

Ferrier-Pagès, C., Hoogenboom, M., and Houlbrèque, F. (2011). The Role of Plankton in Coral Trophodynamics. In Coral Reefs: An Ecosystem in Transition, Z. Dubinsky, and N. Stambler, eds. (Dordrecht: Springer Netherlands), pp. 215–229.

Flannagan, R.S., Jaumouillé, V., and Grinstein, S. (2012). The Cell Biology of Phagocytosis. Annual Review of Pathology: Mechanisms of Disease *7*, 61–98.

Frank, P., and Bleakney, J.S. (1976). Histology and sexual reproduction of the anemone *Nematostella vectensis* Stephenson 1935. Journal of Natural History *10*, 441–449.

Freudenthal, H.D. (1962). *Symbiodinium* gen. nov. and *Symbiodinium microadriaticum* sp. nov., a Zooxanthella: Taxonomy, Life Cycle, and Morphology.*. The Journal of Protozoology *9*, 45–52.

Frith, M.C. (2004). Detection of functional DNA motifs via statistical over-representation. Nucleic Acids Research *32*, 1372–1381.

Furnas, M., Alongi, D., McKinnon, D., Trott, L., and Skuza, M. (2011). Regional-scale nitrogen and phosphorus budgets for the northern (14°S) and central (17°S) Great Barrier Reef shelf ecosystem. Continental Shelf Research *31*, 1967–1990.

Gaither, M.R., and Rowan, R. (2010). Zooxanthellar symbiosis in planula larvae of the coral Pocillopora damicornis. Journal of Experimental Marine Biology and Ecology *386*, 45–53.

Ganley, I.G., Lam, D.H., Wang, J., Ding, X., Chen, S., and Jiang, X. (2009). ULK1.ATG13.FIP200 complex mediates mTOR signaling and is essential for autophagy. J Biol Chem *284*, 12297–12305.

Garrett, T.A., Schmeitzel, J.L., Klein, J.A., Hwang, J.J., and Schwarz, J.A. (2013). Comparative Lipid Profiling of the Cnidarian *Aiptasia* pallida and Its Dinoflagellate Symbiont. PLoS ONE *8*, e57975.

Gleason, D.F., and Hofmann, D.K. (2011). Coral larvae: From gametes to recruits. Journal of Experimental Marine Biology and Ecology *408*, 42–57.

Goad L. J. (1981). Sterol biosynthesis and metabolism in marine invertebrates. Pac *53*, 837.

Gómez, F. (2012). A quantitative review of the lifestyle, habitat and trophic diversity of dinoflagellates (Dinoflagellata, Alveolata). Systematics and Biodiversity *10*, 267–275.

Goreau, T.F., and Goreau, N.I. (1959). The physiology of skeleton formation in corals. II. Calcium deposition by hermatypic corals under various conditions in the reef. The Biological Bulletin *117*, 239–250.

Gotthardt, D., Warnatz, H.J., Henschel, O., Brückert, F., Schleicher, M., and Soldati, T. (2002). High-Resolution Dissection of Phagosome Maturation Reveals Distinct Membrane Trafficking Phases. MBoC *13*, 3508–3520.

Grajales, A., and Rodríguez, E. (2016). Elucidating the evolutionary relationships of the Aiptasiidae, a widespread cnidarian–dinoflagellate model system (Cnidaria: Anthozoa: Actiniaria: Metridioidea). Molecular Phylogenetics and Evolution *94*, 252–263.

Grawunder, D., Hambleton, E.A., Bucher, M., Wolfowicz, I., Bechtoldt, N., and Guse, A. (2015). Induction of Gametogenesis in the Cnidarian Endosymbiosis Model *Aiptasia sp.* Scientific Reports *5*, 15677.

Grottoli, A.G., Warner, M.E., Levas, S.J., Aschaffenburg, M.D., Schoepf, V., McGinley, M., Baumann, J., and Matsui, Y. (2014). The cumulative impact of annual coral bleaching can turn some coral species winners into losers. Global Change Biology *20*, 3823–3833.

Gu, Z., Eils, R., and Schlesner, M. (2016). Complex heatmaps reveal patterns and correlations in multidimensional genomic data. Bioinformatics *32*, 2847–2849.

Habetha, M., Anton-Erxleben, F., Neumann, K., and Bosch, T.C.G. (2003). The Hydra viridis / Chlorella symbiosis. Growth and sexual differentiation in polyps without symbionts. Zoology *106*, 101–108.

Hadano, S., Kunita, R., Otomo, A., Suzuki-Utsunomiya, K., and Ikeda, J.-E. (2007). Molecular and cellular function of ALS2/alsin: Implication of membrane dynamics in neuronal development and degeneration. Neurochemistry International *51*, 74–84.

Hambleton, E.A., Guse, A., and Pringle, J.R. (2014). Similar specificities of symbiont uptake by adults and larvae in an anemone model system for coral biology. The Journal of Experimental Biology *217*, 1613–1619.

Hambleton, E.A., Jones, V.A.S., Maegele, I., Kvaskoff, D., Sachsenheimer, T., and Guse, A. (2019). Sterol transfer by atypical cholesterol-binding NPC2 proteins in coral-algal symbiosis. ELife *8*.

Hanes, S.D., and Kempf, S.C. (2013). Host autophagic degradation and associated symbiont loss in response to heat stress in the symbiotic anemone, *Aiptasia pallida*. Invertebrate Biology *132*, 95–107.

Harrison, P.L. (2011). Sexual Reproduction of Scleractinian Corals. In Coral Reefs: An Ecosystem in Transition, Z. Dubinsky, and N. Stambler, eds. (Dordrecht: Springer Netherlands), pp. 59–85.

Harrison, P.L., and Booth, D.J. (2007). Coral reefs: naturally dynamic and increasingly disturbed ecosystems. In Marine Ecology, S.D. Connell, and B.M. Gillanders, eds. (South Melbourne, Victoria: Oxford University Press), pp. 316–377.

Hecky, R.E., and Kilham, P. (1988). Nutrient limitation of phytoplankton in freshwater and marine environments: A review of recent evidence on the effects of enrichment1: Nutrient enrichment. Limnology and Oceanography *33*, 796–822.

Hill, M., Allenby, A., Ramsby, B., Schönberg, C., and Hill, A. (2011). Symbiodinium diversity among host clionaid sponges from Caribbean and Pacific reefs: Evidence of heteroplasmy and putative host-specific symbiont lineages. Molecular Phylogenetics and Evolution *59*, 81–88.

Hirose, M., Kinzie, R., and Hidaka, M. (2000). Early development of zooxanthella-containing eggs of the corals Pocillopora verrucosa and P. eydouxi with special reference to the distribution of zooxanthellae. The Biological Bulletin *199*, 68–75.

Hirose, M., Yamamoto, H., and Nonaka, M. (2008). Metamorphosis and acquisition of symbiotic algae in planula larvae and primary polyps of Acropora spp. Coral Reefs *27*, 247–254.

Hoegh-Guldberg, O. (1999). Climate change, coral bleaching and the future of the world's coral reefs. Marine and Freshwater Research *50*, 839–866.

Hoegh-Guldberg, O., Mumby, P.J., Hooten, A.J., Steneck, R.S., Greenfield, P., Gomez, E., Harvell, C.D., Sale, P.F., Edwards, A.J., Caldeira, K., et al. (2007). Coral Reefs Under Rapid Climate Change and Ocean Acidification. Science *318*, 1737–1742.

Hohman, T.C., McNeil, P.L., and Muscatine, L. (1982). Phagosome-lysosome fusion inhibited by algal symbionts of Hydra viridis. J Cell Biol *94*, 56.

Inoki, K., Zhu, T., and Guan, K.-L. (2003). TSC2 Mediates Cellular Energy Response to Control Cell Growth and Survival. Cell *115*, 577–590.

Jacobovitz, M.R., Rupp, S., Voss, P.A., Gornik, S.G., and Guse, A. (2019). Dinoflagellate symbionts escape vomocytosis by host cell immune suppression. BioRxiv.

Jolley, E., and Smith, D.C. (1980). The green hydra symbiosis. II. The biology of the establishment of the association. Proceedings of the Royal Society of London. Series B. Biological Sciences *207*, 311–333.

Jones, A., and Berkelmans, R. (2010). Potential costs of acclimatization to a warmer climate: growth of a reef coral with heat tolerant vs. sensitive symbiont types. PloS One *5*, e10437.

Jones, A.M., Berkelmans, R., van Oppen, M.J.H., Mieog, J.C., and Sinclair, W. (2008). A community change in the algal endosymbionts of a scleractinian coral following a natural bleaching event: field evidence of acclimatization. Proc Biol Sci *275*, 1359.

Jones, V.A.S., Bucher, M., Hambleton, E.A., and Guse, A. (2018). Microinjection to deliver protein, mRNA, and DNA into zygotes of the cnidarian endosymbiosis model *Aiptasia sp.* Scientific Reports *8*.

Jovic, M., Sharma, M., Rahajeng, J., and Caplan, S. (2010). The early endosome: a busy sorting station for proteins at the crossroads. Histol Histopathol *25*, 99–112.

Kaandorp, J.A. (2013). Macroscopic Modelling of Environmental Influence on Growth and Form of Sponges and Corals Using the Accretive Growth Model. ISRN Biomathematics *2013*, 159170.

Kalyaanamoorthy, S., Minh, B.Q., Wong, T.K.F., von Haeseler, A., and Jermiin, L.S. (2017). ModelFinder: fast model selection for accurate phylogenetic estimates. Nature Methods *14*, 587.

Kanehisa, M., and Goto, S. (2000). KEGG: kyoto encyclopedia of genes and genomes. Nucleic Acids Res *28*, 27–30.

Kaur, J., and Debnath, J. (2015). Autophagy at the crossroads of catabolism and anabolism. Nature Reviews Molecular Cell Biology *16*, 461.

Kayal, E., Bentlage, B., Sabrina Pankey, M., Ohdera, A.H., Medina, M., Plachetzki, D.C., Collins, A.G., and Ryan, J.F. (2018). Phylogenomics provides a robust topology of the major cnidarian lineages and insights on the origins of key organismal traits. BMC Evolutionary Biology *18*.

Kempf, S.C. (1984). Symbiosis between the zooxanthellae *Symbiodinium (= Gymnodinium) microadriaticum* (Freudenthal) and four species of nudibranchs. The Biological Bulletin *166*, 110–126.

Kennedy, E.V., Foster, N.L., Mumby, P.J., and Stevens, J.R. (2015). Widespread prevalence of cryptic Symbiodinium D in the key Caribbean reef builder, Orbicella annularis. Coral Reefs *34*, 519–531.

Khanna, D.R., and Yadav, P.R. (2005). Biology of coelenterata (New Delhi: Discovery Publ. House).

Kleypas, J., and Langdon, C. (2006). Coral Reefs and Climate Change: Science and Management. AGU Monograph Series, Coastal and Estuarine Studies.

Kopp, C., Domart-Coulon, I., Barthelemy, D., and Meibom, A. (2016). Nutritional input from dinoflagellate symbionts in reef-building corals is minimal during planula larval life stage. Science Advances *2*, e1500681–e1500681.

Krueger, T. (2017). Concerning the cohabitation of animals and algae – an English translation of K. Brandt's 1881 presentation "Ueber das Zusammenleben von Thieren und Algen." Symbiosis *71*, 167–174.

Kwon, H.J., Abi-Mosleh, L., Wang, M.L., Deisenhofer, J., Goldstein, J.L., Brown, M.S., and Infante, R.E. (2009). Structure of N-Terminal Domain of NPC1 Reveals Distinct Subdomains for Binding and Transfer of Cholesterol. Cell *137*, 1213–1224.

LaJeunesse, T.C. (2001). Investigating the biodiversity, ecology, and phylogeny of endosymbiotic dinoflagellates in the genus *Symbiodinium* using the ITS region: in search of a "species" level marker. Journal of Phycology *37*, 866–880.

LaJeunesse, T.C., Smith, R.T., Finney, J., and Oxenford, H. (2009). Outbreak and persistence of opportunistic symbiotic dinoflagellates during the 2005 Caribbean mass coral 'bleaching' event. Proceedings of the Royal Society B: Biological Sciences *276*, 4139–4148.

LaJeunesse, T.C., Smith, R., Walther, M., Pinzón, J., Pettay, D.T., McGinley, M., Aschaffenburg, M., Medina-Rosas, P., Cupul-Magaña, A.L., Pérez, A.L., et al. (2010). Host-symbiont recombination versus natural selection in the response of coral-dinoflagellate symbioses to environmental disturbance. Proc Biol Sci *277*, 2925–2934.

LaJeunesse, T.C., Parkinson, J.E., Gabrielson, P.W., Jeong, H.J., Reimer, J.D., Voolstra, C.R., and Santos, S.R. (2018). Systematic Revision of Symbiodiniaceae Highlights the Antiquity and Diversity of Coral Endosymbionts. Current Biology *28*, 2570-2580.e6.

Lapierre, L.R., De Magalhaes Filho, C.D., McQuary, P.R., Chu, C.-C., Visvikis, O., Chang, J.T., Gelino, S., Ong, B., Davis, A.E., Irazoqui, J.E., et al. (2013). The TFEB orthologue HLH-30 regulates autophagy and modulates longevity in *Caenorhabditis elegans*. Nature Communications *4*.

Lapointe, B.E. (1999). Simultaneous top-down and bottom-up forces control macroalgal blooms on coral reefs (Reply to the comment by Hughes et al.). Limnology and Oceanography *44*, 1586–1592.

Larkin, M.A., Blackshields, G., Brown, N.P., Chenna, R., McGettigan, P.A., McWilliam, H., Valentin, F., Wallace, I.M., Wilm, A., Lopez, R., et al. (2007). Clustal W and Clustal X version 2.0. Bioinformatics *23*, 2947–2948.

Laumer, C.E., Fernández, R., Lemer, S., Combosch, D., Kocot, K.M., Riesgo, A., Andrade, S.C.S., Sterrer, W., Sørensen, M.V., and Giribet, G. (2019). Revisiting metazoan phylogeny with genomic sampling of all phyla. Proceedings of the Royal Society B: Biological Sciences *286*, 20190831.

Lehnert, E.M., Burriesci, M.S., and Pringle, J.R. (2012). Developing the anemone Aiptasia as a tractable model for cnidarian-dinoflagellate symbiosis: the transcriptome of aposymbiotic *A. pallida*. BMC Genomics *13*, 271.

Lehnert, E.M., Mouchka, M.E., Burriesci, M.S., Gallo, N.D., Schwarz, J.A., and Pringle, J.R. (2014). Extensive Differences in Gene Expression Between Symbiotic and Aposymbiotic Cnidarians. G3: Genes\textbarGenomes\textbarGenetics *4*, 277–295.

Letunic, I., and Bork, P. (2017). 20 years of the SMART protein domain annotation resource. Nucleic Acids Research *46*, D493–D496.

Levin, R., Grinstein, S., and Canton, J. (2016). The life cycle of phagosomes: formation, maturation, and resolution. Immunological Reviews *273*, 156–179.

Lewis, D.H., and Smith, D.C. (1971). The Autotrophic Nutrition of Symbiotic Marine Coelenterates with Special Reference to Hermatypic Corals. I. Movement of Photosynthetic Products between the Symbionts. Proceedings of the Royal Society B: Biological Sciences *178*, 111–129.

Li, J., and Pfeffer, S.R. (2016). Lysosomal membrane glycoproteins bind cholesterol and contribute to lysosomal cholesterol export. Elife *5*, e21635.

Lin, K.-L., Wang, J.-T., and Fang, L.-S. (2000). Participation of glycoproteins on zooxanthellal cell walls in the establishment of a symbiotic relationship with the sea anemone, Aiptasia pulchella. Zoological Studies *39*, 172–178.

Little, A.F., Oppen, M.J.H. van, and Willis, B.L. (2004). Flexibility in Algal Endosymbioses Shapes Growth in Reef Corals. Science *304*, 1492–1494.

Lobban, C.S., Modeo, L., Verni, F., and Rosati, G. (2005). Euplotes uncinatus (Ciliophora, Hypotrichia), a new species with zooxanthellae. Marine Biology *147*, 1055–1061.

Marlow, H.Q., and Martindale, M.Q. (2007). Embryonic development in two species of scleractinian coral embryos: Symbiodinium localization and mode of gastrulation. Evolution & Development *9*, 355–367.

Martina, J.A., Chen, Y., Gucek, M., and Puertollano, R. (2012). MTORC1 functions as a transcriptional regulator of autophagy by preventing nuclear transport of TFEB. Autophagy *8*, 903–914.

Matthews, J.L., Sproles, A.E., Oakley, C.A., Grossman, A.R., Weis, V.M., and Davy, S.K. (2016). Menthol-induced bleaching rapidly and effectively provides experimental aposymbiotic sea anemones (*Aiptasia* sp.) for symbiosis investigations. The Journal of Experimental Biology *219*, 306–310.

Matthews, J.L., Crowder, C.M., Oakley, C.A., Lutz, A., Roessner, U., Meyer, E., Grossman, A.R., Weis, V.M., and Davy, S.K. (2017). Optimal nutrient exchange and immune responses operate in partner specificity in the cnidarian-dinoflagellate symbiosis. Proceedings of the National Academy of Sciences *114*, 13194–13199.

McAuley, P.J., and Smith, D.C. (1982). The green hydra symbiosis. V. Stages in the intracellular recognition of algal symbionts by digestive cells. Proceedings of the Royal Society of London. Series B. Biological Sciences *216*, 7–23.

Medrano, E., Merselis, D.G., Bellantuono, A.J., and Rodriguez-Lanetty, M. (2019). Proteomic Basis of Symbiosis: A Heterologous Partner Fails to Duplicate Homologous Colonization in a Novel Cnidarian–Symbiodiniaceae Mutualism. Frontiers in Microbiology *10*, 1153.

Mohamed, A.R., Cumbo, V., Harii, S., Shinzato, C., Chan, C.X., Ragan, M.A., Bourne, D.G., Willis, B.L., Ball, E.E., Satoh, N., et al. (2016). The transcriptomic response of the coral *Acropora digitifera* to a competent Symbiodinium strain: the symbiosome as an arrested early phagosome. Mol Ecol *25*, 3127–3141.

Morariu, V.I., Srinivasan, B.V., Raykar, V.C., Duraiswami, R., and Davis, L.S. (2008). Automatic online tuning for fast Gaussian summation. In Advances in Neural Information Processing Systems 21, Proceedings of the Twenty-Second Annual Conference on Neural Information Processing Systems, Vancouver, British Columbia, Canada, December 8-11, 2008, pp. 1113–1120.

Muscatine, L. (1990). The role of symbiotic algae in carbon and energy flux in reef corals. Ecosystems of the World. Coral Reefs.

Muscatine, L., Falkowski, P., Porter, J., and Dubinsky, Z. (1984). Fate of photosynthetic fixed carbon in light-and shade-adapted colonies of the symbiotic coral Stylophora pistillata. Proceedings of the Royal Society of London. Series B. Biological Sciences *222*, 181–202.

Muscatine, L., Gates, R.D., and Ingrid, L. (1994). Do symbiotic dinoflagellates secrete lipid droplets? Limnology and Oceanography *39*, 925–929.

Muscatine, L., Goiran, C., Land, L., Jaubert, J., Cuif, J.-P., and Allemand, D. (2005). Stable isotopes ($\delta^{13}C$ and $\delta^{15}N$) of organic matrix from coral skeleton. Proc Natl Acad Sci U S A *102*, 1525.

Napolitano, G., Esposito, A., Choi, H., Matarese, M., Benedetti, V., Di Malta, C., Monfregola, J., Medina, D.L., Lippincott-Schwartz, J., and Ballabio, A. (2018). mTOR-dependent phosphorylation controls TFEB nuclear export. Nature Communications *9*, 3312.

Nguyen, L.-T., Schmidt, H.A., von Haeseler, A., and Minh, B.Q. (2014). IQ-TREE: A Fast and Effective Stochastic Algorithm for Estimating Maximum-Likelihood Phylogenies. Molecular Biology and Evolution *32*, 268–274.

Nitschke, M.R., Craveiro, S.C., Brandão, C., Fidalgo, C., Serôdio, J., Calado, A.J., and Frommlet, J.C. (2020). Description of *Freudenthalidium* gen. nov. and *Halluxium* gen. nov. to formally recognize clades Fr3 and H as genera in the family Symbiodiniaceae (Dinophyceae). Journal of Phycology.

Norton, J.H., Shepherd, M.A., Long, H.M., and Fitt, W.K. (1992). The Zooxanthellal Tubular System in the Giant Clam. The Biological Bulletin *183*, 503–506.

Nyholm, S.V., and McFall-Ngai, M. (2004). The winnowing: establishing the squid–vibrio symbiosis. Nature Reviews Microbiology *2*, 632–642.

Oakley, C.A., Ameismeier, M.F., Peng, L., Weis, V.M., Grossman, A.R., and Davy, S.K. (2016). Symbiosis induces widespread changes in the proteome of the model cnidarian *Aiptasia*: Symbiosis and the Aiptasia *proteome*. Cellular Microbiology *18*, 1009–1023.

O'Rourke, E.J., and Ruvkun, G. (2013). MXL-3 and HLH-30 transcriptionally link lipolysis and autophagy to nutrient availability. Nature Cell Biology *15*, 668–676.

Palmieri, M., Impey, S., Kang, H., di Ronza, A., Pelz, C., Sardiello, M., and Ballabio, A. (2011). Characterization of the CLEAR network reveals an integrated control of cellular clearance pathways. Human Molecular Genetics *20*, 3852–3866.

Parmigiani, A., Nourbakhsh, A., Ding, B., Wang, W., Kim, Y.C., Akopiants, K., Guan, K.-L., Karin, M., and Budanov, A.V. (2014). Sestrins Inhibit mTORC1 Kinase Activation through the GATOR Complex. Cell Reports *9*, 1281–1291.

Pearse, V.B., and Muscatine, L. (1971). Role of symbiotic algae (zooxanthellae) in coral calcification. The Biological Bulletin *141*, 350–363.

Peng, S.-E., Chen, W.-N.U., Chen, H.-K., Lu, C.-Y., Mayfield, A.B., Fang, L.-S., and Chen, C.-S. (2011). Lipid bodies in coral–dinoflagellate endosymbiosis: Proteomic and ultrastructural studies. PROTEOMICS *11*, 3540–3555.

Perera, R.M., and Zoncu, R. (2016). The Lysosome as a Regulatory Hub. Annual Review of Cell and Developmental Biology *32*, 223–253.

Pfeffer, S.R. (2019). NPC intracellular cholesterol transporter 1 (NPC1)-mediated cholesterol export from lysosomes. Journal of Biological Chemistry *294*, 1706–1709.

Picelli, S., Faridani, O.R., Björklund, Å.K., Winberg, G., Sagasser, S., and Sandberg, R. (2014). Full-length RNA-seq from single cells using Smart-seq2. Nat. Protocols *9*, 171–181.

Plickert, G., Kroiher, M., and Munck, A. (1988). Cell proliferation and early differentiation during embryonic development and metamorphosis of Hydractinia echinata. Development *103*, 795.

Pochon, X., and Gates, R.D. (2010). A new Symbiodinium clade (Dinophyceae) from soritid foraminifera in Hawai'i. Molecular Phylogenetics and Evolution *56*, 492–497.

Pochon, X., and Pawlowski, J. (2006). Evolution of the soritids-Symbiodinium symbiosis. Symbiosis *42*, 77–88.

Porstmann, T., Santos, C.R., Griffiths, B., Cully, M., Wu, M., Leevers, S., Griffiths, J.R., Chung, Y.-L., and Schulze, A. (2008). SREBP Activity Is Regulated by mTORC1 and Contributes to Akt-Dependent Cell Growth. Cell Metabolism *8*, 224–236.

Porter, J.W., and Tougas, J.I. (2001). Reef Ecosystems: Threats to their Biodiversity. In Encyclopedia of Biodiversity, (Elsevier), pp. 73–95.

Rabilloud, T. (2018). Optimization of the cydex blue assay: A one-step colorimetric protein assay using cyclodextrins and compatible with detergents and reducers. PLOS ONE *13*, e0195755.

Rebsamen, M., Pochini, L., Stasyk, T., de Araújo, M.E.G., Galluccio, M., Kandasamy, R.K., Snijder, B., Fauster, A., Rudashevskaya, E.L., Bruckner, M., et al. (2015). SLC38A9 is a component of the lysosomal amino acid sensing machinery that controls mTORC1. Nature *519*, 477.

Revel, J., Massi, L., Mehiri, M., Boutoute, M., Mayzaud, P., Capron, L., and Sabourault, C. (2016). Differential distribution of lipids in epidermis, gastrodermis and hosted Symbiodinium in the sea anemone Anemonia viridis. Comparative Biochemistry and Physiology Part A: Molecular & Integrative Physiology *191*, 140–151.

Rhyne, A.L., Lin, J., and Deal, K.J. (2004). Biological control of aquarium pest anemone Aiptasia pallida Verrill by peppermint shrimp Lysmata Risso. Journal of Shellfish Research *23*, 227–230.

Rinkevich, B. (2014). Rebuilding coral reefs: does active reef restoration lead to sustainable reefs? Current Opinion in Environmental Sustainability *7*, 28–36.

Roczniak-Ferguson, A., Petit, C.S., Froehlich, F., Qian, S., Ky, J., Angarola, B., Walther, T.C., and Ferguson, S.M. (2012). The transcription factor TFEB links mTORC1 signaling to transcriptional control of lysosome homeostasis. Sci Signal *5*, ra42–ra42.

Rodriguez-Lanetty, M., Chang, S.-J., and Song, J.-I. (2003). Specificity of two temperate dinoflagellate-anthozoan associations from the north-western Pacific Ocean. Marine Biology *143*, 1193–1199.

Rowan, R. (2004). Coral bleaching: thermal adaptation in reef coral symbionts. Nature *430*, 742.

Rowan, R., and Knowlton, N. (1995). Intraspecific diversity and ecological zonation in coral-algal symbiosis. Proc Natl Acad Sci USA *92*, 2850.

Rowan, R., and Powers, D., A. (1991). A Molecular Genetic Classification of Zooxanthellae and the Evolution of Animal-Algal Symbioses. Science *251*, 1348.

Rowan, R., and Powers, D.A. (1992). Ribosomal RNA sequences and the diversity of symbiotic dinoflagellates (zooxanthellae). Proc Natl Acad Sci USA *89*, 3639.

Sampayo, E.M., Ridgway, T., Bongaerts, P., and Hoegh-Guldberg, O. (2008). Bleaching susceptibility and mortality of corals are determined by fine-scale differences in symbiont type. Proceedings of the National Academy of Sciences *105*, 10444–10449.

Sancak, Y., Peterson, T.R., Shaul, Y.D., Lindquist, R.A., Thoreen, C.C., Bar-Peled, L., and Sabatini, D.M. (2008). The Rag GTPases bind raptor and mediate amino acid signaling to mTORC1. Science *320*, 1496–1501.

Sancak, Y., Bar-Peled, L., Zoncu, R., Markhard, A.L., Nada, S., and Sabatini, D.M. (2010). Ragulator-Rag Complex Targets mTORC1 to the Lysosomal Surface and Is Necessary for Its Activation by Amino Acids. Cell *141*, 290–303.

Santos, S.R., Taylor, D.J., Kinzie, III, R.A., Hidaka, M., Sakai, K., and Coffroth, M.A. (2002). Molecular phylogeny of symbiotic dinoflagellates inferred from partial chloroplast large subunit (23S)-rDNA sequences. Molecular Phylogenetics and Evolution *23*, 97–111.

Sardiello, M. (2016). Transcription factor EB: from master coordinator of lysosomal pathways to candidate therapeutic target in degenerative storage diseases. Annals of the New York Academy of Sciences *1371*, 3–14.

Sardiello, M., Palmieri, M., di Ronza, A., Medina, D., Valenza, M., Gennarino, V., Di Malta, C., Donaudy, F., Embrione, V., Polishchuk, R., et al. (2009). A Gene Network Regulating Lysosomal Biogenesis and Function. Science *325*, 473–477.

Saxton, R.A., and Sabatini, D.M. (2017). mTOR Signaling in Growth, Metabolism, and Disease. Cell *168*, 960–976.

Schindelin, J., Arganda-Carreras, I., Frise, E., Kaynig, V., Longair, M., Pietzsch, T., Preibisch, S., Rueden, C., Saalfeld, S., Schmid, B., et al. (2012). Fiji: an open-source platform for biological-image analysis. Nature Methods *9*, 676.

Schindelin, J., Rueden, C.T., Hiner, M.C., and Eliceiri, K.W. (2015). The ImageJ ecosystem: An open platform for biomedical image analysis. Molecular Reproduction and Development *82*, 518–529.

Schoenberg, D.A., and Trench, R.K. (1980). Genetic variation in *Symbiodinium (=Gymnodinium) microadriaticum* Freudenthal, and specificity in its symbiosis with marine invertebrates. II. Morphological variation in *Symbiodinium microadriaticum*. Proceedings of the Royal Society of London. Series B. Biological Sciences *207*, 429–444.

Schubert, N., Brown, D., and Rossi, S. (2017). Symbiotic versus non-symbiotic octocorals: physiological and ecological implications. Marine Animal Forests 887–918.

Schwarz, J.A., Krupp, D.A., and Weis, V.M. (1999). Late Larval Development and Onset of Symbiosis in the Scleractinian Coral Fungia scutaria. The Biological Bulletin *196*, 70–79.

Sebé-Pedrós, A., Saudemont, B., Chomsky, E., Plessier, F., Mailhé, M.-P., Renno, J., Loe-Mie, Y., Lifshitz, A., Mukamel, Z., Schmutz, S., et al. (2018). Cnidarian Cell Type Diversity and Regulation Revealed by Whole-Organism Single-Cell RNA-Seq. Cell *173*, 1520-1534.e20.

Settembre, C., Di Malta, C., Polito, V.A., Arencibia, M.G., Vetrini, F., Erdin, S., Erdin, S.U., Huynh, T., Medina, D., Colella, P., et al. (2011). TFEB Links Autophagy to Lysosomal Biogenesis. Science *332*, 1429–1433.

Settembre, C., Zoncu, R., Medina, D.L., Vetrini, F., Erdin, S., Erdin, S., Huynh, T., Ferron, M., Karsenty, G., Vellard, M.C., et al. (2012). A lysosome-to-nucleus signalling mechanism senses and regulates the lysosome via mTOR and TFEB: Self-regulation of the lysosome via mTOR and TFEB. The EMBO Journal *31*, 1095–1108.

Settembre, C., De Cegli, R., Mansueto, G., Saha, P.K., Vetrini, F., Visvikis, O., Huynh, T., Carissimo, A., Palmer, D., Jürgen Klisch, T., et al. (2013). TFEB controls cellular lipid metabolism through a starvation-induced autoregulatory loop. Nature Cell Biology *15*, 647–658.

Sheppard, C., Davy, S.K., Pilling, G.M., and Graham, N.A.J. (2018). The Biology of Coral Reefs (Oxford University Press).

Siebert, S., Farrell, J.A., Cazet, J.F., Abeykoon, Y., Primack, A.S., Schnitzler, C.E., and Juliano, C.E. (2019). Stem cell differentiation trajectories in *Hydra* resolved at single-cell resolution. Science *365*, eaav9314.

Slobodkin, L.B., and Bossert, P.E. (2010). Cnidaria. In Ecology and Classification of North American Freshwater Invertebrates, (Elsevier), pp. 125–142.

Sommer, C., Straehle, C., Köthe, U., and Hamprecht, F.A. (2011). Ilastik: Interactive learning and segmentation toolkit. In 2011 IEEE International Symposium on Biomedical Imaging: From Nano to Macro, pp. 230–233.

Sorokin, Y.I. (2013). Coral reef ecology (Springer Science & Business Media).

Spalding, M.D., and Grenfell, A.M. (1997). New estimates of global and regional coral reef areas. Coral Reefs *16*, 225–230.

Sproles, A.E., Oakley, C.A., Matthews, J.L., Peng, L., Owen, J.G., Grossman, A.R., Weis, V.M., and Davy, S.K. (2019). Proteomics quantifies protein expression changes in a model cnidarian colonised by a thermally tolerant but suboptimal symbiont. The ISME Journal.

Stat, M., Carter, D., and Hoeghguldberg, O. (2006). The evolutionary history of Symbiodinium and scleractinian hosts—Symbiosis, diversity, and the effect of climate change. Perspectives in Plant Ecology, Evolution and Systematics *8*, 23–43.

Steen, R.G., and Muscatine, L. (1984). Daily budgets of photosynthetically fixed carbon in symbiotic zoanthids. The Biological Bulletin *167*, 477–487.

Stimson, J.S. (1987). Location, Quantity and Rate of Change in Quantity of Lipids in Tissue of Hawaiian Hermatypic Corals. Bulletin of Marine Science *41*, 889–904.

Subramanian, K., and Balch, W.E. (2008). NPC1/NPC2 function as a tag team duo to mobilize cholesterol. Proc Natl Acad Sci USA *105*, 15223.

Suggett, D.J., and Smith, D.J. (2020). Coral bleaching patterns are the outcome of complex biological and environmental networking. Global Change Biology *26*, 68–79.

Sunagawa, S., Wilson, E.C., Thaler, M., Smith, M.L., Caruso, C., Pringle, J.R., Weis, V.M., Medina, M., and Schwarz, J.A. (2009). Generation and analysis of transcriptomic resources for a model system on the rise: the sea anemone Aiptasia pallida and its dinoflagellate endosymbiont. BMC Genomics *10*, 258.

Szmant-Froelich, A., Reutter, M., and Riggs, L. (1985). Sexual reproduction of Favia fragum (Esper): lunar patterns of gametogenesis, embryogenesis and planulation in Puerto Rico. Bulletin of Marine Science *37*, 880–892.

Takeuchi, R., Jimbo, M., Tanimoto, F., Tanaka, C., Harii, S., Nakano, Y., Yasumoto, K., and Watabe, S. (2017). Establishment of a model for chemoattraction of Symbiodinium and characterization of chemotactic compounds in Acropora tenuis. Fisheries Science *83*, 479–487.

Taylor, F.J.R. (1987). The Biology of dinoflagellates (Oxford ; Boston: Blackwell Scientific Publications).

Thornhill, D.J., LaJeunesse, T.C., Kemp, D.W., Fitt, W.K., and Schmidt, G.W. (2006). Multi-year, seasonal genotypic surveys of coral-algal symbioses reveal prevalent stability or post-bleaching reversion. Marine Biology *148*, 711–722.

Thornhill, D.J., Xiang, Y., Pettay, D.T., Zhong, M., and Santos, S.R. (2013). Population genetic data of a model symbiotic cnidarian system reveal remarkable symbiotic specificity and vectored introductions across ocean basins. Molecular Ecology *22*, 4499–4515.

Todd, P.A. (2008). Morphological plasticity in scleractinian corals. Biological Reviews *83*, 315–337.

Tremblay, P., Grover, R., Maguer, J.F., Legendre, L., and Ferrier-Pagès, C. (2012). Autotrophic carbon budget in coral tissue: a new ^{13}C-based model of photosynthate translocation. J. Exp. Biol. *215*, 1384.

Vandermeulen, J.H., and Watabe, N. (1973). Studies on reef corals. I. Skeleton formation by newly settled planula larva of Pocillopora damicornis. Marine Biology *23*, 47–57.

de Vargas, C., Audic, S., Henry, N., Decelle, J., Mahé, F., Logares, R., Lara, E., Berney, C., Le Bescot, N., Probert, I., et al. (2015). Eukaryotic plankton diversity in the sunlit ocean. Science *348*, 1261605.

Voss, P.A., Gornik, S.G., Jacobovitz, M.R., Rupp, S., Dörr, M.S., Maegele, I., and Guse, A. (2019). Nutrient-dependent mTORC1 signaling in coral-algal symbiosis. BioRxiv.

Waller, R.F., and Kořený, L. (2017). Plastid Complexity in Dinoflagellates: A Picture of Gains, Losses, Replacements and Revisions. In Advances in Botanical Research, (Elsevier), pp. 105–143.

Wang, J., and Douglas, A.E. (1998). Nitrogen recycling or nitrogen conservation in an alga-invertebrate symbiosis? Journal of Experimental Biology *201*, 2445–2453.

Wang, S., Tsun, Z.-Y., Wolfson, R.L., Shen, K., Wyant, G.A., Plovanich, M.E., Yuan, E.D., Jones, T.D., Chantranupong, L., Comb, W., et al. (2015). Lysosomal amino acid transporter SLC38A9 signals arginine sufficiency to mTORC1. Science *347*, 188.

Weis, V.M. (2008). Cellular mechanisms of Cnidarian bleaching: stress causes the collapse of symbiosis. Journal of Experimental Biology *211*, 3059–3066.

Weis, V.M., Davy, S.K., Hoegh-Guldberg, O., Rodriguez-Lanetty, M., and Pringle, J.R. (2008). Cell biology in model systems as the key to understanding corals. Trends in Ecology & Evolution *23*, 369–376.

Whitehead, L.F., and Douglas, A.E. (2003). Metabolite comparisons and the identity of nutrients translocated from symbiotic algae to an animal host. Journal of Experimental Biology *206*, 3149–3157.

Wilkinson, C. (2004). Status of Coral Reefs of the World: 2004 Volume 1-Volume 2 (Australian Institute of Marine Science).

Winchester, B.G. (2001). Lysosomal membrane proteins. European Journal of Paediatric Neurology *5*, 11–19.

Wolfowicz, I., Baumgarten, S., Voss, P.A., Hambleton, E.A., Voolstra, C.R., Hatta, M., and Guse, A. (2016). *Aiptasia sp.* larvae as a model to reveal mechanisms of symbiont selection in cnidarians. Sci Rep *6*.

Wolfson, R.L., Chantranupong, L., Saxton, R.A., Shen, K., Scaria, S.M., Cantor, J.R., and Sabatini, D.M. (2016). Sestrin2 is a leucine sensor for the mTORC1 pathway. Science *351*, 43.

Wood-Charlson, E.M., Hollingsworth, L.L., Krupp, D.A., and Weis, V.M. (2006). Lectin/glycan interactions play a role in recognition in a coral/dinoflagellate symbiosis. Cellular Microbiology *8*, 1985–1993.

Xiang, T., Hambleton, E.A., DeNofrio, J.C., Pringle, J.R., and Grossman, A.R. (2013). Isolation of clonal axenic strains of the symbiotic dinoflagellate Symbiodinium and their growth and host specificity1. J. Phycol. *49*, 447–458.

Yamashita, H., Suzuki, G., Kai, S., Hayashibara, T., and Koike, K. (2014). Establishment of Coral–Algal Symbiosis Requires Attraction and Selection. PLoS ONE *9*, e97003.

Yellowlees, D., Rees, T.A.V., and Leggat, W. (2008). Metabolic interactions between algal symbionts and invertebrate hosts. Plant Cell Environ. *31*, 679–694.

Yu, G., Wang, L.-G., Han, Y., and He, Q.-Y. (2012). clusterProfiler: an R Package for Comparing Biological Themes Among Gene Clusters. OMICS: A Journal of Integrative Biology *16*, 284–287.

Yuyama, I., Ishikawa, M., Nozawa, M., Yoshida, M., and Ikeo, K. (2018). Transcriptomic changes with increasing algal symbiont reveal the detailed process underlying establishment of coral-algal symbiosis. Scientific Reports *8*.

Zoncu, R., Bar-Peled, L., Efeyan, A., Wang, S., Sancak, Y., and Sabatini, D.M. (2011). mTORC1 Senses Lysosomal Amino Acids Through an Inside-Out Mechanism That Requires the Vacuolar H^+-ATPase. Science *334*, 678.

Acknowledgements

First and foremost, I would like to thank Annika for giving me the amazing opportunities to do research in her group on this exciting topic and that I was allowed to conduct field work in Sesoko, Okinawa. I learned a lot form you! I am grateful to my TAC members and examiners Thomas Holstein and Steffen Lemke, who have devoted a lot of time and efforts to give me critical input over the years which improved the research. My thanks also goes to Masayuki Hatta for his guidance during field work in Okinawa and his abounding knowledge and contagious enthusiasm about coral biology. This work would not have been possible without the great research environment in Heidelberg. I got much advice from many researchers at COS, but also from Dinko Pavlinic (who knew preparing sequencing libraries could be so much fun) and Vladimir Benes at EMBL, David Ibberson at Bioquant, Jan Siemens and Shiying Lu at DKFZ and many others. During my time PhD, I was in the HBIGS graduate school, which offered great courses and instant support anywhere they could. Thank you Sandra, Martina and Rolf!

At COS, I want to thank all members of the Grossmann, Evers, Holstein and Özbek and Acebron groups for creating the wonderful work environments in INF329 for the first 2 years of my PhD and in INF230 thereafter. But in particular, I want to thank all the members of the Guse Lab throughout the years. There were the original "Guse girls" Annika, Liz, Natascha, Madeline, Iliona, and Desirée, who welcomed me into the group and Heidelberg and showed me the ropes. Even with most of them in other places, luckily the spirit of the Guse girls lives on forever in the COS party costumes, hopefully for a long time coming! Over the years, I had so much support from the amazing techs Natascha, Ira, Diana, and Harald who supported the research, helped out where they could and made working fun. I want to thank the PhD and Postdocs Marie, Victor, Seb, and Sebastian for the great time in the last two years of my research. Marie for lending an open ear and advice on experiments and for the time spent winding down in the boulder house after an exhausting lab day. And of course for . Victor for his random knowledge and initiating and hosting Sunday dinners so often. And Seb for his help with the bioinformatic analysis, starting when he let me stay with his family in Galway to figure out transcriptome analysis, and of course the endless discussions.

Outside the lab, I was supported by friends and family. Thanks Rik for inviting over to your place for bear and pizza and fun times. Iliona and Oli for becoming such good neighbors and nice evenings with board games or in the park, even it was only shortly before your move to Portugal. Of course this whole ordeal would not have been possible without my family. Thanks Mom and Dad, Christopher, Agnes and Mia for raising me to be ever curious and hardly ever asking when I'd finally finish my PhD. And of course to Gaby and Siggi Koch, as well as Miriam and Gerhard Pfeiffer, who welcomed me into their home and showed me to enjoy the finer things in life (expensive wine and food). Last but not least I

want to thank my wife Sarah for the support throughout the years, her patience for my experience in the PhD (even if she sometimes knew better from her own) and her support when I needed to finish something last-minute. I could always count on you!